Investigation into the Anticancer Mechanism of Action of Novel 4-Substituted Phenylthiazoles and Antihelminthic Benzimidazoles

Jakeb Scott Stuart Marsden Petersen

A thesis submitted for the degree of **Masters of Science** at the University of Otago, Dunedin NZ

Abstract

Recently, two novel 4-substituted phenylthiazoles, D1 and D2, have been synthesised based upon the marine bacterial secondary metabolite anithiactin A/thiasporine C, and shown to be cytotoxic towards cancer cells below 100 μM, with suggestions of inhibition of tubulin polymerisation. D1 and D2 were then further screened for cytotoxicity in three cancer cell lines (MDA-MB-231, MCF-7, HT-29) and one non-transformed mesenchymal stem-cell line (RCB2157), using the MTT assay. Their effects on the cell cycle and cell death mechanisms were analysed using flow cytometry and fluorescent microscopy and spectroscopy. Unfortunately, no significant changes in cell death mechanisms were observed and previous cytotoxicity results were unable to be replicated. This was attributed to the degradation of the compounds in DMSO solution, likely to cause a loss in biological activity.

Antihelminthic benzimidazole drugs mebendazole and albendazole are commonly used to treat a variety of worm infestations in humans. Their mechanism of action against helminths is well-established and involves the inhibition of microtubule formation. Mebendazole has recently shown promising results in pre-clinical *in vitro* and *in vivo* cancer studies and is currently in Phase I trials for treatment of glioma. However, the way in which it causes cell death in cancer cells has not been fully explored.

Here, the *in vitro* analysis of the anticancer mechanism of action of mebendazole and a structural analogue albendazole was undertaken. The two drugs were screened for cytotoxicity in three cancer cell lines (MDA-MB-231, MCF-7, HT-29) and one non-transformed mesenchymal stem-cell line (RCB2157), using the MTT assay. Their effects on the cell cycle and cell death mechanisms were analysed using flow cytometry and fluorescent microscopy and spectroscopy.

Mebendazole and albendazole were found to selectively kill cancer cells, being most potent in the colorectal cancer cell line HT-29, with IC_{50} values of 1.3 ± 0.1 μM and 1.4 ± 0.1 μM,

respectively. Both mebendazole and albendazole induced caspase-3 activation. Phosphatidylserine exposure, mitochondrial and lysosomal membrane permeability and reactive oxygen species production were all significantly increased compared to control and peaked at 24 hours, with DNA fragmentation increasing in a time-dependent manner peaking at 48 hours. Using Hoechst 33342 staining, nuclear features of apoptosis such as chromatin condensation were found following treatment with both drugs. Cell cycle arrest in the G2/M phase was found, and tubulin structures were significantly altered. Mebendazole and albendazole appear to cause cancer cell death via a mechanism of classical apoptosis and cell cycle arrest, which may originate from the destabilisation of microtubules.

Acknowledgements

First and foremost, I would like to thank my supervisor Dr Sarah Baird, without whom none of this would have been possible. From a lab rotation during my undergraduate studies, a summer studentship and now a Master's of Science, it has been an amazing journey and I have greatly appreciated all your guidance, support and continuous kindness that you have shown me over the past few years. I would like to thank the Hawkins Lab group from the Department of Chemistry for synthesising and providing the phenylthiazole compounds. Thank you to Chloe and Gowthami for helping me get accommodated in the Baird Lab and for being great lab mates! Special thanks to Jackmil for all her help with many experiments and troubleshooting. To everyone in the Department of Pharmacology & Toxicology, thank you for welcoming me into the department and continuously making me feel part of our pharmacology family. Thank you to all the staff for always offering an ear to listen and providing help and support whenever I needed it, and especially to Jo our department mother! To all the post-grads, it has been great getting to know all of you over the years and we have spent some great times together and hopefully they will continue.

To my flatmates and friends thank you for always offering your support and interest, I've enjoyed the many discussions and rants we've had about our studies over the past couple of years, and thoroughly appreciate the multiple opportunities of procrastination you have provided me. Lastly to my family, this hasn't been the easiest of journeys for me but was only made possible thanks to the continuous love and caring support of my Mum and Dad and my sister Sammi.

List of Abbreviations

ABZ	Albendazole
ADC	Antibody Drug Conjugate
AIF	Apoptosis Inducing Factor
ANOVA	Analysis of Variance
AO	Acridine Orange
APAF-1	Apoptotic Protease Activating Factor – 1
ATP	Adenosine Triphosphate
BH3	BH3-only proteins
BSA	Bovine Serum Albumin
CAD	Caspase Activated DNase
D1	4-Thiazolecarboxylic acid, 4, 5-dihydro-2-(4-nitrophenyl)-methyl ester
D2	4-Thiazolecarboxylic acid, 2-(4-nitrophenyl) -methyl ester
DISC	Death-Inducing Signalling Complex
DMEM	Dulbecco's Modified Eagle Medium
DMSO	Dimethyl Sulfoxide
DR4	Death Receptor 4\
DTNB	5, 5"-dithio-bis-(2-nitrobenzoic acid)
FADD	Fas-Associated Death Domain
FBS	Fetal Bovine Serum
GBM	Glioblastoma Multiforme
GDP	Guanidine Diphosphate
GTP	Guanidine Triphosphate
h	Hour
IAP	Inhibitor of Apoptosis Proteins
i.p.	Intraperitoneal Injection
LMP	Lysosomal Membrane Permeabilisation
MAC	Mitochondrial Apoptosis-induced Channel
MBZ	Mebendazole
MDA	Microtubule Destabilising Agent
MDR	Multidrug Resistance

MMP	Mitochondrial Membrane Permeabilisation
MOA	Mechanism of Action
MSA	Microtubule Stabilising Agent
MSC	Mesenchymal Stem Cell
MTA	Microtubule Targeting Agent
MTT	3-(4,5-dimethylthiazol-2-yl)-2,5-diphenyltetrazolium bromide
NAC	N-acetylcysteine
NSCLC	Non-Small Cell Lung Cancer
PBS	Phosphate Buffered Saline
PI	Propidium Iodide
PS	Penicillin Streptomycin
PLA2	Phospholipase A2
ROS	Reactive Oxygen Species
SEM	Standard Error of the Mean
SMAC	Second Mitochondrial-derived Activator of Caspases
TMRE	Tetramethylrhodamine Ester
TNF	Tumour Necrosis Factor
TNFR1	TNF Receptor 1
TRADD	TNF Receptor-Associated Death Domain
v/v	Volume per Volume
XIAP	X-linked Inhibitor of Apoptosis Protein

List of Figures

Table of Contents

Chapter 1: Introduction

1.1 Cancer

Cancer is a range of diseases defined by the abnormal, uncontrolled growth of cells in a variety of tissue types. It is caused by mutations in various genes responsible for cell proliferation, differentiation, survival, DNA repair and cell death or apoptotic control. Cancer is a leading cause of morbidity and mortality in New Zealand, accounting for nearly one third of all deaths. Among the many types of cancers, lung, colorectal, prostate and breast cancers are the biggest killers in New Zealand (Ministry of Health. 2016). Each year approximately 1200 people in New Zealand die of colorectal cancer, a mortality rate similar to breast and prostate cancers combined (BPAC, 2012). Chemotherapy is one of the primary treatment methods used to combat these cancers. Traditional chemotherapy agents need to be used at high therapeutic doses, which often result in detrimental side effects for patients, reducing quality of life of the patient and also the effectiveness of the therapy. Additional issues with chemotherapy involve the development of resistance to therapeutic drugs, through a variety of possible mechanisms such as resistance-associated point mutations, altered membrane transport, activated DNA repair systems, and altered enzyme activity (Raguz *et al.*, 2008). The growing resistance to the available anticancer drugs thus drives the search for novel anticancer compounds, which may potentially be used as new chemotherapeutic agents.

1.2. Apoptosis

The term apoptosis was first used in a now-classic paper by Kerr, Wyllie, and Currie in 1972 to describe a morphologically distinct form of cell death, although certain components of the apoptosis concept had been explicitly described many years previously (Kerr *et al.*, 1972; Paweletz, 2001; Kerr, 2002). Apoptosis is commonly referred to cellular suicide and occurs normally during development and aging and acts as a homeostatic mechanism to maintain cell populations in tissues, such as in the overproduction of cells giving rise to the nervous and immune systems. This initial overproduction is

then followed by the death of those cells that fail to establish functional synaptic connections or productive antigen specificities, respectively (Nijhawan *et al.*, 2000; Opferman *et al.*, 2003). Apoptosis also occurs as a defence mechanism such as in immune reactions when cells are damaged by pathogenic or noxious agents, and is a vital component of wound healing in that it is involved in the removal of inflammatory cells and the evolution of granulation tissue into scar tissue (Greenhalgh, 1998; Norbury *et al.*, 2001). Apoptosis is morphologically classified by cell shrinkage, chromatin condensation (pyknosis), nuclear fragmentation and membrane blebbing which are indicative of the execution phase of apoptosis (Kerr *et al.*, 1972; Elmore, 2007). There are two main apoptotic pathways: the extrinsic or death receptor pathway and the intrinsic or mitochondrial pathway, both of which rely on the cleavage of pro-caspases to execute apoptosis, however an additional caspase-independent, granzyme/perforin-mediated pathway has been described (Fan *et al.*, 2003; Elmore, 2007). The caspases involved are divided into 'initiator' caspases (caspase-8 and -9) and 'effector' caspases (caspase-3, -6 and -7) which are responsible for the execution phase of apoptosis (Fesik *et al.*, 2001; Delgado *et al.*, 2013).

1.2.1 Intrinsic Pathway

In the intrinsic pathway, death signals caused by various stimuli, including heat stress and radiation, act directly or indirectly on the mitochondria to cause the release of pro-apoptotic proteins from their intermembrane space. This cell death pathway is generally thought to be controlled by Bcl-2 family proteins (involved in the regulation of cytochrome c release), inhibitor of apoptosis proteins (IAPs) (inhibition of caspases), second mitochondrial-derived activator of caspases (SMAC), and Omi (negative regulation of IAPs) (Orrenius *et al.*, 2011). The initial stages of the intrinsic pathway are regulated by the Bcl-2 family of proteins, which govern mitochondrial membrane permeability and can be either pro-apoptotic or anti-apoptotic (Cory *et al.*, 2002; Kim *et al.*, 2009). To date, a total of 25 genes have been identified in the Bcl-2 family. Some of the anti-apoptotic proteins include Bcl-2, Bcl-x, Bcl-XL, Bcl-XS, Bcl-w, BAG, and some of the pro-apoptotic proteins include Bcl-10, Bax,

Bak, Bid, Bad, Bim, Bik, and Blk (Cory *et al.*, 2002; Elmore, 2007). The pro-apoptotic members are divided into a further subclass known as the BH3-only proteins (BH3s) of which Bim, Bid, Puma and Bik are members. BH3s are responsible for activating Bax and Bak, which then go on to alter the mitochondrial outer membrane integrity, the critical step in intrinsic apoptosis which leads to cytochrome C release and subsequent caspase activation (Youle *et al.*, 2008). A few possible mechanisms for the activation of Bax and Bak by BH3s have been studied, but none have been proven definitively (Elmore, 2007).

Once activated by BH3 proteins, Bax translocates from the cytosol to the mitochondria, where it inserts into the outer membrane via its C- terminal and then proceeds to form homo-oligomers (Kim *et al.*, 2009). Bak behaves in the same way once activated, however it does not require translocation as it is an integral mitochondrial membrane protein (Dewson *et al.*, 2009). The BH3 domain-only protein t-Bid then facilitates the activation and oligomerisation of Bax and Bak to form MAC (Mitochondrial Apoptosis-Induced Channel), which can be predominantly composed of either Bax or Bak (Figure 1). The anti-apoptotic protein Bcl-2 suppresses MAC formation (Dejean *et al.*, 2006). Once formed, the MAC pore aids the release of cytochrome c, SMAC, Omi and apoptosis inducing factor (AIF) which all promote apoptosis. SMAC and OMI act by binding and inhibiting x-linked inhibitor of apoptosis protein (XIAP) which normally inhibits caspase-9, -3 and -7 (Verhagen *et al.*, 2000; Suzuki *et al.*, 2001). Cytochrome c goes on and binds to the regulatory domain of apoptotic protease activating factor-1 (Apaf-1) (Yuan *et al.*, 2010). This stimulates dATP binding to Apaf-1 leading to Apaf-1 activation (Kim *et al.*, 2005b). Once activated, Apaf-1 homo-oligomerises to form a circular structure known as the apoptosome (Figure 2). The apoptosome contains seven activated Apaf-1 molecules associated with one cytochrome c molecule each (Yuan

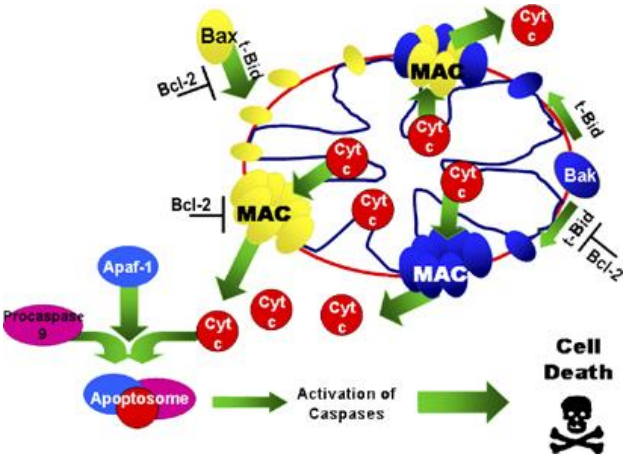

Figure 1: Diagram of MAC formation. From (Dejean et al., 2006).

et al., 2010). The assembled apoptosome recruits and activates procaspase-9, by cleaving the caspase recruitment domain (CARD) (Kim *et al.*, 2005a). This in turn activates the proteolytic caspase cascade. The now active initiator caspase, caspase-9, cleaves the procaspases giving rise to the effector caspases, caspase-3, -7 and -6, and leads to degradation of cellular components for apoptosis, resulting in the morphological changes previously described (Logue *et al.*, 2008).

1.2.2 Extrinsic Pathway

The extrinsic signalling pathways that initiate apoptosis involve transmembrane receptor-mediated interactions. These include death receptors that are members of the tumour necrosis factor (TNF) receptor gene superfamily such as TNF receptor 1 (TNFR1), FasR, TRAILR1/2 and Death Receptor 4 (DR4) (Locksley *et al.*, 2001). The sequence of events that define the extrinsic phase of apoptosis are best characterized with the FasL/FasR and TNF-α/TNFR1 models (Elmore, 2007). TNF-α is a cytokine produced mainly by activated macrophages, and is the major extrinsic mediator of apoptosis. It binds to TNF receptors and results in the binding of the adaptor protein TNF receptor-associated death domain (TRADD) with recruitment of Fas-associated death domain protein (FADD) and RIP. The binding of Fas ligand to Fas receptor also results in the binding of the adaptor protein FADD (Hsu *et al.*, 1995; Wajant, 2002). FADD then associates with procaspase-8 via dimerization of the death effector domain. At this point, a death-inducing signalling complex (DISC) is formed, resulting in the auto-catalytic activation of procaspase-8 (Kischkel *et al.*, 1995). Once caspase-8 is activated, the execution phase of apoptosis is triggered and is where the intrinsic and extrinsic pathways of apoptosis conjoin (Fig 6). Death receptor-mediated apoptosis can

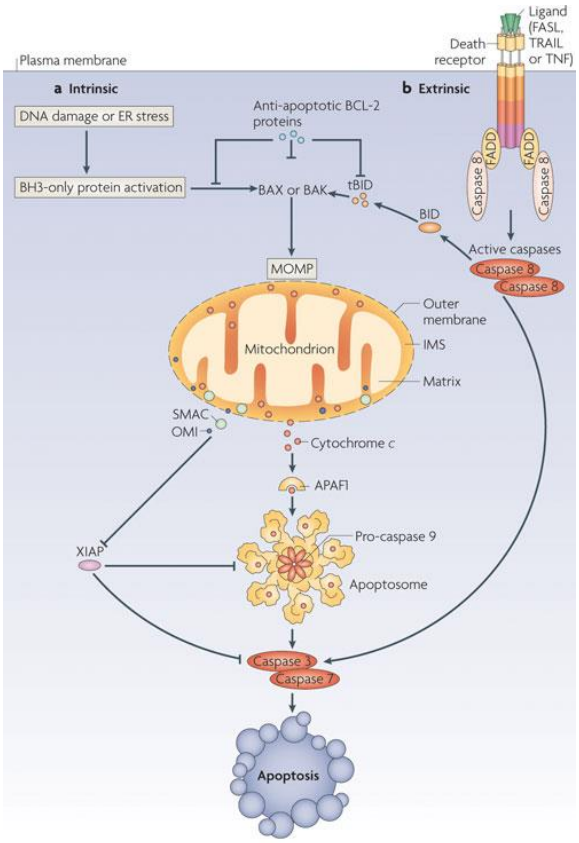

Figure 2: Diagram detailing major steps in the intrinsic and extrinsic pathways of apoptosis. From (Tait et al., 2010).

be inhibited by a protein called c-FLIP which will bind to FADD and caspase-8, rendering them ineffective (Kataoka *et al.*, 1998; Scaffidi *et al.*, 1999). Another point of potential apoptosis regulation involves a protein called Toso, which has been shown to block Fas-induced apoptosis in T cells via inhibition of caspase-8 processing (Hitoshi *et al.*, 1998).

The extrinsic and intrinsic pathways both end at the point of the execution phase, considered the final pathway of apoptosis. It is the activation of the execution caspases that begins this phase of apoptosis. Execution caspases activate cytoplasmic endonuclease, which degrades nuclear material, and proteases that degrade the nuclear and cytoskeletal proteins. Caspase-3, caspase-6, and caspase-7 function as effector or "executioner" caspases, cleaving various substrates including cytokeratins, PARP, the plasma membrane cytoskeletal protein α-fodrin, the nuclear protein NuMA and others, that ultimately cause the morphological and biochemical changes seen in apoptotic cells (Slee *et al.*, 2001; Elmore, 2007). Caspase-3 is considered to be the most important of the executioner caspases and is activated by any of the initiator caspases (caspase-8, caspase-9, or caspase-10). Caspase-3 specifically activates the endonuclease Caspase-Activated-DNase (CAD). In proliferating cells CAD is complexed with its inhibitor, ICAD. In apoptotic cells, activated caspase-3 cleaves ICAD to release CAD (Sakahira *et al.*, 1998). CAD then degrades chromosomal DNA within the nuclei and causes chromatin condensation, by cleaving DNA at internucleosomal linker sites between nucleosomes, protein-containing structures that occur in chromatin at approximately 180-bp intervals (Enari *et al.*, 1998; Sakahira *et al.*, 1998). This apoptotic characteristic can be easily detected following cell fixation, where the fragmented DNA multimers leak out of the cells, leaving a population of cells with reduced DNA content which can be quantified using DNA-binding dyes such as propidium iodide (PI) with flow cytometry (Riccardi *et al.*, 2006; Kajstura *et al.*, 2007). Caspase-3 also further induces cytoskeletal reorganization into the apoptotic microtubule network (AMN) and disintegration of the cell into apoptotic bodies during a process called "budding" (Elmore, 2007; Povea-Cabello *et al.*, 2017).

1.3 Necrosis

Necrosis is commonly thought of as an unregulated form of cell death brought on by such cellular insults as infection or toxins. Traditionally necrosis is identified morphologically by the swelling of organelles, increased cell volume, disruption of the plasma membrane and loss of intracellular contents (Rello *et al.*, 2005). It is the less desirable form of cell death as the release of cellular contents into the surrounding extracellular matrix results in an inflammatory response which leads to tissue damage (Rock *et al.*, 2008). This is contrasted with the "clean" and organised response seen with apoptosis, where cells undergoing apoptotic cell death have externalised phosphatidylserine residues, which provide an "eat me" signal to phagocytic macrophages and are then internalised and recycled, leaving no immune response (Fadok *et al.*, 1992).

1.4 Lysosomes in Cell Death

Lysosomes are small vesicular organelles that serve as cellular recycling centres and are responsible for the breakdown of a variety of biomolecules, into nutrients and building blocks for future cellular components. The lumen of lysosomes are maintained at a low pH (4.5 – 5) by membrane-bound V-ATPase proton pumps, which drive protons across the lysosomal membrane into the lumen, providing optimal conditions for the various lysosomal hydrolases to carry out their functions (Mindell, 2012). Lysosomes contain many different types of hydrolytic enzymes including cathepsins, lipases, nucleases, glycosidases, phospholipases, phosphatases and sulfatases (Boya *et al.*, 2008a).

Lysosomal membrane permeabilisation (LMP) is a potentially lethal event whereby the rupture of the lysosome causes the release of these cathepsins and other hydrolases from the lysosomal lumen into the cytosol, setting off indiscriminate degradation of cellular components. LMP can be caused by a plethora of stimuli, including pharmacological lysosomotropic compounds, reactive oxygen species and endogenous cell death effectors such as Bax (Kagedal *et al.*, 2001a; Boya *et al.*, 2003; Yu *et al.*, 2003; Kagedal *et al.*, 2005; Feldstein *et al.*, 2006; Terman *et al.*, 2006). A quantitative relationship between the amount of lysosomal rupture and the mode of cell death has been suggested to explain

the widely different morphological outcomes following LMP (Kagedal *et al.*, 2001b). With extensive lysosomal leakage caused by high intensity stresses, cytosolic acidification occurs and the cell undergoes uncontrolled necrosis. However, partial or selective LMP, caused by low stress intensity, triggers limited release of lysosomal contents to the cytoplasm followed by apoptosis or apoptotic-like death. Accordingly, low concentrations of sphingosine, an acid ceramidase-generated metabolite of ceramide with detergent-like properties at low pH, induces partial LMP and caspase-mediated apoptosis, whereas higher concentrations result in massive LMP and caspase-independent necrotic cell death (Kagedal *et al.*, 2001b). LMP-induced apoptosis is usually activated due to the leakage of lysosomal proteases such as cysteine cathepsins B and L and aspartyl cathepsin D, which remain active at neutral pH (Boya *et al.*, 2008a; Aits *et al.*, 2013b). These cathepsins then go on to initiate MOMP (mitochondrial outer membrane permeabilisation) by cleavage of pro-apoptotic proteins (Bid) or inhibiting cleavage of anti-apoptotic Bcl-2 proteins (Bcl-2, Bcl-XL and Mcl-1) (Cirman *et al.*, 2004; Droga-Mazovec *et al.*, 2008; Appelqvist *et al.*, 2012). Cytosolic cathepsins can also activate apoptotic caspases themselves, by cleaving either them or their inhibitor E3 ubiquitin-protein ligase XIAP, which can further enhance either MOMP-dependent or -independent apoptotic death (Vancompernolle *et al.*, 1998; Zhao *et al.*, 2003; Conus *et al.*, 2008; Droga-Mazovec *et al.*, 2008).

ROS contribute to LMP that is induced by a wide range of oxidative stimuli (e.g. drugs, heavy metals and ionising radiation) and conditions (e.g. ischaemia–reperfusion injury, inflammation and neurodegenerative disorders) (Kurz *et al.*, 2008a). Upon oxidative stress, excess H_2O_2 diffuses into lysosomes, where it reacts with redox-active iron, resulting in the production of hydroxyl radicals in Fenton-type reactions (Kurz *et al.*, 2008b). Hydroxyl radicals are highly reactive and can destabilise the lysosomal membrane by causing lipid peroxidation and damaging lysosomal membrane proteins. Additionally, ROS might contribute to LMP by activating lysosomal Ca^{2+} channels or altering the activity of lysosomal enzymes such as phospholipase A2 (PLA2) (Sumoza-Toledo *et al.*, 2011). Not all lysosomes are permeabilised at the same time following lethal stimuli, however the reason for this heterogeneity remains unclear. The production of intracellular ROS, which have a spatially limited

range of activity, may induce the permeabilisation of lysosomes only in those subcellular regions that are near to mitochondria, the major ROS-generating organelles. Therefore, lysosomes that are localised in the proximity of uncoupled mitochondria are more likely to suffer damage to their membranes than distant lysosomes. Furthermore, lysosomes contain the primary reservoir of chelatable iron, which accumulates upon the autophagic degradation of iron-containing proteins including mitochondrial cytochromes and ferritin. Iron-catalysed Fenton reactions, which produce highly reactive pro-oxidants, thus may damage lysosomal membranes, and go on to damage proteins and DNA.

1.5 Microtubules

The cytoskeleton of eukaryotic cells is made up of three principal components – microfilaments, intermediate filaments and microtubules. Microtubules are responsible for maintaining cell shape and motility, they provide platforms for intracellular transport and are involved in a variety of cellular processes, including the movement of organelles, secretory vesicles, and intracellular macromolecular assemblies such as the motor proteins dynein and kinesin (Vale, 2003). They also play a major role in cell division, in both mitosis and meiosis, where they are the main constituents of mitotic spindles, which are required for chromosomal separation and cytokinesis.

Microtubules are filamentous, heterodimeric proteins made up of α- and β-tubulin dimers that polymerise to form microtubules which consist of 13 linear protofilaments around a hollow lumen with an approximate diameter of 24 nm (Nogales, 2000). The protofilaments composed of head-to-tail arrays of tubulin dimers are arranged in parallel and are therefore polar structures with two distinct ends: a fast-growing plus end and a slow-growing minus end, which is important in determining the direction of movement along microtubules. They are constantly lengthening and shortening throughout all phases of the cell cycle and are in a dynamic equilibrium with the pool of free soluble tubulin heterodimers (Desai *et al.*, 1997). Tubulin dimers can bind two molecules of GTP – one for each of the of α- and β-tubulin monomers – which functions analogously to the ATP bound to actin

to regulate polymerisation of microfilaments. In particular, the GTP bound to β-tubulin (though not that bound to α-tubulin) is hydrolysed to GDP during or shortly after polymerisation. This GTP hydrolysis weakens the binding affinity of tubulin for adjacent molecules, thereby favouring depolymerisation and resulting in the dynamic behaviour of microtubules (Weisenberg *et al.*, 1976). GTP hydrolysis to GDP causes a conformational change in β-tubulin subunits and places the polymer under conformational tension while in the microtubule lattice, but is stabilised by a "GTP cap" – a layer of GTP-containing subunits – at its ends, and when this is lost, rapid depolymerisation occurs (Mitchison *et al.*, 1984; Nogales *et al.*, 2003). In microtubules, GTP hydrolysis also results in the behaviour known as dynamic instability, in which individual microtubules alternate between cycles of growth and shrinkage. Whether a microtubule grows or shrinks is determined by the rate of tubulin addition relative to the rate of GTP hydrolysis. As long as new GTP-bound tubulin molecules are added more rapidly than GTP is hydrolysed, the microtubule retains a GTP cap at its plus end and microtubule growth continues (Figure 3). However, if the rate of polymerisation slows, the GTP bound to tubulin at the plus end of the microtubule will be hydrolysed to GDP. If this occurs, the GDP-bound tubulin will dissociate, resulting in rapid depolymerisation and shrinkage of the microtubule (Desai *et al.*, 1997).

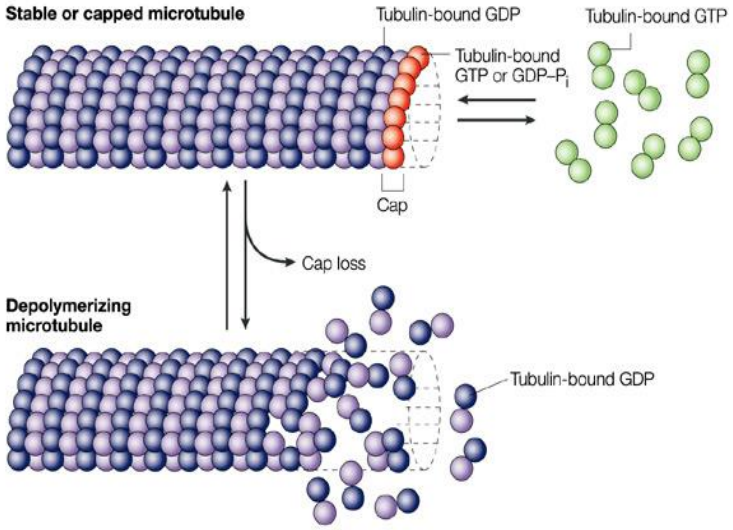

Figure 3: Microtubule assembly. From (Jordan et al., 2004)

1.5.1 Microtubule Targeting Agents

Because microtubules are implicated in such key cellular activities as mentioned previously, compounds that interfere with microtubule cytoskeleton functions have been developed as cytotoxic agents, not only for basic research experiments to demonstrate the dependence of cellular processes

on microtubules, but most importantly to combat parasites and cancer, and have been in clinical practice for decades (Jordan *et al.*, 2004). Not long after the discovery of microtubules in the late 1950s by transmission electron microscopy and identification in the early 60s (Slautterback, 1963; Brinkley, 1997), the drug colchicine – commonly used to treat gout – was identified as the first microtubule targeting agent (MTA) and found that it bound to tubulin, at what is now called the colchicine-binding site (Borisy *et al.*, 1967a; Borisy *et al.*, 1967b). Since then a variety of MTAs have been developed, with the majority being natural products or synthetic derivatives thereof that originate from natural sources such as marine sponges, plants or bacteria. These can be broadly categorised into two classes, microtubule-stabilising agents (MSAs) and microtubule-destabilising agents (MDAs). Arguably the most famous of MTAs is paclitaxel (Taxol), a gold-standard of chemotherapeutics, first isolated from the Pacific yew tree in 1971 and approved in 1992 where it became a first-line treatment for ovarian, breast, bladder, prostate and lung cancers (Wani *et al.*, 1971; Jordan *et al.*, 2004; Yang *et al.*, 2017).

MTAs have largely been successful in clinical use, due to their novel mechanism of action. Microtubules are present in both interphase cells and dividing cells; in the latter, microtubules constituting the mitotic spindle are highly dynamic and exquisitely sensitive to therapeutic inhibitors. Therefore, in rapidly dividing cells, such as with cancer, MTAs are seen to have a profound effect. However, in addition to massive success in the clinic, the application of MTAs is hampered by toxicity and the development of resistance (Kavallaris, 2010; Miltenburg *et al.*, 2014). Similar to other chemotherapeutics, MTAs such as taxanes and the vinca alkaloids are hindered by peripheral neuropathy, a potentially dose limiting side effect where these agents are suggested to damage axons and neuronal bodies. Resistance to these drugs also provides a major obstacle to overcome, as multidrug resistance (MDR) results in the loss of activity of anticancer agents against cells possessing the MDR phenotype. The two mechanisms most commonly associated with the development of MDR are the overexpression of members of the ATP-binding cassette family of transporters, of which P-

glycoprotein is the best known, and mutations in the structure of tubulin, which directly affects the binding and efficacy of most MTAs (Fojo *et al.*, 2005; Kavallaris, 2010).

To overcome these challenges additional chemotherapeutic MTAs such as epothilone (Ixempra®), eribulin (Halaven®), auristatin (Adcetris®), and maytansine (Kadcyla®) have been approved by the FDA in the past 10 years and introduced into the clinic either as classical drugs or as antibody–drug conjugates (ADCs). Numerous compounds are also under investigation which supposedly act upon microtubules through novel mechanisms, as well as an ongoing effort in repurposing already approved drugs not initially indicated for cancer treatment, such as in the case of the compounds involved in this thesis (Nathwani *et al.*, 2009; Pantziarka *et al.*, 2014; Medellin *et al.*, 2016).

1.5.2 Microtubule Stabilising and Destabilising Agents

MTAs are generally categorised into two major groups – MSAs and MDAs – based upon their effects at high concentrations on microtubule polymer mass. Colchicine-site ligands are probably the most extensively studied class of MTAs and promote the destabilisation of tubulin by binding to the colchicine site, which is a deep pocket buried in the intermediate domain of β-tubulin, located near the intra-dimer interface between the α- and β-tubulin subunits (Ravelli *et al.*, 2004; Dorléans *et al.*, 2009). In the course of microtubule assembly, tubulin dimers undergo conformational changes from a ‘curved’ conformation in their free state to a ‘straight’ structure in microtubules, which is accompanied by a contraction of the colchicine site (Akhmanova *et al.*, 2015). Thus, binding of a ligand to the colchicine site inhibits microtubule formation mainly by preventing the curved-to-straight conformational change in tubulin. Vinca-site ligands are another major class of MDAs, with the vinca alkaloids representing the oldest family of compounds that target this site. Vinblastine and vincristine have received extensive clinical evaluation and have proved effective against a variety of malignancies (Johnson *et al.*, 1963). The vinca site-targeting agents known to date comprise several chemical classes of compounds of both natural and synthetic origin, such as the highly potent cytotoxic peptides dolastatins, auristatins, and tubulysins which are used as payloads for ADCs, as

well as eribulin, diazonamides, and triazolopyrimidines (Steinmetz *et al.*, 2018). Ligands targeting the vinca site bind at the inter-dimer interface between two longitudinally aligned tubulin dimers. Microtubule destabilisation by vinca-site ligands is achieved either by introducing a molecular 'wedge' at the tip of microtubules, which prevents the curved-to-straight transition of tubulin necessary for proper incorporation into microtubules, or by sequestering tubulin dimers into ring-like oligomers that are incompatible with the straight protofilament structure in microtubules. Ligand binding further inhibits proper positioning of the catalytic α-tubulin residues that promote GTP-hydrolysis on β-tubulin (Gigant *et al.*, 2005; Ranaivoson *et al.*, 2012).

Unlike MDAs, MSAs interact with microtubules by rather enhancing polymerisation and stabilising microtubule formation. Paclitaxel, as mentioned previously, is a historic chemotherapeutic agent, and falls into this class of MTAs. Paclitaxel, along with other MSAs such as epothilone, zampanolide, discordermolide, taccalonolide and other taxanes, all show high affinity for the taxane binding region, which is located in the lumen of microtubules, whereas other more recently discovered marine MSAs such as laulimalide and peloruside A bind to a site on β-tubulin, distinct from the taxane site, located on the outside of the microtubule (Prota *et al.*, 2014; Kellogg *et al.*, 2017). Paclitaxel binds to the taxane region on GDP-bound β-tubulin in the microtubule lumen, and reduces strain from curvature by strengthening longitudinal tubulin contacts via an allosteric mechanism, leading to the favoured straightened conformation and increased intracellular concentration of the polymerised protein (Elie-Caille *et al.*, 2007; Alushin *et al.*, 2014).

1.6 Drug Repurposing

In the context of cancer, the tubulin family of proteins is recognised as the target of the tubulin-binding chemotherapeutics or MTAs, which suppress the dynamics of the mitotic spindle to cause mitotic arrest and cell death. Importantly, changes in microtubule stability and the expression of different tubulin isotypes as well as altered post-translational modifications have been reported for a range of cancers. These changes have been correlated with poor prognosis and chemotherapy

resistance in solid and haematological cancers (Kavallaris *et al.*, 2001; Sale *et al.*, 2002; Martello *et al.*, 2003; Verdier-Pinard *et al.*, 2003; Mozzetti *et al.*, 2005). However, the mechanisms underlying these observations have remained poorly understood. Emerging evidence suggests that tubulins and microtubule-associated proteins may play a role in a range of cellular stress responses, thus conferring survival advantage to cancer cells. This opens the door for new potential drug candidates that may be either novel compounds or repurposed from another indication, and may potentially act through a new mechanism of action or binding site and/or ability to avoid resistance. Currently, the method of obtaining new drugs is a long and expensive process involving drug-screening, a range of *in vitro* and pre-clinical work all the way up to clinical trials and drug approval. However, a solution to this is the Repurposing Drugs in Oncology (ReDO) Project, which seeks to repurpose well-known and well-characterised non-cancer drugs for new uses in oncology. Interest in oncological drug repurposing (also sometimes called drug repositioning) is driven by a range of concerns: productivity issues in current drug development; the need to address existing unmet patient needs; and the economic impact of existing and projected cancer incidence on health systems in both advanced and developing countries. A recent analysis has shown that the number of new drugs approved per billion US dollars spent on research and development has halved every nine years since 1950, falling around 80-fold in inflation-adjusted terms (Scannell *et al.*, 2012). The crisis is particularly acute in oncology, where the success rate for new drugs from Phase I trial to US Food and Drug Administration (FDA) approval in the period 2003 to 2011 was around 6.7%, a figure that is about half the rate for non-oncological drugs (Hay *et al.*, 2014). In contrast to the *de novo* development of new molecules, drug repurposing begins with known pharmaceutical agents with a history of clinical use. There is, therefore, a wealth of data that is accessible to the clinician and researcher, including published data on pharmacokinetics, bioavailability, toxicities (common and uncommon), established protocols, and dosing. This is data that is far in excess of what can be derived from Phase I clinical trials of new drugs, particularly for first in class drugs. In one review of drug repositioning versus *de novo* drug development, a 10–17 year development lifecycle for *de novo* development is contrasted with a 3–12

year process for repurposed drugs (Ashburn *et al.*, 2004). One of the aims of the ReDO project is to further truncate this development time. Currently, the first six drugs that are part of the ReDO project include: mebendazole, nitroglycerin, cimetidine, clarithromycin, diclofenac and itraconazole (Pantziarka *et al.*, 2014).

1.7 Study Compounds

Recently, anithiactin A, a bacterial secondary metabolite, was isolated from *Streptomyces* sp., found in a sample of intertidal mudflat sediment collected on the southern coast of the Korean peninsula (Kim *et al.*, 2014). At approximately the same time, a separate research group isolated the same compound from marine-derived *Actinomycetospora chlora* SNC-032 from a mangrove swamp in Tonga and named it thiasporine C (Fu *et al.*, 2015). Anithiactin A/thiasporine C contains a 2-phenylthiazole core which has previously been shown to be a useful scaffold in the design of compounds with anti-cancer properties (Gududuru *et al.*, 2005). In particular, methoxybenzoyl phenylthiazoles have been shown to possess low nanomolar activity with selectivity for both melanoma and prostate cancer cell lines and preliminary investigations on their mode of action suggests they operate via inhibition of tubulin polymerisation (Lu *et al.*, 2009). The Hawkins Lab group from the Department of Chemistry, University of Otago, were interested in the structure of this compound and developed an original synthesis to produce anithiactin A/thiasporine C along with a range of novel structural analogues. Although anithiactin A/thiasporine C previously displayed no significant biological activity against a range of non-small-cell lung cancer cell lines, two structural analogues 4-thiazolecarboxylic acid, 4, 5-dihydro-2-(4-nitrophenyl)-methyl ester (D1 (11c – Lamb *et al.* paper)) and 4-thiazolecarboxylic acid, 2-(4-nitrophenyl) -methyl ester (D2 (12c – Lamb *et al.* paper)), with nitro groups substituted at the 4-position on the phenyl ring (Figure 4), were observed to significantly decrease cell viability of breast and colon cancer cells over 24-72 hrs in the micromolar range (Lamb *et al.*, 2015). Following these findings, the investigation of the mechanism of action of these compounds in cancer cells became a focus of this research.

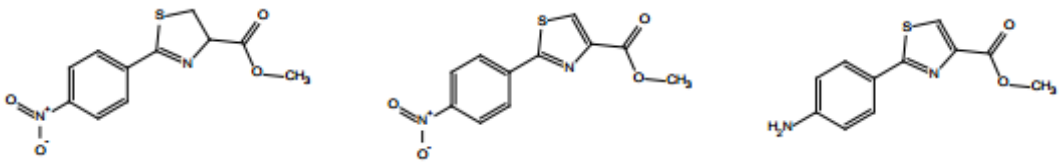

Figure 4: Chemical structures of D1, D2 and D3 (left to right).

The novel compounds D1 and D2 were the primary focus of this investigation however, over a period of months and with a newly synthesised batch of compounds, D1 and D2 lost their biological activity most likely due to degradation in solution and two new compounds were then selected for investigation based upon a similar MOA involving tubulin interaction. Mebendazole (MBZ) and albendazole (ABZ) are broad-spectrum benzimidazole anti-helminthic drugs, in the same class as thiabendazole, flubendazole, oxfendazole, and others (Figure 5). They are commonly prescribed to treat a range of parasitical worm infections, including threadworm, tapeworms, roundworms, and other nematode and trematode infections in humans and domestic animals. MBZ is available as a generic drug: common trade names have included Vermox (Janssen Pharamceutica) and Ovex (McNeil Products Ltd) in the US and Europe. MBZ is one of the primary drug candidates of the ReDO Project (Repurposing Drugs in Oncology), aiming to reposition already approved drugs with known safety profiles, for new indications in cancer treatment (Pantziarka *et al.*, 2017). MBZ has recently been shown to have promising anticancer effects in a range of pre-clinical *in vitro* and *in vivo* studies (Mukhopadhyay *et al.*, 2002; Sasaki *et al.*, 2002; Martarelli *et al.*, 2008), with albendazole also showing potent anti-tumour properties *in vivo* (Castro *et al.*, 2016). Although the anti-helminthic mechanism of action is well understood and involves the inhibition of tubulin polymerisation, leading to reduced glucose uptake in gastrointestinal cells of helminths, the mechanism of action leading to cytotoxicity in cancer cells, particularly in breast and colorectal cancers, remains to be fully explored.

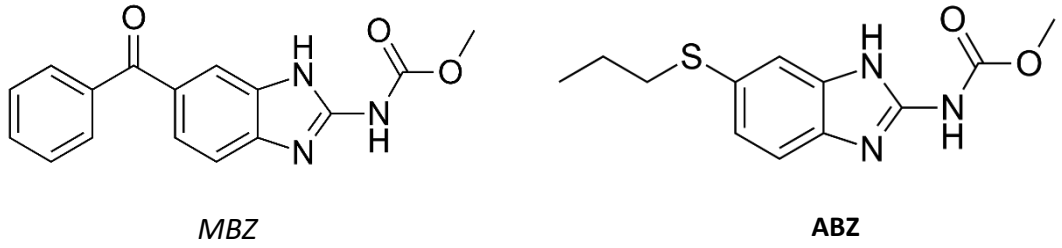

Figure 5: Chemical structures of mebendazole (MBZ) and albendazole (ABZ).

1.8 Aims and Hypothesis

The aim of this study was to identify the *in vitro* anticancer mechanism of action of the novel substituted phenylthiazoles D1 and D2, as well as the antihelminthic benzimidazoles MBZ and ABZ. This would be carried out by first screening the drugs for cytotoxicity in three cancer cell lines and one non-cancerous mesenchymal stem cell line. Then using an array of *in vitro* assays, flow cytometry and fluorescent microscopy to observe changes in apoptotic or necrotic markers and interaction with microtubules and their involvement in cell death.

It is hypothesised that MBZ and ABZ will produce cell death in cancer cells via apoptosis, and in a similar manner to which they cause death in helminths through interactions with microtubule polymerisation.

Chapter 2: Materials and Methods

2.1 Materials

Dimethyl sulfoxide (DMSO) was purchased from Scharlau (Barcelona, Spain). Fetal Bovine Serum (FBS), Penicillin Streptomycin (PS), PBS (8 g NaCl, 0.2 g KCl, 1.44 g Na2HPO4, 0.24 g KH2PO4; pH 8.0) and Trypsin (2.69 mM EDTA, 1 g/L trypsin, 0.14 M NaCl, 76.78 mM Tris HCl; pH 8.0) were purchased from Gibco (Carlsbad, CA). 3-(4,5-dimethylthiazol-2-yl)-2,5-diphenyl tetrazolium bromide (MTT), Acridine Orange (A6014), DTNB (D8130), Propidium Iodide (PI) (P4170) and RNAse A (R6513) were purchased from Sigma-Aldrich (St. Louis, MO). Annexin V-FITC (OPSB00049), Ac-DEVD-AMC (14986) and z-VAD-FMK (AB120382) were purchased from Sapphire Biosciences (NSW, Australia). Hoechst 33342 (Excitation/Emission 352 nm/461 nm) and TMRE (T669) were purchased from Life Technologies (California, USA). α-tubulin (DM1A) Mouse mAB, Acetyl-α-tubulin (Lys40) (D20G3) XP® Rabbit mAB, Anti-rabbit IgG (H+L), $F(ab')_2$ Fragment (Alexa Fluor® 488 Conjugate) and Anti-mouse IgG ($F(ab')_2$ Fragment (Alexa Fluor® 594 Conjugate) were all purchased from Cell Signaling Technology (MA, U.S.A). MCF-7 and MDA-MB-231 breast cancer cell lines were kindly gifted from Professor Rhonda Rosengren (University of Otago). HT-29 colorectal cancer cell line was purchased from ATCC (HTB-38). RCB2157 mesenchymal stem-cell line were obtained from the Riken BioResource Centre through the National Bio-resource Project of the MEXT, Japan.

2.2 Treatment Compounds

D1 (4-Thiazolecarboxylic acid, 4,5-dihydro-2-(4-nitrophenyl)-methyl ester) and D2 (4-Thiazolecarboxylic acid, 2-(4-nitrophenyl)-methyl ester) were obtained from the Department of Chemistry, University of Otago, where they were synthesised by the Hawkins' lab group and given at 10 mM dissolved in DMSO, stored in the dark at room temperature. Mebendazole ≥98% and Albendazole ≥98% were purchased from Sigma-Aldrich (St. Louis, MO) and dissolved in DMSO at

5 mM stock concentrations, stored at 4°C in the dark. Paclitaxel ≥98% was purchased from Cayman Chemical (Michigan, U.S.A) and dissolved in DMSO at a stock concentration of 1 mM also stored at 4°C in the dark. DMSO was therefore used as a vehicle control for all experiments and treated at 0.1% v/v which was deemed to be non-toxic to all cell lines.

2.3 Cell Culture

Three human cancer cell lines were used in experiments and included; MCF-7 – breast adenocarcinoma, MDA-MB-231 – triple negative breast cancer, and HT-29 – colorectal adenocarcinoma. The non-cancerous, human bone marrow mesenchymal stem cell (MSC) line RCB2157 was also used. All cell lines were cultured in Dulbecco's Modified Eagle Medium (DMEM) with 5% heat inactivated fetal bovine serum (FBS)/10% for MSCs, 100 units/mL penicillin and 100 µg/mL streptomycin, in Corning T75 flasks. Cells were incubated at 37°C in humidified conditions with 5% CO_2. At 90% confluency, cells were passaged by the addition of 2 mL trypsin solution (2.69 mM EDTA, 1 g/L trypsin, 0.14 M NaCl, 76.78 mM Tris HCl; pH 8.0) followed by a 2-min incubation at 37°C, to allow cells to detach from the bottom of the flask. Cells were rescued using fresh supplemented growth medium (10 mL). Cell-trypsin-medium solution was centrifuged at 1200 rpm for 3 min at 4°C. Supernatant was removed, and cells were resuspended in supplemented DMEM 5% FBS medium (20 mL).

2.4 MTT Assay

Cells were seeded onto 96-well plates at 5000 cells/well. The quantity of live cells present following 24 and 48hr treatment exposure was measured. Treatments with D1, D2, MBZ, ABZ, paclitaxel, DMSO (vehicle control) or untreated control were compared using the MTT assay, which assesses mitochondrial and endoplasmic reticulum dehydrogenase activity. Live cells lead to the formation of purple formazan crystals which can be further quantified (Mosmann, 1983; Sylvester, 2011). Cells were treated with 50 µM of D1 and D2 (dissolved in serum-free media), as a previous study had found

the IC_{50} of these compounds to be approximately 50-100 µM (Lamb R, 2015). DMSO was used as a vehicle control (0.1% v/v). MTT was made up to 5 mg/mL in phosphate buffered saline (PBS), added to cells at a final concentration of 0.5 mg/mL, and incubated at 37ºC for 3 hrs following treatment exposure. Media was then aspirated and the formazan crystals were then dissolved with DMSO, and the resulting absorbance was read at 560 nm using the Bio Rad Benchmark Plus microplate spectrophotometer. Three individual experiments were carried out with four replicate wells for each treatment.

2.5 Caspase-3 Assay

HT-29 cells were plated at 300,000 cells/well and treated for 24 hrs with MBZ (2 µM), ABZ (2 µM), paclitaxel (50 nM), DMSO 0.1% v/v or left untreated. Cells were harvested and frozen in -80^{O}C for a minimum of 24 hrs. Samples were then suspending in 1mL of caspase buffer (100 mM HEPES pH 7.25; 10% sucrose; 0.1% CHAPS; 0.0001% NP-40), with 5 µL of DTT (1 M) and 3.4 µL of the caspase-3 substrate Acetyl-DEVD-AMC (50 mM, dissolved in DMSO). Following 1 hr of incubation at 37^{O}C the fluorescent intensity was measured using a fluorescent spectrophotometer with 10 mm excitation and emission slits, with the excitation wavelength set at 380 nm and emission wavelength 400-600 nm.

2.6 Flow Cytometry

Flow cytometry was carried out using a BD FACSCantoII® flow cytometer and data analysed using FlowJo® VX software. Cells were seeded in 6-well plates at 300,000 cells/well in 5% FBS DMEM and left to adhere for 24 hrs. Where indicated in their respective figure legends, cells were then treated with 50 µM D1, D2, 2 µM MBZ, ABZ, 50 nM paclitaxel or DMSO (0.1% v/v), or left as untreated control. After either 24 or 48 hrs, cells were then stained with propidium iodide (PI) alone, annexin V/PI, acridine orange (AO) or tetramethylrhodamine ester (TMRE) and analysed using the appropriate filters FITC and/or PE. Three separate experiments were carried out for each stain, where each individual experiment analysed 150,000 stopping events (cells) per treatment sample.

2.6.1 Apoptosis/Necrosis

Annexin V/PI double stain is a common method used to determine if cells are viable, apoptotic, or necrotic through differences in plasma membrane integrity and permeability (Vermes *et al.*, 1995; Rieger *et al.*, 2011). The ability of PI to enter a cell is dependent upon the permeability of the membrane: PI does not stain live or early apoptotic cells due to the presence of an intact plasma membrane. In late apoptotic and necrotic cells, the integrity of the plasma and nuclear membranes decrease, allowing PI to pass through the membranes, intercalate into nucleic acids, and display red fluorescence. Annexin V cannot cross the plasma membrane either however, it binds to externalised phosphatidylserine residues, which commonly occurs during apoptosis, and displays green fluorescence due to conjugation with the dye FITC (Vermes *et al.*, 1995). Therefore, using these two stains in conjunction, it can be determined whether cells are viable, apoptotic, or necrotic, based on the intensity of the fluorescence of the stains.

Following incubation with respective treatments for 24 or 48 hrs, media from each well was collected into labelled tubes and the wells then washed with PBS. Cells were then harvested using 200 µL trypsin per well and incubated at 37^{o}C for 2 mins, where the cell suspension was then collected by adding 1 mL of 5% DMEM and centrifuged at 4^{o}C, 2000 rpm for 3 mins. The supernatant was aspirated and the pellet was washed twice in 1 mL of 4^{o}C PBS and centrifuged. Following this, the supernatant was aspirated and the cells resuspended in 100 µL of Annexin V binding buffer (HEPES; 10.0 mM (pH 7.4), NaCl; 140.0 mM, and $CaCl_2$; 2.5 mM) supplemented with 5 µL of PI (10 µg/mL) and 5 µL of annexin V conjugated to FITC. The cells were incubated for 15 min in the dark at room temperature before the cells were resuspended in an additional 300 µL of FACS binding buffer.

Compensation controls were carried out using single-stained Annexin V and single-stained PI samples. Data were analysed using FlowJo® VX software. Cellular debris was gated out using a dot-plot with FSC-A and SSC-A parameters and apoptosis/necrosis or viable cells determined using a

quadrant gate separating cell populations that are Annexin+/PI-, Annexin+/PI+, Annexin-/PI+, and Annexin-/PI- based upon fluorescence intensity, using the compensated FITC and PE channels.

2.6.2 Cell Cycle

As PI binds to DNA stoichiometrically, it can be used in conjunction with flow cytometry to determine cell cycle (Pozarowski *et al.*, 2004).

Following incubation with respective treatments for 24 or 48 hrs, media from each well was collected into labelled tubes and the wells then washed with PBS. Cells were then harvested using 200 µL trypsin per well and incubated at 37ºC for 2 mins, where the cell suspension was then collected by adding 1 mL of 5% DMEM and centrifuged at 4ºC, 2000 rpm for 3 mins. The supernatant was aspirated and the pellet was washed twice in 1 mL of 4ºC PBS and centrifuged. As PI is impermeable to intact cell membranes, cells were first fixed with 70% ethanol dropwise (500 µL) to allow permeabilisation of the plasma membrane, and left at 4ºC for a minimum of 30 mins. Cell were then washed twice in phosphate-citrate buffer (Na_2HPO_4; 192 mM, Citric acid; 4 mM (pH 7.8)) and centrifuged at 4ºC, 2000 rpm for 3 mins. Supernatant was discarded and cells then treated with 50 µL of 100 µg/mL RNAse A to remove potential binding between PI and RNA. Three hundred µL of 50 µg/mL of PI was then added to each sample. Following PI treatment, cells were analysed following flow cytometry using FlowJo® VX software, where cell cycle is measured from a histogram of PI fluorescence using the PE channel. Cellular debris was initially gated out using a dot-plot with FSC-A and SSC-A parameters. Using a linear scale, the G2 peak should be double the intensity of the G1 peak due to double the amount of DNA present in those cells (2n). From here gates were applied manually or through the separate cell cycle function where available. Cells were not synchronised before treatment

2.6.3 Mitochondrial Membrane Integrity

Mitochondrial dysfunction has been shown to be part of the induction of apoptosis and has been suggested to be central to the apoptotic pathway (Ly *et al.*, 2003). The opening of the mitochondrial

permeability transition pore has been demonstrated to induce depolarisation of the transmembrane potential (Δψm), release of apoptogenic factors such as cytochrome c and loss of oxidative phosphorylation. In some apoptotic systems, loss of Δψm can be an early event in the apoptotic process. TMRE is a fluorescent dye that is readily sequestered by active mitochondria, allowing for flow cytometric or imaging analysis to assess for apoptosis or mitochondrial depolarisation (Crowley *et al.,* 2016a). Non-apoptotic or cells with polarised mitochondria will fluoresce red while apoptotic or cells with depolarised mitochondria will have diminished levels of red fluorescence, which can be quantified.

Following incubation with respective treatments for 24 or 48 hrs, media from each well was collected into labelled tubes and the wells then washed with PBS. Cells were then harvested using trypsin and incubation at 37^{o}C for 2 mins, when the cell suspension was then collected by adding 5% DMEM and centrifuged at 4^{o}C, 2000 rpm for 3 mins. Cells were resuspended in 5% DMEM and TMRE was added to give a final concentration of 40 nM, followed by incubation at 37^{o}C for 10 mins. Cells were then centrifuged and washed in PBS then resuspended in 5% DMEM.

Following flow cytometry, using FlowJo® VX, cellular debris was initially gated out using a dot-plot with FSC-A and SSC-A parameters. Then, using a histogram vs PE on a logarithmic scale and a gate to the left of the high-intensity peak seen in untreated control samples, the percentage of cells with low-intensity fluorescence, indicating compromised mitochondria, was found (Figure 6).

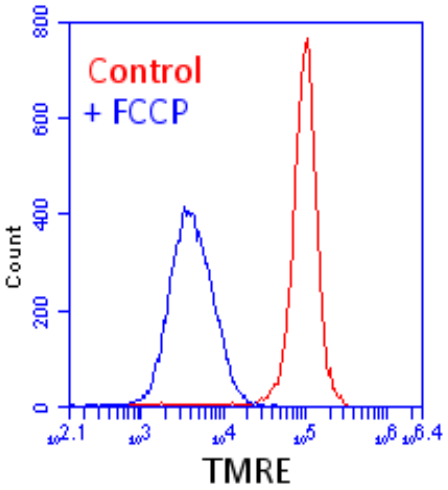

Figure 6: An example of a histogram measuring depolarised/permeabilised mitochondria. Flow cytometry histogram of Jurkat cells stained with TMRE with (blue) or without (red) treatment with 100µM FCCP, an ionophore uncoupler of oxidative phosphorylation. Treating cells with FCCP eliminates mitochondrial membrane potential and TMRE staining. (From Abcam® TMRE-Mitochondrial Membrane Potential Assay Kit ab113852 product datasheet)

2.6.4 Lysosome Membrane Integrity

Lysosomal membrane permeabilisation (LMP) and the consequent leakage of the lysosomal content into the cytosol leads to so-called "lysosomal cell death" (Boya *et al.*, 2008b; Aits *et al.*, 2013a; Repnik *et al.*, 2014). This form of cell death is mainly carried out by the lysosomal cathepsin proteases and can have necrotic, apoptotic or apoptosis-like features depending on the extent of the leakage and the cellular context. LMP can be induced by a wide range of pharmacological agents and endogenous factors, such as reactive oxygen species and cell death effectors such as Bax (Boya *et al.*, 2008b). Acridine orange (AO) is a lipophilic amine that readily diffuses into cells. Inside the cell it enters the acidic lysosomal compartment where it is protonated and sequestered, shifting its emission spectrum towards a longer wavelength that is red (Moriyama *et al.*, 1982). Once inside the lysosomes, the metachromatic AO sensitises the lysosomal membrane to photo-oxidation by blue light (Brunk *et al.*, 1997). Upon light-induced loss of the lysosomal pH gradient and subsequent leakage of AO into the cytosol, the emission spectrum of AO shifts from red to green, where there is a decrease in intensity of red fluorescence which can be quantified, much like TMRE and the depolarisation of the mitochondrial membrane potential.

Following incubation with respective treatments for 24 or 48 hrs. AO was added to each well giving a final concentration of 4 µg/mL and incubated in the dark at 37ºC for 15 mins. Supernatants were then collected and cells washed with PBS before being harvested with trypsin. Cells and supernatants were centrifuged at 4ºC, 2000 rpm for 3 mins, washed with PBS then resuspended in 5% DMEM. Following flow cytometry, using FlowJo® VX, cellular debris was initially gated out using a dot-plot with FSC-A and SSC-A parameters. Then, using a histogram vs PE or vs FITC on a logarithmic scale and a gate to the left of the high-intensity peak seen in untreated control samples, the percentage of cells with low-intensity fluorescence, indicating compromised lysosomal or outer membrane were measured, similar to the TMRE stain (Figure 6).

2.7 DTNB Assay (Free Sulfhydryl Content)

Free sulfhydryl content following treatment was assessed using the DTNB (5, 5"-dithio-bis-(2-nitrobenzoic acid)) assay. DTNB is a versatile, water-soluble compound that can quantify free sulfhydryl groups in solution by reacting with them and producing a measurable yellow-coloured product (Ellman, 1959). Using the molar extinction coefficient of 14,150 M^{-1} cm^{-1} and the absorbance measured by a spectrophotometer, the free sulfhydryl content can be calculated.

Cells were plated in 6-well plates at 300,000 cells/well and left to adhere for 24 hrs. Cells were then treated with DMSO 0.1% v/v, D2 50 µM, MBZ 2 µM, ABZ 2 µM, paclitaxel 50 nM or were untreated and were incubated at 37ºC for 48 hrs. Following treatment, media from each well was collected into labelled tubes and the wells then washed with PBS. Cells were then harvested using 200 µL trypsin per well and incubated at 37ºC for 2 mins, where the cell suspension was then collected by adding 1 mL of 5% DMEM and centrifuged at 4ºC, 2000 rpm for 3 mins and washed with PBS twice. Cells were resuspended in 1 mL of PBS and sonicated for 2 mins. Five hundred µL of 10% SDS and DTNB at a final concentration of 30 µM were added and incubated at room temperature for 30 mins. Samples were then placed in 1 mL cuvettes and absorbance measured at 412 nm using a spectrophotometer.

2.8 Fluorescent Microscopy

Cells were plated in 8-well microscope slides at approximately 25,000 cells per well. They were treated with D2 (50 µM), MBZ (2 µM), ABZ (2 µM), paclitaxel (50 nM), DMSO (0.1% v/v) and untreated control for 48 hrs. Following treatment, the media from the wells were aspirated and cells fixed with 4% paraformaldehyde (pH 7.2) and washed three times with PBS. They were then stained with the DNA-selective dye Hoechst 33342 at 10 µg/mL to analyse the nuclear morphology of the cells, as nuclear/chromatin condensation (pyknosis) and blebbing are indicative of apoptosis. Following washing with distilled water, the slides were dried and Prolong Gold was placed on the slides along with coverslips. The cells were then analysed using the Nikon AI-R inverted fluorescent microscope with Nikon Intensilight C-HGFI mercury lamp (Olympus, Japan) at 20x magnification.

For tubulin staining, the steps above were repeated with MBZ (2 µM), ABZ (2 µM), paclitaxel (50 nM), DMSO (0.1% v/v) treatments for 8 hrs. Following fixation cells were first blocked for 60 mins using blocking buffer (1X PBS; 5% BSA; 0.3% Triton X-100). Then stained with a primary antibody solution containing (1X PBS; 5% BSA; 0.3% Triton X-100; anti-α-tubulin – 1;16,000; anti-acetyl-α-tubulin – 1:800) overnight at 4^{o}C. Following washing cells were then incubated with respective secondary anti-mouse and anti-rabbit antibodies, in conjunction with Hoechst 33342 at 10 µg/mL for 1 hr at room temperature in the dark. Coverslips were placed along with Prolog Gold antifade reagent and left to cure overnight. Photos were then taken using the Nikon AI-R inverted fluorescent microscope with Nikon Intensilight C-HGFI mercury lamp (Olympus, Japan) at 20x magnification using consistent exposure. Images were then analysed using Fiji Image J software.

2.9 Statistical Analyses

All results were analysed using GraphPad Prism® 6.0 software. Cell viability experiments contained four replicates for each treatment, however this is a form of pseudoreplication (Lazic, 2010) and only represents n=1, therefore a minimum of three separate experiment each with four pseudoreplicates were carried out to give n=3. Flow cytometry experiments were similar in that each sample was

measured at least three times for each treatment, again pseudoreplication, however, three separate experiments were carried out to give n=3. All data from both cell viability, flow cytometry and DTNB assay experiments were analysed using one-way analysis of variance (ANOVA). ANOVAs were used as there were more than two treatment groups in each experiment, where the samples were independent and only one variable was measured. Dunnett's post hoc tests were used in conjunction to compare treatment groups and untreated control where statistical significance was determined at $p<0.05$.

Chapter 3: D1 and D2 Results

3.1 Caspase Inhibition

To determine whether caspases played a role in the mechanism of cell death induced by these substituted phenylthiazoles, the pan-caspase inhibitor z-VAD-FMK was employed, where it was used to see if it had any change on cell viability following drug treatment. In MCF-7 cells, the caspase inhibitor had no effect on cell viability alone at 0.1 and 1.0μM compared to DMSO control, D2 treatment caused a 65% decrease in cell viability (35.6 ± 2.8% vs 100 ± 10.4%, $p < 0.0001$) (Figure 7), which could not be rescued by the caspase inhibitor at either 0.1 or 1.0μM (33.1 ± 0.3%, 31.9 ± 0.5% respectively) ($p < 0.0001$). Paclitaxel 100nM also decreased cell viability by 26% ($p = 0.012$). In the triple-negative breast cancer cell line MDA-MB-231, the caspase inhibitor had no effect on cell viability at 1.0μM, whereas at 0.1 μM it led to a small (6%) but statistically significant ($p = 0.002$) increase in cell viability compared to DMSO control. D2 and paclitaxel treatments led to significant decreases in cell viability (42.9 ± 0.7%, 45.2 ± 0.5% respectively) ($p < 0.0001$). The caspase inhibitor again showed no difference in cell viability in conjunction with D2 compared to D2 alone, at both concentrations, and gave similar cell viability results compared to DMSO control (43.1 ± 0.5% (0.1 μM); 44.9 ± 0.8%, $p < 0.0001$) (Figure 7). In HT-29 cells, the caspase inhibitor alone at both 0.1 and 1.0 μM caused statistically significant decreases in cell viability compared to DMSO control (92.6 ± 1.7%, 87.2 ± 1.6% vs 100.0 ± 1.1% respectively, $p < 0.0001$). Similar to MCF-7 and MDA-MB-231 the caspase inhibitor at both 0.1 and 1.0 μM could not rescue the decrease in cell viability seen in D2 treatment alone, when treated together (D2 + CI 0.1 μM – 35.9 ± 0.4%; D2 + CI 1.0 μM – 35.8 ±0.4%; D2 alone – 38.8 ± 0.4%, $p < 0.0001$) (Figure 7).

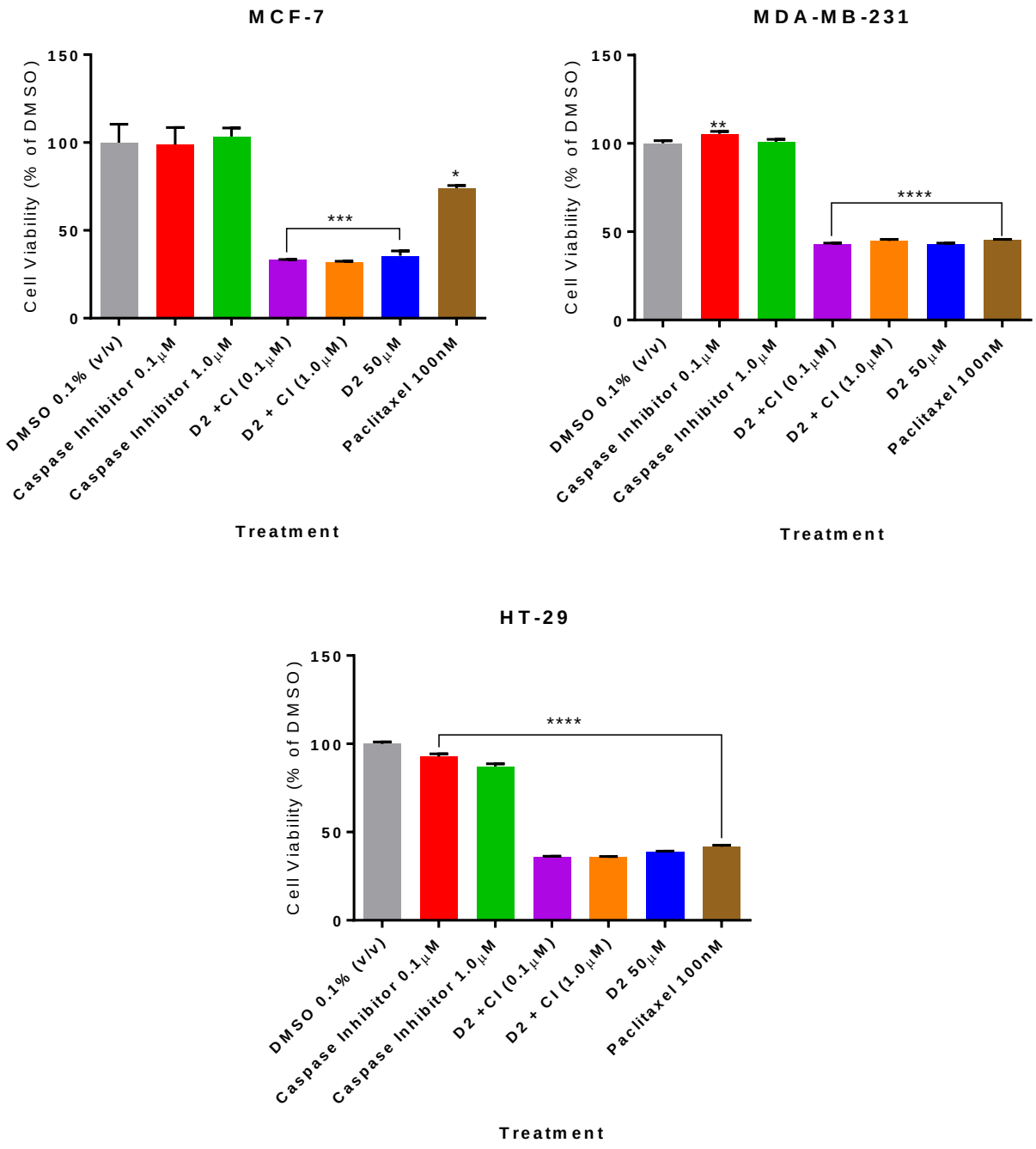

Figure 7. Viability of MCF-7, MDA-MB-231 and HT-29 cells following treatment with the pan-caspase inhibitor (CI) z-VAD-FMK (0.1, 1.0μM), D2 (50μM), D2 + CI and paclitaxel 100 nM compared to DMSO 0.1% v/v vehicle control, determined using MTT assays. Cells were drug treated for 48hr, with z-VAD-FMK exposed 30 mins prior to drug treatment. Data represents means ± SEM of three separate experiments performed in quadruplicate (n = 3). Data was analysed using One-way ANOVAs with Dunnett's post-hoc test comparing to DMSO control, where $p < 0.05$ was considered statistically significant. *p<0.05, **p<0.01, ***p<0.001, ****p<0.0001

3.2 Cell Cycle

Cell cycle analysis was carried out in cells treated with D1, D2, DMSO or untreated for 48 hrs using propidium iodide staining and flow cytometry to quantify DNA content. There were no significant changes in percentages of cells in each cell cycle stage following treatments with either DMSO, D1 or D2 compared to control ($p > 0.05$) in MCF-7 cells (Figure 8).

In MDA-MB-231 cells the only statistically significant difference observed was an approximate 5% decrease in the percentage of cells in the G1 phase following D1 treatment compared to control (52.85% vs 48.04%, $p = 0.016$) (Figure 8).

HT-29 cells also showed statistically significant changes compared to control following D1 treatment. Percentage of cells in the G1 stage were increased by 7.5% (51.83% vs 59.42%, $p = 0.002$), which subsequently led to a 5.6% decrease in the percentage of cells in the S phase (24.01% vs 18.40%, $p = 0.026$) (Figure 8).

3.3 Mitochondrial Membrane Potential ($\Delta\Psi m$)

Cells were treated with D1, D2, DMSO or untreated control for 48hrs and their mitochondrial membrane potential ($\Delta\psi m$) assessed using flow cytometry with the fluorescent dye TMRE, which is sequestered by active mitochondria producing high fluorescence intensity. All three cell lines displayed no change in percentage of cells with depolarised mitochondrial membrane potential compared to control (MCF-7 – 2.00 ± 0.17 %; MDA-MB-231 – 9.01 ± 2.43%; HT-29 – 5.70 ± 1.73%) following treatments with DMSO 0.1%, D1 50µM or D2 50µM ($p > 0.05$) (Figure 9)

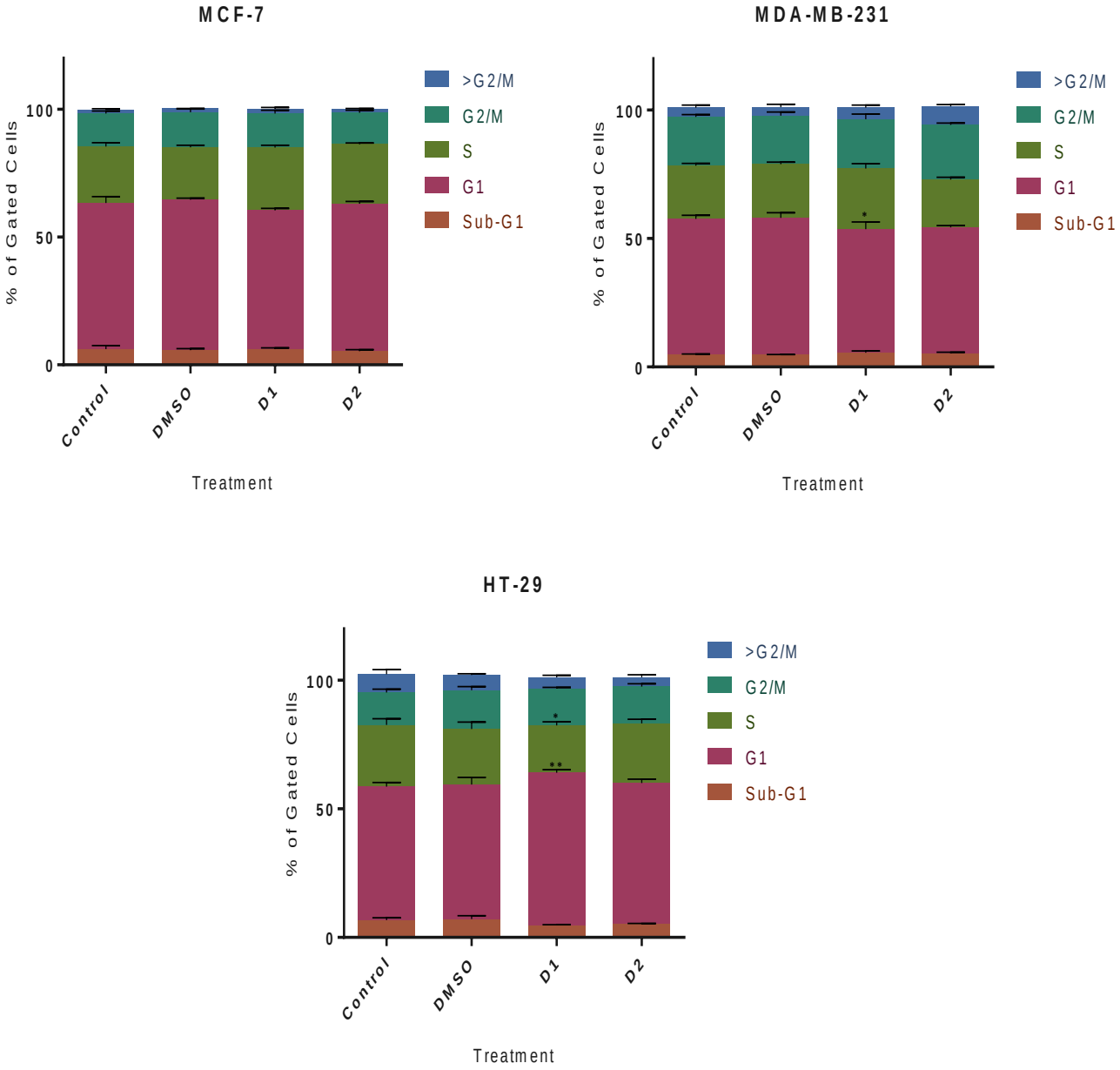

Figure 8*:* Cell cycle analysis of MCF-7, MDA-MB-231 and HT-29 cells following 48hr treatment with D1 (50µM), D2 (50µM), DMSO (0.1% v/v) or untreated control. DNA content was assessed using PI staining. Data represent mean ± SEM of the percentage of cells at each cell cycle stage (Sub-G1; G1; S; G2/M; >G2/M). Three independent experiments were conducted in triplicate with a minimum of 10,000 stopping events for each sample. Data were analysed using a Two-way ANOVA with Dunnett's post-hoc test comparing to untreated control, where $p < 0.05$ was considered statistically significant. *$p < 0.05$, **$p < 0.01$

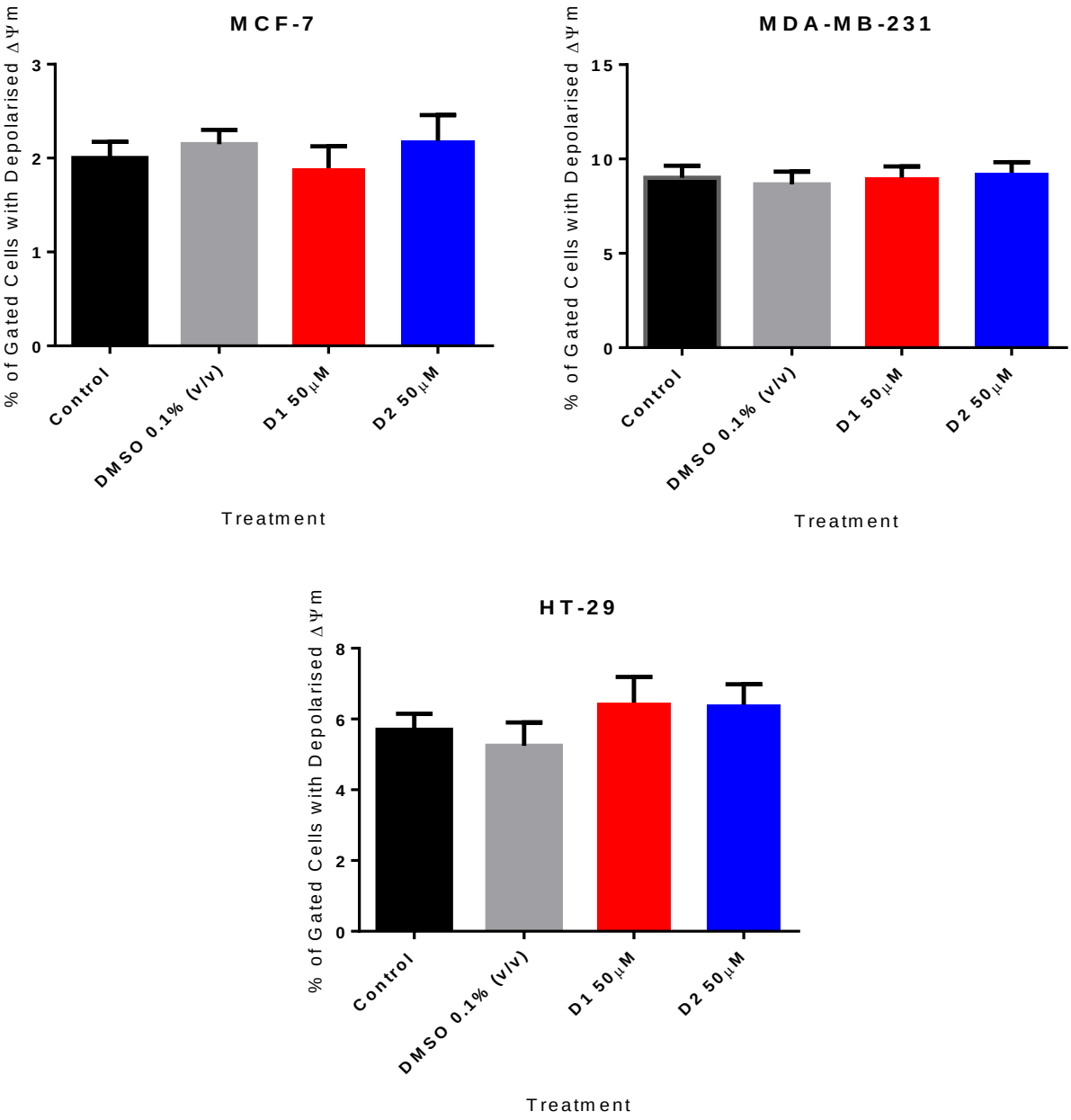

Figure 9: Percentage of cells (MCF-7, MDA-MB-231, HT-29) with depolarised mitochondrial membrane potential (Ψ) determined by TMRE fluorescence intensity, following 48hr treatment with D1 (50µM), D2 (50µM), DMSO (0.1% v/v) or untreated control. Data represent means ± SEM, of three separate experiments (n = 3) performed in triplicate, where each sample includes a minimum of 10,000 stopping events. One-way ANOVAs were performed, with Dunnett's post-hoc test where $p < 0.05$ was considered as statistically significant.

3.4 Lysosomal Membrane Permeabilisation

To determine whether lysosomal membrane permeabilisation was involved in the mechanism of action of D1 and D2, cells were treated for 48hrs with D1 and D2 (50µM) then exposed to acridine orange and using flow cytometry the percentage of cells with permeabilised lysosome membranes were measured. In MCF-7 and HT-29 cells there were no statistically significant differences in the percentage of cell with lysosomal membrane permeabilisation following treatments with either DMSO, D1 or D2 compared to control ($p > 0.05$) (Figure 10.). Whereas the MDA-MB-231 cell line displayed a 0.8% decrease following treatment with D2 compared to control ($1.94 \pm 0.16\%$ vs $1.14 \pm 0.10\%$, $p = 0.012$) (Figure 10.).

3.5 Nuclear Staining

Cells were stained with Hoechst 33342 following drug treatment and nuclear morphology was examined using fluorescent microscopy. MCF-7 cells showed no obvious changes in nuclear morphology following treatment with DMSO and D2 compared to untreated control, whereas D1 treatment displayed some cells with shrinking nuclei (pyknosis) with a greater fluorescent intensity (Figure 11). MDA-MB-231 cells provided difficulty in determining whether drug treatment had any effect on nuclear morphology as in all three treatment groups as well in untreated control there were cells with variable nuclei shape, size and fluorescent intensity. Therefore, it could not be concluded that D1 or D2 treatment had any effect on nuclei morphology. In HT-29 cells, D1, D2 and DMSO treatment were observed to have no change on nuclear morphology compared to untreated control (Figure 11).

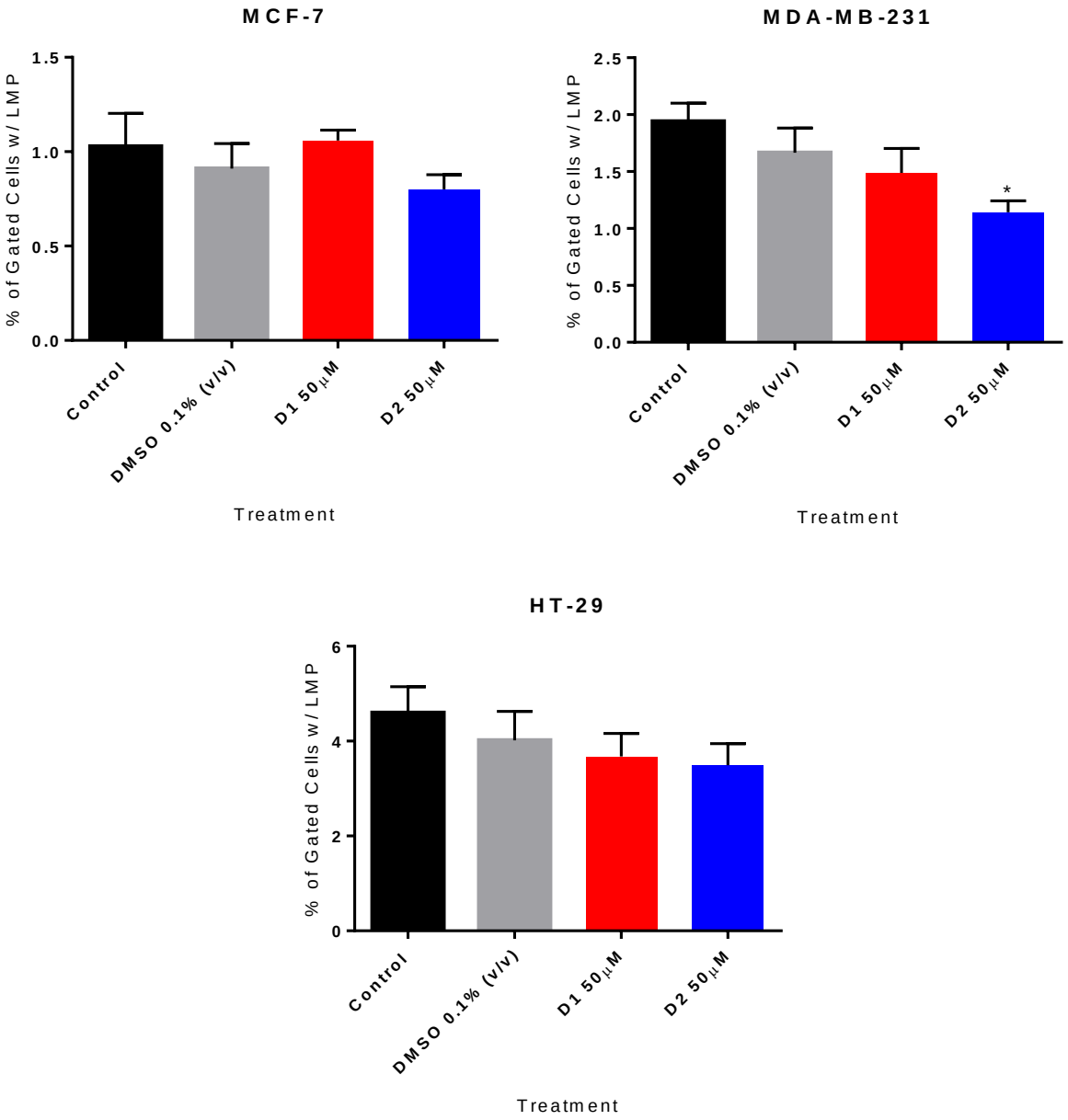

Figure 10. Percentage of cells (MCF-7, MDA-MB-231, HT-29) with lysosomal membrane permeabilisation (LMP) determined by acridine orange fluorescence intensity using flow cytometry, following 48hr treatment with D1 (50µM), D2 (50µM), DMSO (0.1% v/v) or untreated control. Data represent means ± SEM, of three separate experiments (n = 3) performed in triplicate, where each sample includes a minimum of 10,000 stopping events. One-way ANOVAs were performed, with Dunnett's post-hoc test comparing to untreated control, where $p < 0.05$ was considered as statistically significant.

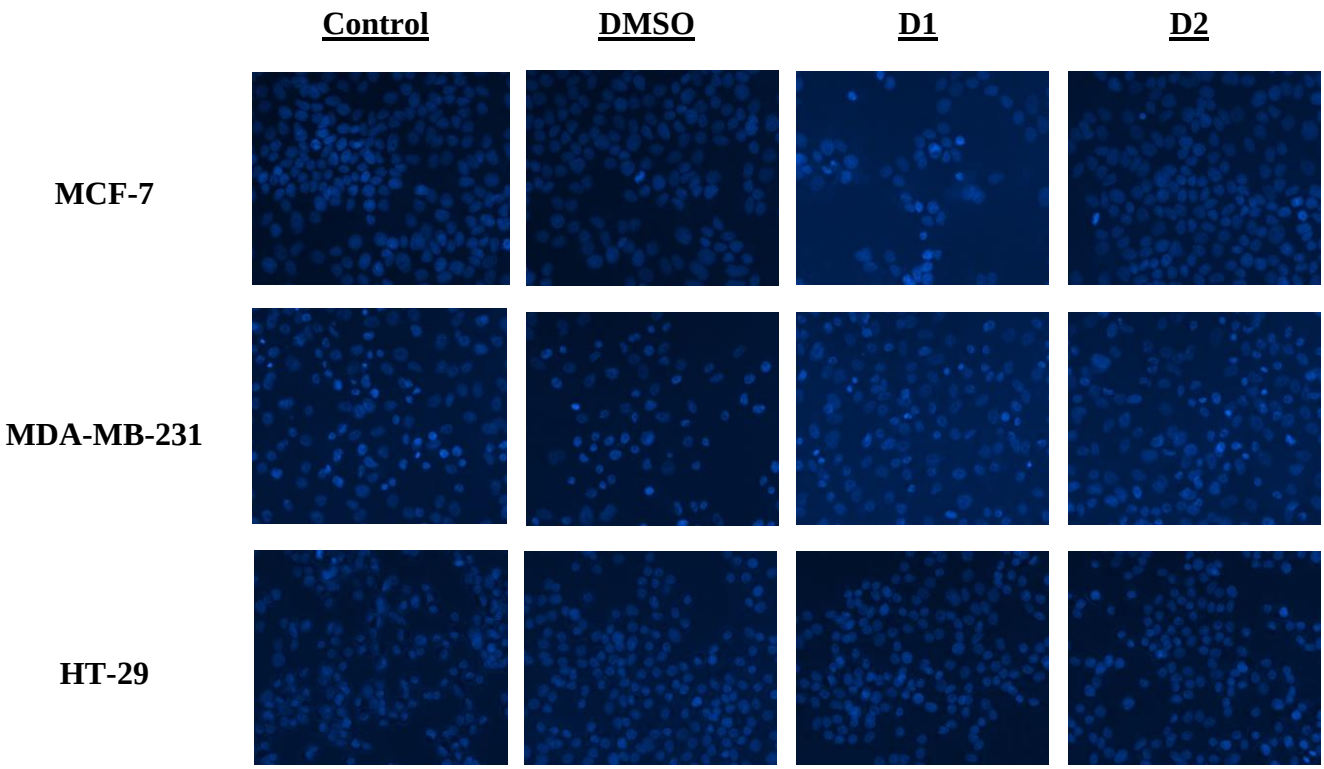

Figure 11. Nuclear morphology of MCF-7, MDA-MB-231 and HT-29 cells stained with Hoechst 33342 and imaged using fluorescence microscopy. Cells were plated in 8-well microscope slides at approximately 25,000 cells per well. They were treated with D1, D2 (80 µM), DMSO 0.1% v/v and untreated control for 48 hrs.

3.6 D1 and D2 Cell Viability

D1 and D2 cell viability was determined in three cancer cell lines and one non-transformed cell line using the MTT assay, where live cells were quantified by functioning mitochondrial oxidoreductase enzymes to reduce MTT to measurable formazan crystals. The IC_{50} values for D1 and D2 after 24hr exposure were; 536.7 µM and 66.3 µM for MCF-7; 393.8 µM and 137.3 µM for MDA-MB-231; 770.1 µM and 155.0 µM for HT-29; 603.8 µM and 1223 µM for RCB2157 respectively (Figure 12).

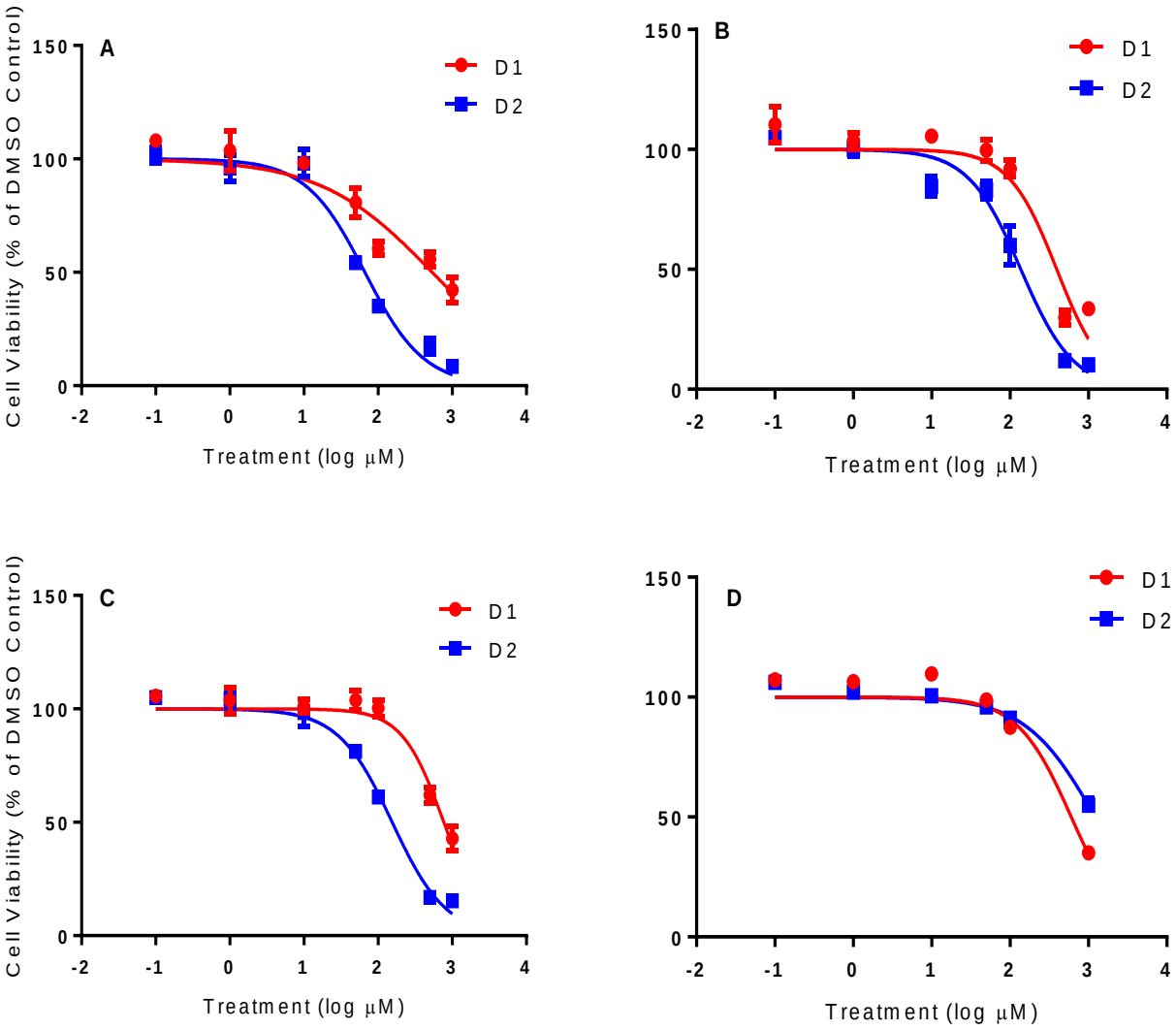

Figure 12. IC_{50} curves of the human cancer cell lines MCF-7 (A), MDA-MB-231 (B), HT-29 (C) and the mesenchymal stem cell line RCB2157 (D) following 24 hr treatment with D1 and D2 (0.1-1000 µM) compared to DMSO control, determined using MTT assays. IC_{50} calculated using non-linear regression. Experiments were carried out in sextuplicate (n = 1).

Chapter 4: MBZ and ABZ Results

4.1 MBZ and ABZ Cell Viability

The IC_{50} values of MBZ and ABZ over 24 hrs were determined in the three cancer cell lines MCF-7, MDA-MB-231 and HT-29 and the non-transformed mesenchymal stem-cell line RCB2157 using MTT cell viability assays. Both MBZ and ABZ were observed to be the most potent in the HT-29 cell line, giving IC_{50} values of 1.3 ± 0.1 µM and 1.4 ± 0.1µM respectively (Figure 13). In MCF-7 cells, MBZ had an IC_{50} of 9.5 ± 1.1 µM and ABZ 50.2 ± 1.1 µM. Both MBZ and ABZ were the least potent in MDA-MB-231 cells of the cancer cell lines, with 31.2 ± 1.2 µM and 928.0 ± 1.6 µM respectively

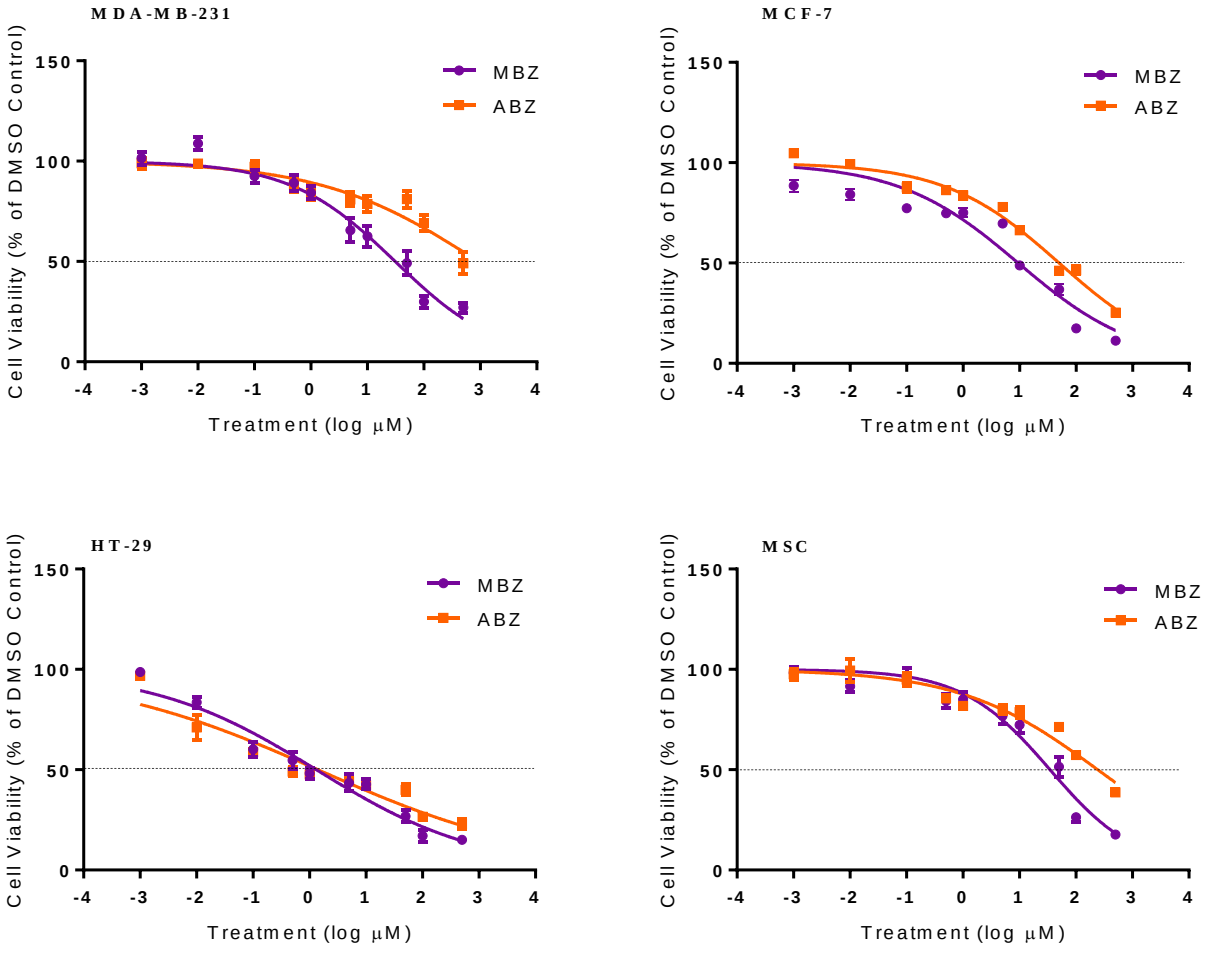

Figure 13. IC_{50} curves of MCF-7, MDA-MB-231, HT-29 and RCB2157 cell lines following treatment with MBZ and ABZ (1 nM – 500 µM) for 24 hrs, compared to DMSO control, determined using MTT assays. IC_{50} values and line-of-best-fit calculated using non-linear regression. Each data point represents means ± SEM of three independent experiments (n = 3) carried out in quadruplicate.

and in RCB2157 mesenchymal stem cells, with 34.8 ± 0.1 µM and 243.1 ± 0.1 µM respectively (Figure 13).

The IC_{50} curves following 48 hr treatment with MBZ and ABZ are shown in Figure 14. HT-29 again was the cell line with the lowest IC_{50} values for both MBZ and ABZ; 0.11 ± 0.07 µM and 0.69 ± 0.42 µM respectively. MCF-7 cells gave values of 1.1 ± 1.3 µM for MBZ and 8.1 ± 1.2 µM for ABZ. Of the cancer cells, MBZ and ABZ were again least potent in the MDA-MB-231 cell line with values of 15.0 ± 0.1 µM and 53.3 ± 0.2 µM. The highest IC_{50} values were seen in the mesenchymal stem-cell line RCB2157, with 19.9 ± 0.1 µM for MBZ and 129.5 ± 0.1 µM for ABZ, suggesting that these drugs may be selective for cancer cells.

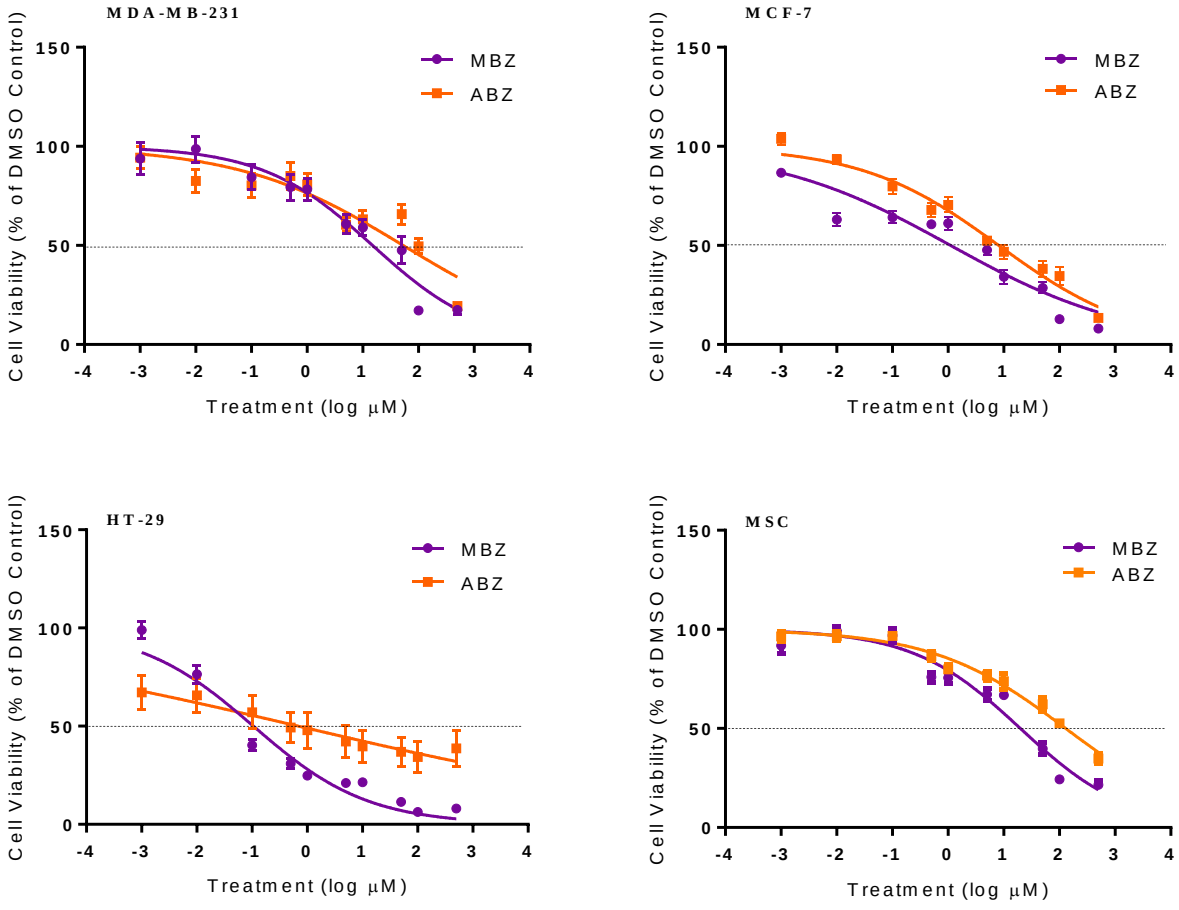

Figure 14 IC_{50} curves of MCF-7, MDA-MB-231, HT-29 and RCB2157 cell lines following treatment with MBZ and ABZ (1 nM – 500 µM) for 48 hrs, compared to DMSO control, determined using

MTT assays. IC_{50} values and line-of-best-fit calculated using non-linear regression. Each data point represents means ± SEM of three independent experiments (n = 3) carried out in quadruplicate.

4.2 Caspase-3 Activity

Caspase activity was measured in HT-29 cells following treatment using the fluorescent intensity of the cleaved substrate Ac-DEVD-AMC as shown in Figure 15. Both untreated control and DMSO vehicle control caused a peak fluorescent intensity of approximately 150 F.U (fluorescence units) at 440 nm. ABZ treatment and MBZ treatment both increased fluorescent intensities to approx. 200 and 250 F.U respectively. Paclitaxel treatment caused the greatest increase in fluorescent intensity, up to approx. 450 F.U, which is not surprising as paclitaxel is a classical apoptosis inducer and activates caspase-3. Both MBA and ABZ, and paclitaxel all caused significant increases in fluorescent intensity compared to control, however no statistical analysis was possible as only one replicate was obtained.

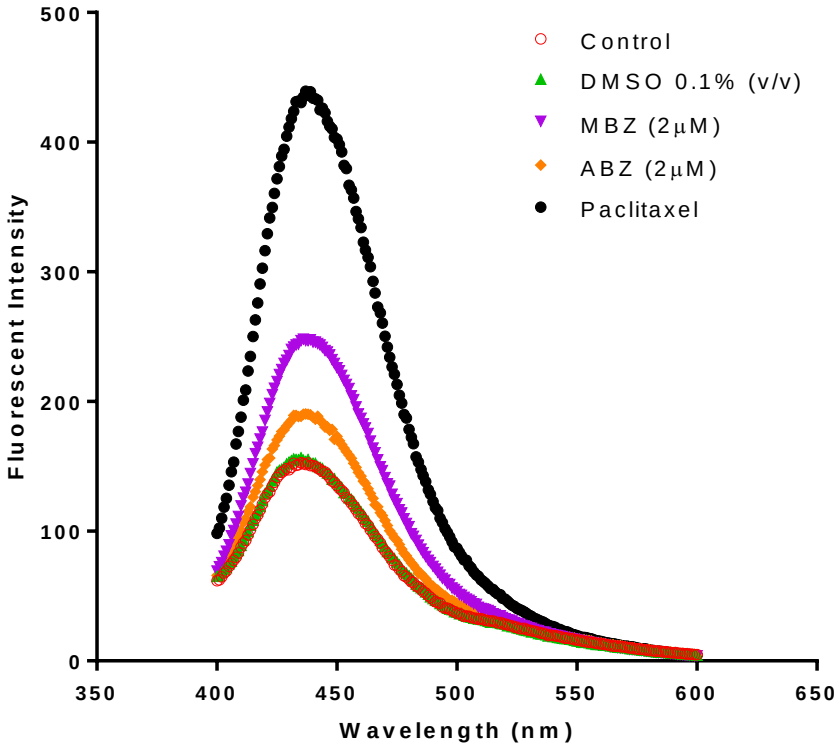

Figure 15: MBZ, ABZ and Paclitaxel cause increased caspase-3 activity. Caspase-3 activity measured by fluorescent intensity of HT-29 cells treated for 24hrs with MBZ (2µM), ABZ (2µM), paclitaxel (50nM), DMSO 0.1% v/v or left as untreated control using the caspase-3 specific substrate Ac-DEVD-AMC. Excitation wavelength – 380 nm; Emission wavelength – 400-440 nm. n = 1

4.3 Apoptosis vs Necrosis

Following both 24 and 48 hr treatments, cells were double-stained with Annexin-V to identify external phosphatidylserine residues, markers of early apoptosis, and PI to detect cell membrane permeabilisation, a sign of necrosis, in order to suggest which route of cell death MBZ and ABZ cause. Following 24hr treatment, MBZ and ABZ caused approximate 25% decreases in the percentage of viable cells (negative for both Annexin V and PI) compared to control ($P < 0.0001$), similar to that of the positive control paclitaxel (Figure 16). MBZ and ABZ caused a significant 20% increase in the percentage of cells with phosphatidylserine exposure – a sign of early apoptosis – with 22.83% of MBZ treated cells positive for Annexin V only and 24.17% of ABZ treated cells, whereas only 3.37% of control cells were positive ($P < 0.0001$). Paclitaxel also showed a large increase of 20.72% of cells with phosphatidylserine exposure. Paclitaxel, MBZ and ABZ all showed small but significant increases in cells positive for both Annexin V and PI - an indicator of secondary/late apoptosis – MBZ; 5.78%, ABZ; 5.99%, paclitaxel; 7.94% vs Control; 2.12% ($P < 0.0001$). Cells positive for PI only due to membrane permeabilisation, an indicator of necrosis, were increased in MBZ and ABZ treatments only, compared to control, 3.58% and 3.48% vs 0.54% respectively. DMSO vehicle control produced no significant changes in any cell state compared to control.

Forty-eight-hour treatments produced similar results to that of 24hr treatments, with significant reduction of the percentage of viable cells observed with MBZ, ABZ and paclitaxel compared to control (Figure 17). MBZ; 75.67%, ABZ; 74.97% and paclitaxel 74.54% vs control; 86.39% ($P < 0.0001$). Interestingly, DMSO treatment resulted in a small but significant increase in the percentage of viable cells – 88.87% ($P < 0.05$). The percentage of cells positive for Annexin V only were also significantly increased following MBZ, ABZ and paclitaxel treatments compared to control. MBZ; 19.50%, ABZ 19.53% and paclitaxel; 19.81% vs control; 4.00% ($P < 0.0001$). There were no significant differences in the percentage of cells positive for both Annexin V and PI following any treatment compared to control ($P > 0.05$). Surprisingly, MBZ and paclitaxel treatment resulted in small but statistically significant decreases in the percentage of cells positive for PI only, an indicator

of necrosis, MBZ; 0.80% and paclitaxel 0.72% vs control 3.52% ($P < 0.05$). Other than a 2.5% increase in the percentage of viable cells, DMSO again had no significant change on the percentage of cells stained with either Annexin V, PI or both, compared to control.

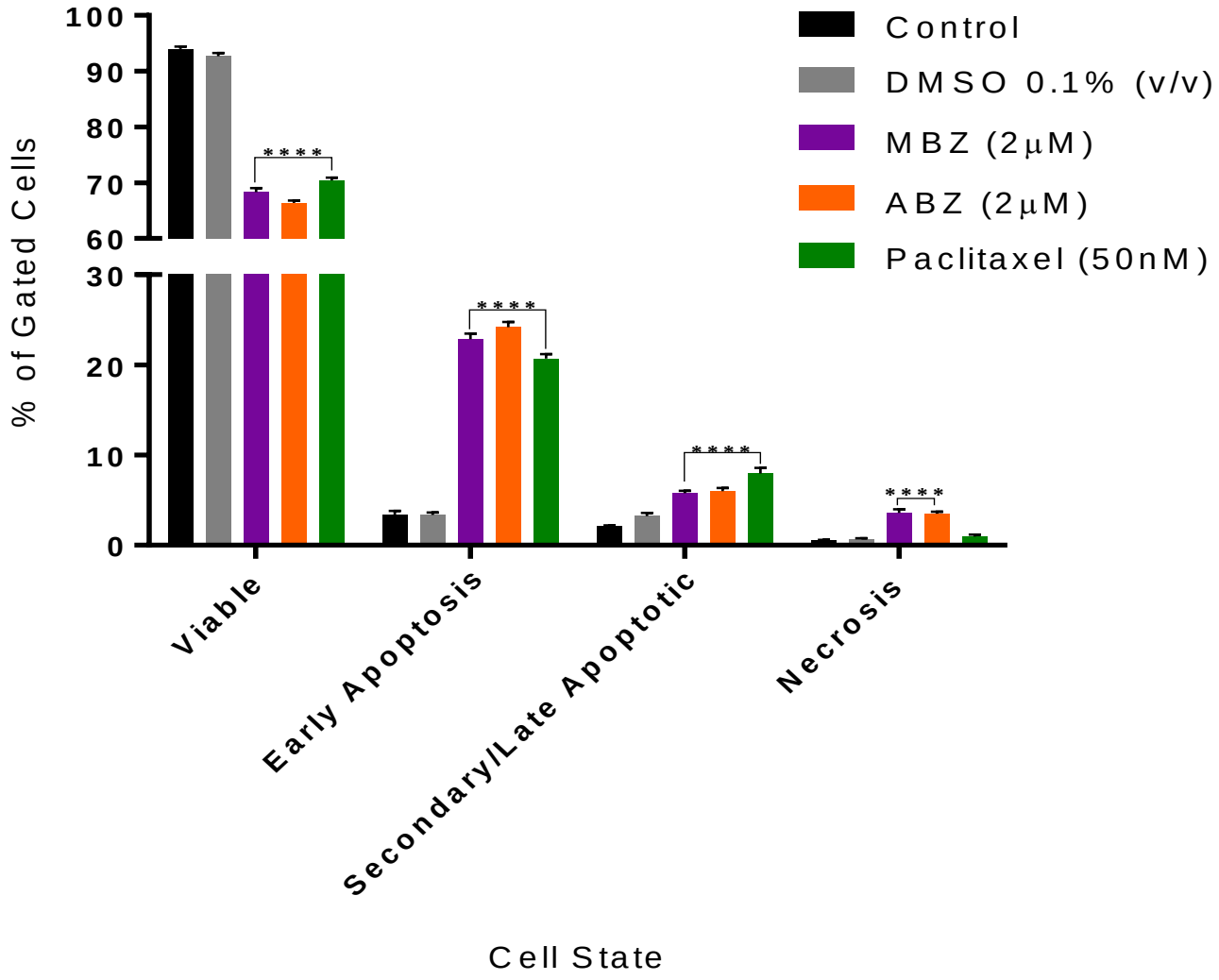

Figure 16. MBZ, ABZ and Paclitaxel cause significant increases in phosphatidylserine exposure. Percentage of HT-29 cells in viable (Annexin V^-/PI^-), early apoptotic (Annexin V^+/PI^-), secondary/late necrotic (Annexin V^+/PI^+), or necrotic (Annexin V^-/PI^+) states, determined by staining with Annexin V and PI. Cells were treated for 24hrs with MBZ (2µM), ABZ (2µM), paclitaxel (50nM), DMSO 0.1% v/v or left as untreated control. Data represents mean ± SEM of three independent experiments carried out in triplicate, where each sample consisted of a minimum of 50,000 stopping events. One-way ANOVAs were performed with a post-hoc Dunnett's test comparing against untreated control, where $p < 0.05$ was considered statistically significant. ****$p < 0.0001$

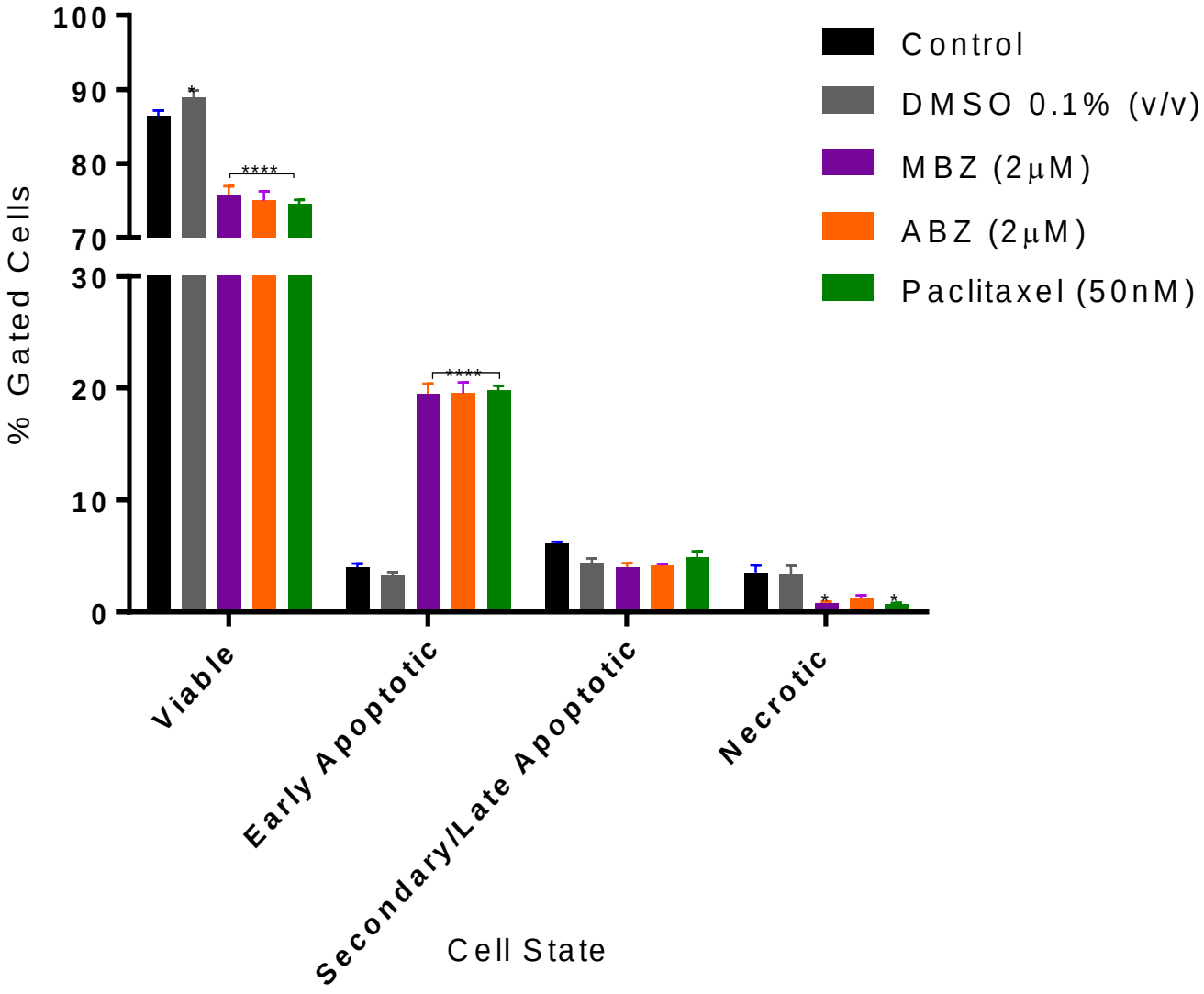

Figure 17. MBZ, ABZ and Paclitaxel cause significant increases in phosphatidylserine exposure. Percentage of HT-29 cells in viable (Annexin V^-/PI^-), early apoptotic (Annexin V^+/PI^-), secondary/late necrotic (Annexin V^+/PI^+), or necrotic (Annexin V^-/PI^+) states, determined by staining with Annexin V and PI. Cells were treated for 48hrs with MBZ (2µM), ABZ (2µM), paclitaxel (50nM), DMSO 0.1% v/v or left as untreated control. Data represents mean ± SEM of three independent experiments carried out in triplicate, where each sample consisted of a minimum of 50,000 stopping events. One-way ANOVAs were performed with a post-hoc Dunnett's test, comparing against untreated control, where $p < 0.05$ was considered statistically significant. *$p < 0.05$, ****$p < 0.0001$

4.4 Sub-G1

Another indicator of apoptosis is the fractionation of DNA content following treatment. This Sub-G1 DNA content can be estimated using PI. Here, following both 24 and 48 hour treatments with MBZ, ABZ and paclitaxel, the percentage of cells with Sub-G1 DNA content were significantly increased compared to control (Figure 18). After 24hrs MBZ resulted in 13.84% ($P = 0.001$) of cells with Sub-G1 DNA content, ABZ; 11.53% ($P = 0.026$), paclitaxel; 19.33% ($P < 0.0001$) vs control; 6.45%. DMSO caused no significant change to the percentage of cells with Sub-G1 DNA content, 6.11% ($P > 0.05$).

Following 48hr treatment with MBZ, 21.96% ($P < 0.0001$) of cells contained Sub-G1 DNA content, ABZ; 15.33%b ($P < 0.0001$), paclitaxel; 23.10% ($P < 0.0001$), whereas control only contained 4.32%. DMSO again showed no significant difference to that of control, 5.12% ($P > 0.05$).

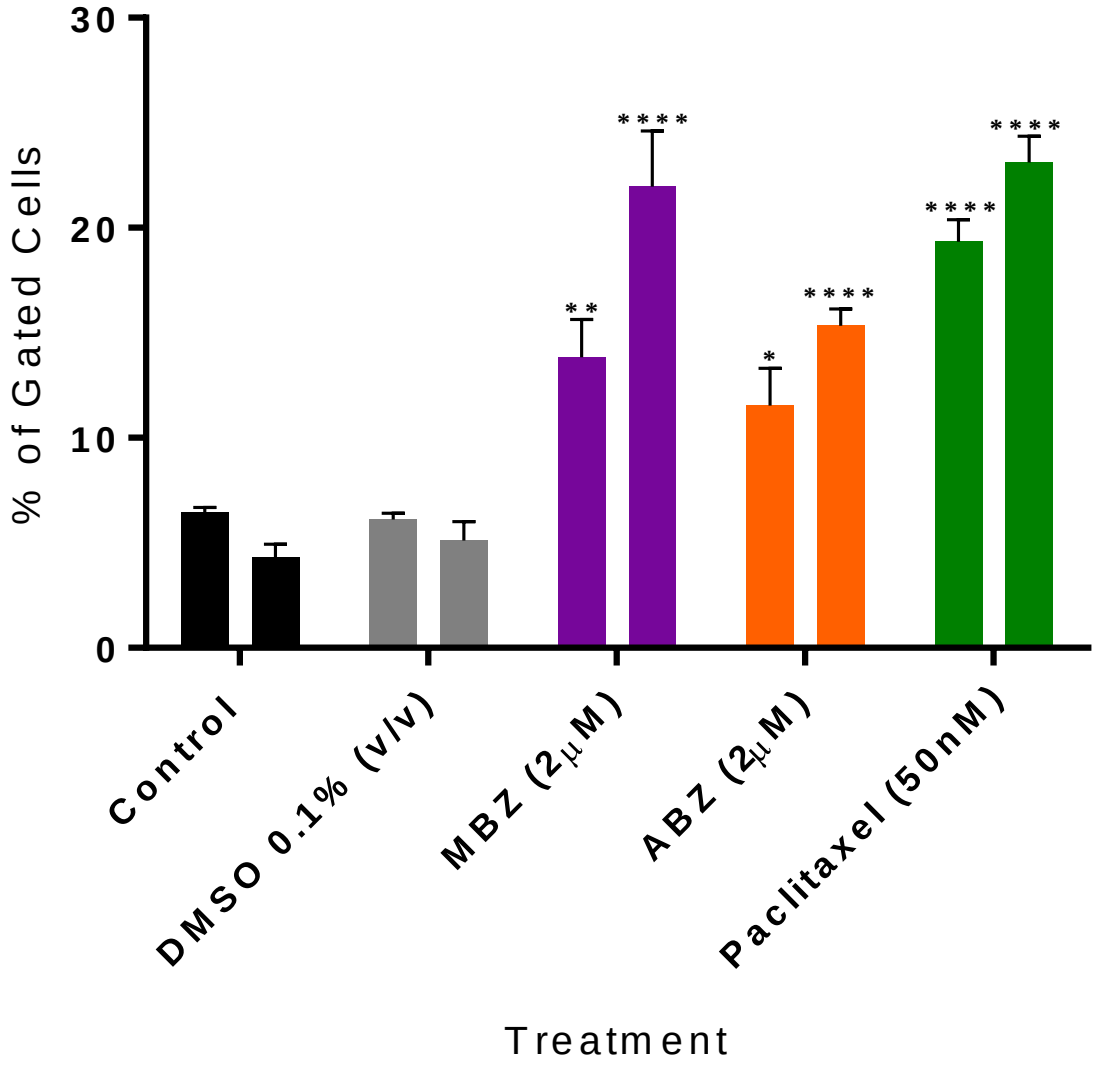

Figure 18. MBZ, ABZ and Paclitaxel cause significant increases in cells with Sub-G1 DNA content. Percentage of HT-29 cells with Sub-G1 DNA content, determined by PI fluorescence using flow cytometry, following 24 hr (left bar) and 48 hr (right bar) treatment with MBZ (2 µM), ABZ (2 µM), paclitaxel (50 nM), DMSO (0.1% v/v) or untreated control. Data represent means ± SEM, of three separate experiments (n = 3) performed in triplicate, where each sample includes a minimum of 50,000 stopping events. One-way ANOVAs were performed, with Dunnett's post-hoc test comparing to respective untreated controls, where $p < 0.05$ was considered as statistically significant. *P < 0.05, **P < 0.01, ****P < 0.0001

4.5 Mitochondrial Membrane Potential ($\Delta\Psi m$)

HT-29 cells were treated with MBZ, ABZ, paclitaxel, DMSO or left untreated for 24 and 48 hrs and the percentage of cells with depolarised mitochondrial membrane potentials, indicative of apoptosis, were determined using the mitochondrial-targeted stain TMRE in conjunction with flow cytometry.

In the 24 hr treatments there were no significant differences between both DMSO vehicle control (3.49 ± 0.38%) and D2 (4.70 ± 0.41 %) compared to control (3.36 ± 0.29%, $p > 0.05$). However, in MBZ, ABZ and paclitaxel treatments there were approximate 6-fold increases in the percentage of cells with depolarised mitochondrial membrane potentials compared to control. MBZ – 19.17 ± 2.23%; ABZ – 18.12 ± 1.32%; paclitaxel – 18.68 ± 1.40%, all of which were statistically significant and gave p values less than 0.0001, (Figure 19).

Cells exposed to the treatments for 48 hrs exhibited similar results to that of the 24 hr treatments. DMSO (3.87 ± 0.10%) showed no difference compared to control (4.79 ± 0.17%, $p > 0.05$), D2 (6.38 ± 0.23%) exhibited a slight increase compared to control however, this was not statistically significant ($p > 0.05$). MBZ, ABZ and paclitaxel similarly showed a large 4-fold increase in the percentage of cells with depolarised mitochondrial membrane potentials compared to control. MBZ – 15.74 ± 1.14%; ABZ – 15.90 ± 1.60%; paclitaxel – 16.87 ± 0.78%, $p < 0.0001$ (Figure 19).

The difference between the two treatment times in respect in control, DMSO and D2 treatments where there is a greater percentage of cells with depolarised mitochondrial membrane potentials in the 48 hr group compared to the 24 hr group, may be attributed to a much larger population of cells as they had an additional 24 hrs to grow. Therefore, there would be a greater percentage of baseline cells with depolarised mitochondrial membrane potentials. On the other hand, there is a decrease in the percentage of cells with depolarised mitochondrial membrane potentials in the 48 hr treatment groups of ABZ, MBZ and paclitaxel compared to the 24 hr group. This may be explained by the increased exposure time of these cytotoxic agents on the cells, thereby killing more cells and decreasing the population of cells that would be included in the gate that would be further analysed.

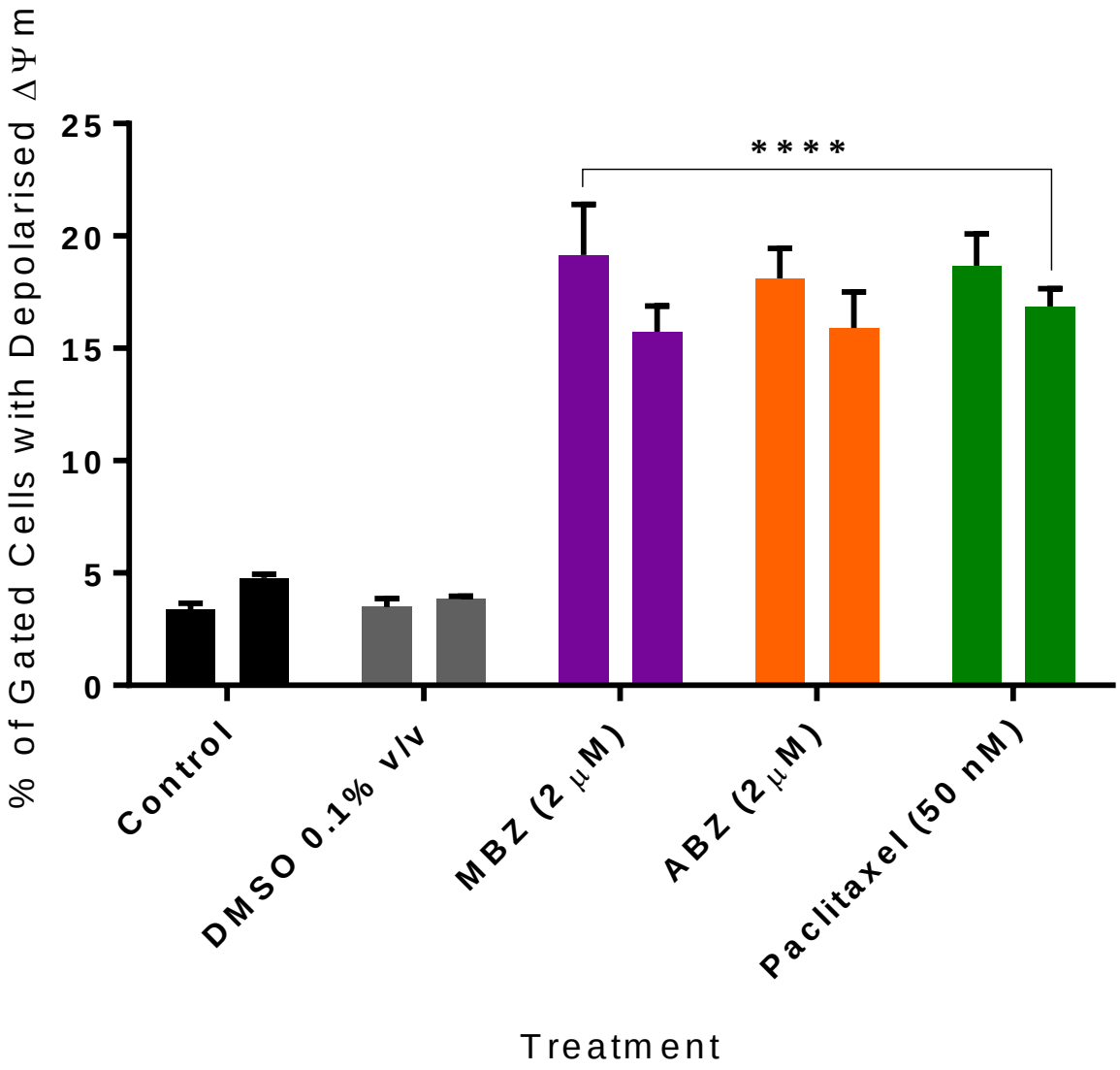

Figure 19. MBZ, ABZ and Paclitaxel cause depolarisation of the mitochondrial membrane potential (Ψ). Percentage of HT-29 cells with depolarised mitochondrial membrane potential (Ψ) determined by TMRE fluorescence intensity, following 24 hr (left bar) and 48 hr (right bar) treatment with MBZ (2 µM), ABZ (2 µM), paclitaxel (50 nM), DMSO (0.1% v/v) or untreated control. Data represent means ± SEM, of three separate experiments (n = 3) performed in triplicate, where each sample includes a minimum of 50,000 stopping events. One-way ANOVAs were performed, with Dunnett's post-hoc test comparing to respective untreated controls, where $p < 0.05$ was considered as statistically significant. ****P < 0.0001

4.6 Lysosomal and Outer Membrane Permeability

Following treatment with MBZ, ABZ, paclitaxel, DMSO or untreated control for both 24 and 48 hrs, lysosomal and outer cell membrane permeability was assessed using the metachromatic dye AO, in conjunction with flow cytometry, which emits green fluorescence in monomeric forms bound to dsDNA, and red fluorescence when accumulated in acidic vesicles, i.e. lysosomes.

Figure 20 shows the percentage of HT-29 cells with LMP following 24 and 48 hr treatments. Twenty-four-hour treatment of MBZ, ABZ and paclitaxel all displayed large significant increases of cells with LMP, 36.28%, 36.76% and 24.16% respectively, vs control 3.81% ($p < 0.0001$). DMSO displayed no significant difference compared to control, 4.35% ($p > 0.05$). Forty-eight-hour treatment yielded similar results, with a notable increase in cells with LMP following paclitaxel treatment compared to 24 hr treatment. MBZ – 35.01%; ABZ – 35.03%; paclitaxel – 34.17% vs control – 4.50% ($p < 0.0001$), whereas DMSO showed no significant difference, 4.79% ($p > 0.05$).

Figure 21 shows the percentage of HT-29 cells with outer cell membrane permeabilisation following 24 and 48 hr treatments, and closely matches the results seen in Figure 10 of cells with LMP. Following 24 hr treatment, MBZ, ABZ and paclitaxel showed significant increases in the percentage of cells with outer cell membrane permeabilisation compared to control. MBZ – 37.40%; ABZ – 37.92%; paclitaxel – 24.20% vs control 4.29% ($p < 0.0001$), whereas DMSO showed no significant difference, 4.63% ($p > 0.05$). Following 48 hr treatment, MBZ – 34.18%; ABZ - 34.17%; paclitaxel 35.76%, vs control 4.73% ($p < 0.0001$), with DMSO again showing no significant difference, 4.99% ($p > 0.05$).

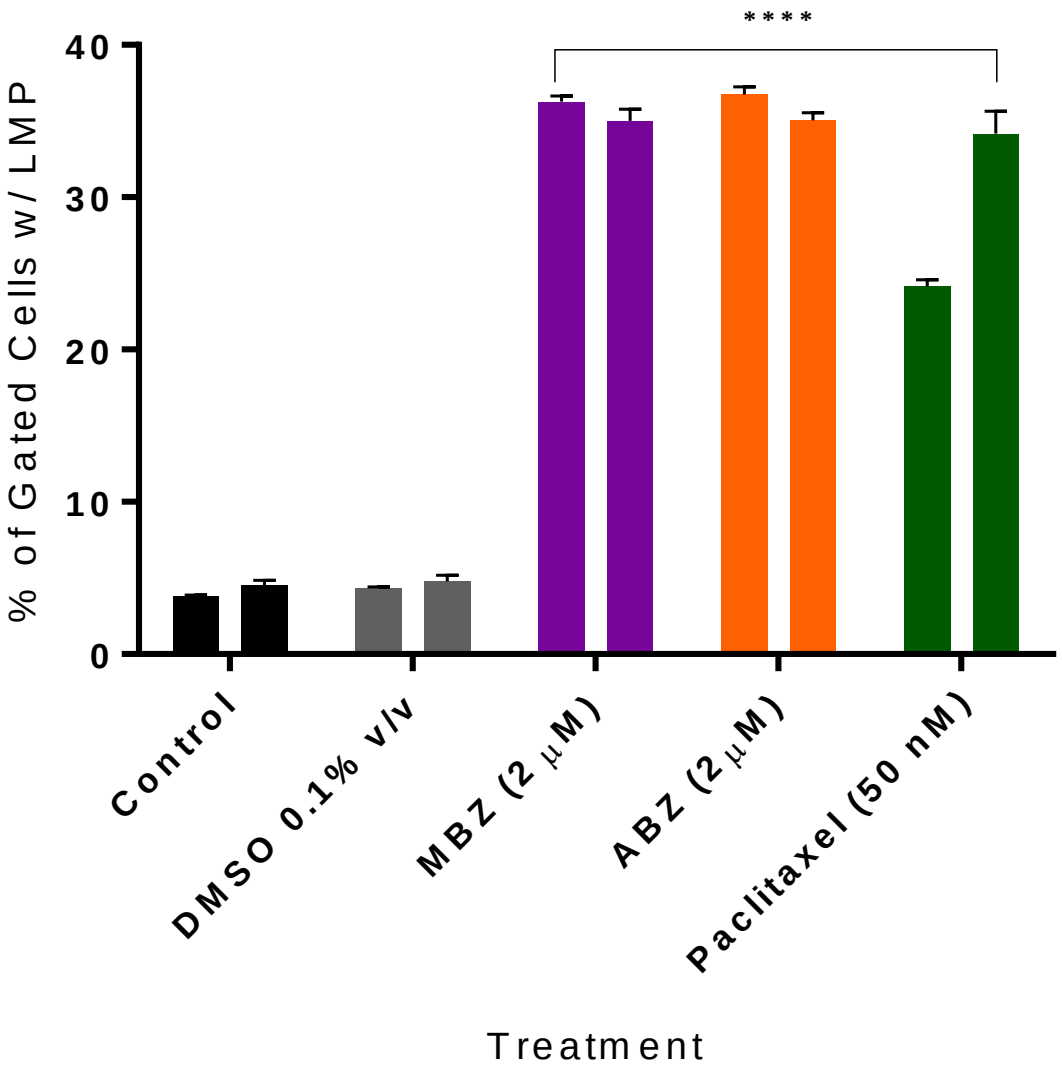

Figure 20. MBZ, ABZ and Paclitaxel cause significant increases in cells with permeabilised lysosomal membranes. Percentage of HT-29 cells with lysosomal membrane permeabilisation determined by AO fluorescence intensity using the PE filter, following 24 hr (left bar) and 48 hr (right bar) treatment with MBZ (2 µM), ABZ (2 µM), paclitaxel (50 nM), DMSO (0.1% v/v) or untreated control. Data represent means ± SEM, of three separate experiments (n = 3) performed in triplicate, where each sample includes a minimum of 50,000 stopping events. One-way ANOVAs were performed, with Dunnett's post-hoc test comparing to respective untreated controls, where $p < 0.05$ was considered as statistically significant. ****$P < 0.0001$

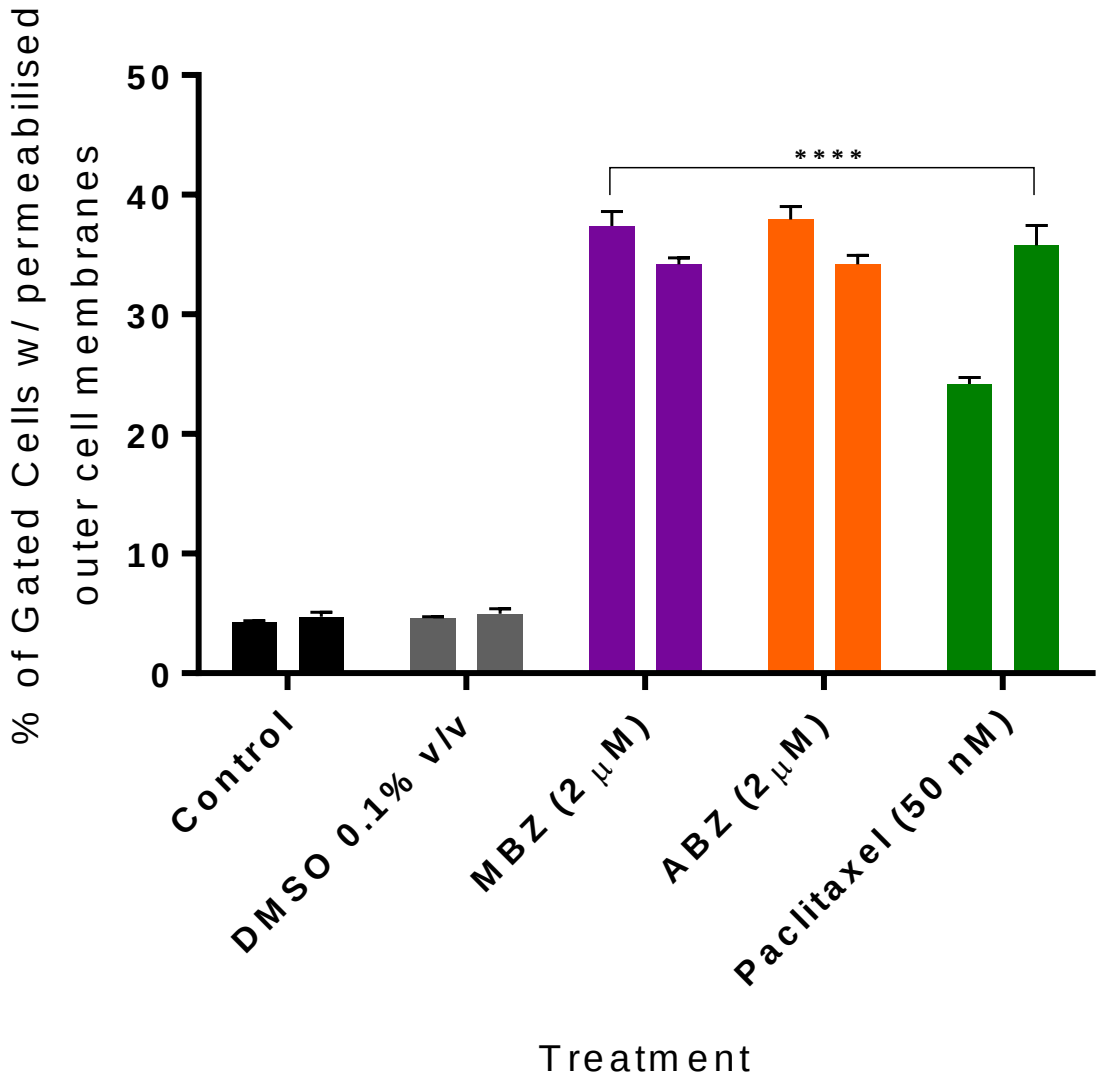

Figure 21. MBZ, ABZ and Paclitaxel cause significant increases in cells with permeabilised outer membranes. Percentage of HT-29 cells with lysosomal membrane permeabilisation determined by AO fluorescence intensity using the FITC filter, following 24 hr (left bar) and 48 hr (right bar) treatment with MBZ (2 µM), ABZ (2 µM), paclitaxel (50 nM), DMSO (0.1% v/v) or untreated control. Data represent means ± SEM, of three separate experiments (n = 3) performed in triplicate, where each sample includes a minimum of 50,000 stopping events. One-way ANOVAs were performed, with Dunnett's post-hoc test comparing to respective untreated controls, where $p < 0.05$ was considered as statistically significant. ****P < 0.0001

4.7 ROS

Indirect measurement of ROS damage was assessed using the DTNB assay, which is used to determine the free sulfhydryl content of cells samples, which is decreased as a consequence of oxidation from ROS and can be calculated using the molar extinction coefficient (**ε**) of DTNB.

Following 48 hr treatments, the free sulfhydryl concentration was significantly decreased in cells treated with; MBZ – 2.671 x 10^{-5} M ($p = 0.0094$); ABZ – 2.646 x 10^{-5} M ($p = 0.0086$) and paclitaxel - 2.539 x 10^{-5} M ($p = 0.0058$) vs control – 4.630 x 10^{-5} M (Figure 22). DMSO exhibited a small increase (4.857 x 10^{-5} M) compared to control but was not statistically significant.

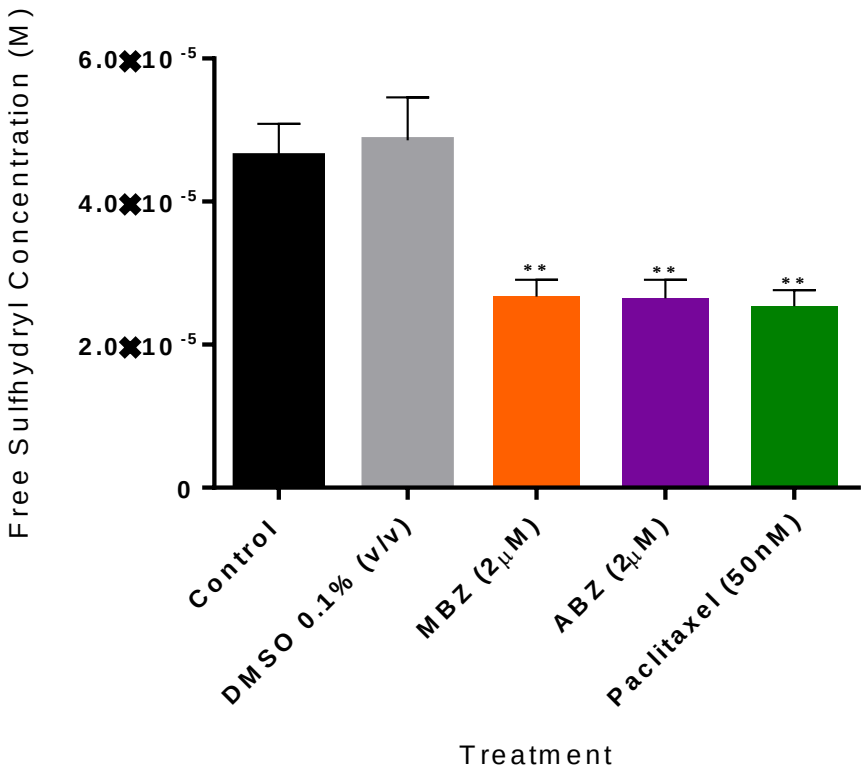

Figure 22. MBZ, ABZ and Paclitaxel cause significant decreases in cellular free sulfhydryl content. The concentration of free sulfhydryls (M) in HT-29 cells following 48 hr treatment with MBZ (2 µM), ABZ (2 µM), paclitaxel (50 nM), DMSO (0.1% v/v) or untreated control. Three independent experiments were carried out (n = 3), where each sample included the entire contents of one well of a 6-well plate seeded at 300,000 cells. Data were analysed using a One-way ANOVA with Dunnett's post-hoc test comparing to untreated control, where $p < 0.05$ was considered statistically significant. **$p < 0.01$

4.8 Cell Cycle

Cell cycle analysis was carried out on HT-29 cells treated with MBZ, ABZ, paclitaxel, DMSO or untreated control for 24 or 48 hrs, and assessed using PI staining in conjunction with flow cytometry.

Following 24 hr treatments, MBZ, ABZ and paclitaxel exhibited significantly large increases in the percentage of cells in the G2/M phase compared to control (Figure 23 and 24). As shown in Figure 11, MBZ, ABZ and paclitaxel treatments all lead to significant increases in cells with Sub-G1 content compared to control. Cells in the G2/M phase were significantly increased in; MBZ – 60.18%; ABZ – 58.68% and paclitaxel – 62.42%, vs control – 19.28% ($p < 0.0001$). DMSO showed no significant difference, 21.37% ($p > 0.05$). Subsequently, MBZ, ABZ and paclitaxel treated cells showed significant decreases in the percentage of cells in the G1 and S phases. MBZ – 2.67% (G1), 11.84% (S); ABZ – 3.52% (G1), 10.56% (S); paclitaxel – 1.78% (G1), 6.92% (S); vs control 45.02 (G1) ($p < 0.0001$), 22.87% (S) ($p < 0.0001$). The percentage of cells in the >G2/M phase were also increased following treatment with MBZ – 11.53% ($p = 0.0027$) and ABZ – 15.57% ($p < 0.0001$), vs control 6.53%. DMSO showed no significant difference at any cell cycle phase compared to control ($p > 0.05$).

Forty-eight-hour treatments produced similar results to that seen of the 24 hr treatments, with G2/M arrest being the most significant observation in the MBZ, ABZ and paclitaxel groups. Cells in the G2/M phase were significantly increased in; MBZ – 54.42%; ABZ – 64.03% and paclitaxel – 51.10%, vs control – 16.79% ($p < 0.0001$) (Figure 25). This again lead to subsequent decreases in the percentage of cells in G1 and S phases. MBZ – 4.01% (G1) ($p < 0.0001$), 5.54% (S) ($p < 0.0001$); ABZ – 2.33% (G1) ($p < 0.0001$), 3.50% (S) ($p < 0.0001$); paclitaxel – 1.97% (G1) ($p < 0.0001$), 8.02% (S) ($p = 0.0001$); vs control – 51.84% (G1), 19.72% (S). The percentage of cells in the >G2/M phase were also increased following treatment with MBZ – 13.66% ($p = 0.0006$); ABZ – 14.06% ($p = 0.0003$) and paclitaxel – 15.72% ($p < 0.0001$). There were no significant differences following 48 hr treatment with DMSO compared to control ($p > 0.05$).

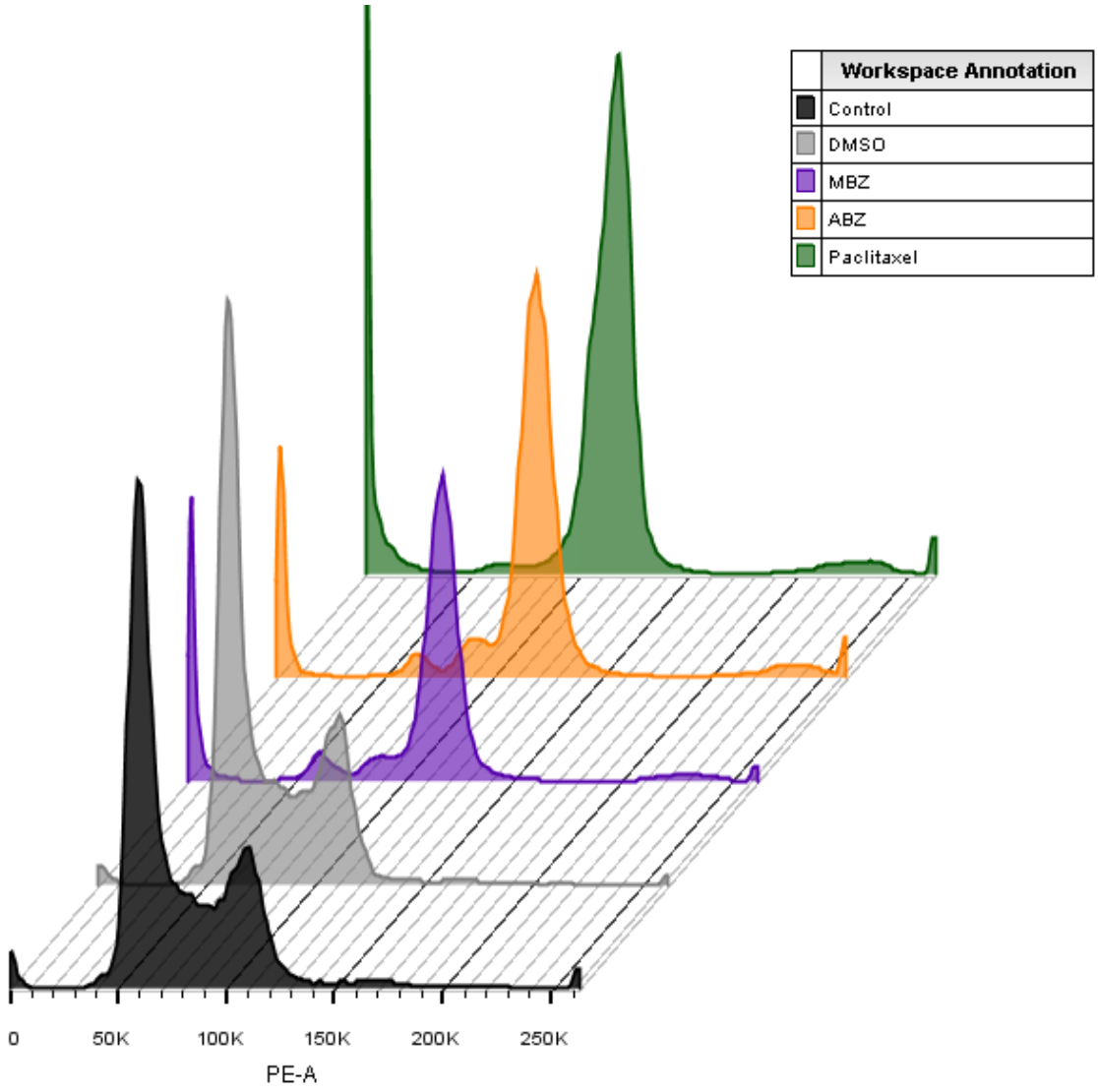

Figure 23. MBZ, ABZ and Paclitaxel cause G2/M arrest in cell cycle following 24hr treatment. Histogram analysis of cell cycle in HT-29 cells following 24 hr drug treatment. Control and DMSO vehicle control (0.1% v/v) displaying "normal" G1 peaks at approx. 50K PE-A intensity, which is significantly diminished following MBZ (2 µM), ABZ (2 µM) and paclitaxel (50 nM) treatments, where large sub-G1 and G2/M peaks are evident.

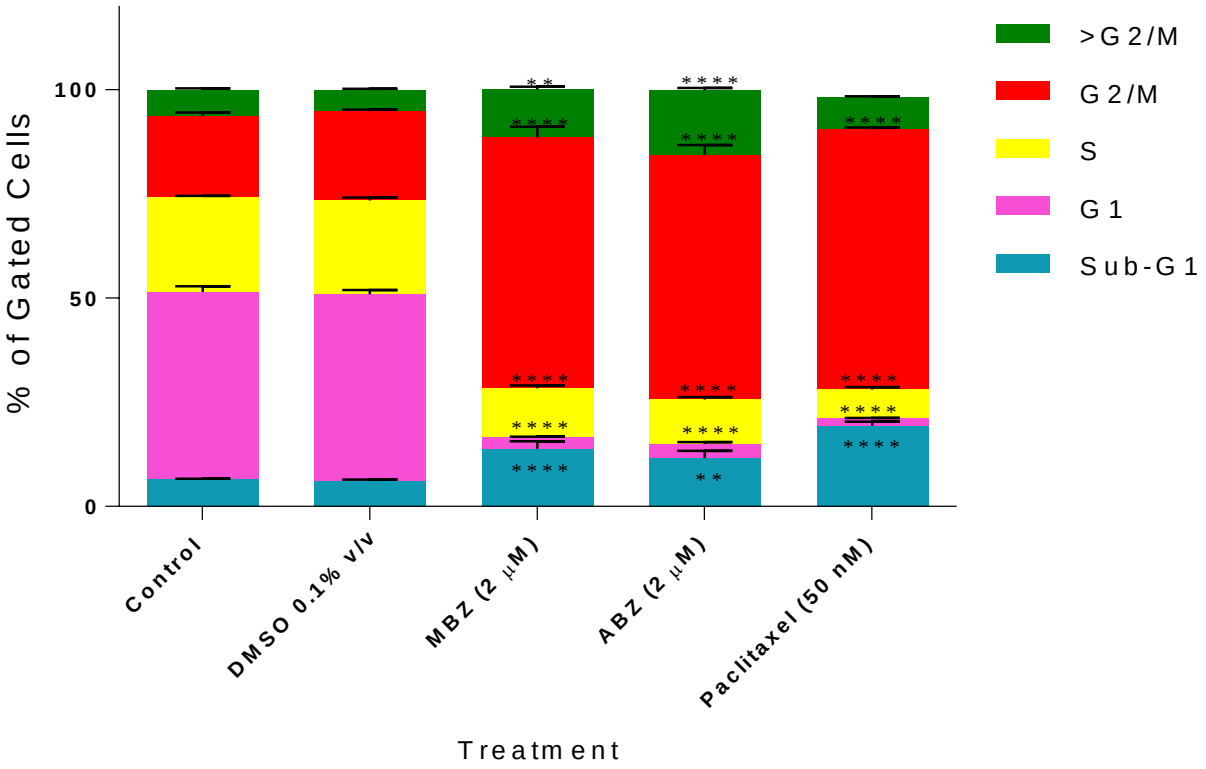

Figure 24. MBZ, ABZ and Paclitaxel cause G2/M arrest in cell cycle following 24hr treatment. Cell cycle analysis of HT-29 cells following 24 hr treatment with MBZ (2 µM), ABZ (2 µM), paclitaxel (50 nM), DMSO (0.1% v/v) or untreated control. DNA content was assessed using PI staining. Data represent mean ± SEM of the percentage of cells at each cell cycle stage (Sub-G1; G1; S; G2/M; >G2/M). Three independent experiments were conducted in triplicate with a minimum of 50,000 stopping events for each sample. Data were analysed using a Two-way ANOVA with Dunnett's post-hoc test comparing to untreated control, where $p < 0.05$ was considered statistically significant. **$p < 0.01$, ****$p < 0.0001$

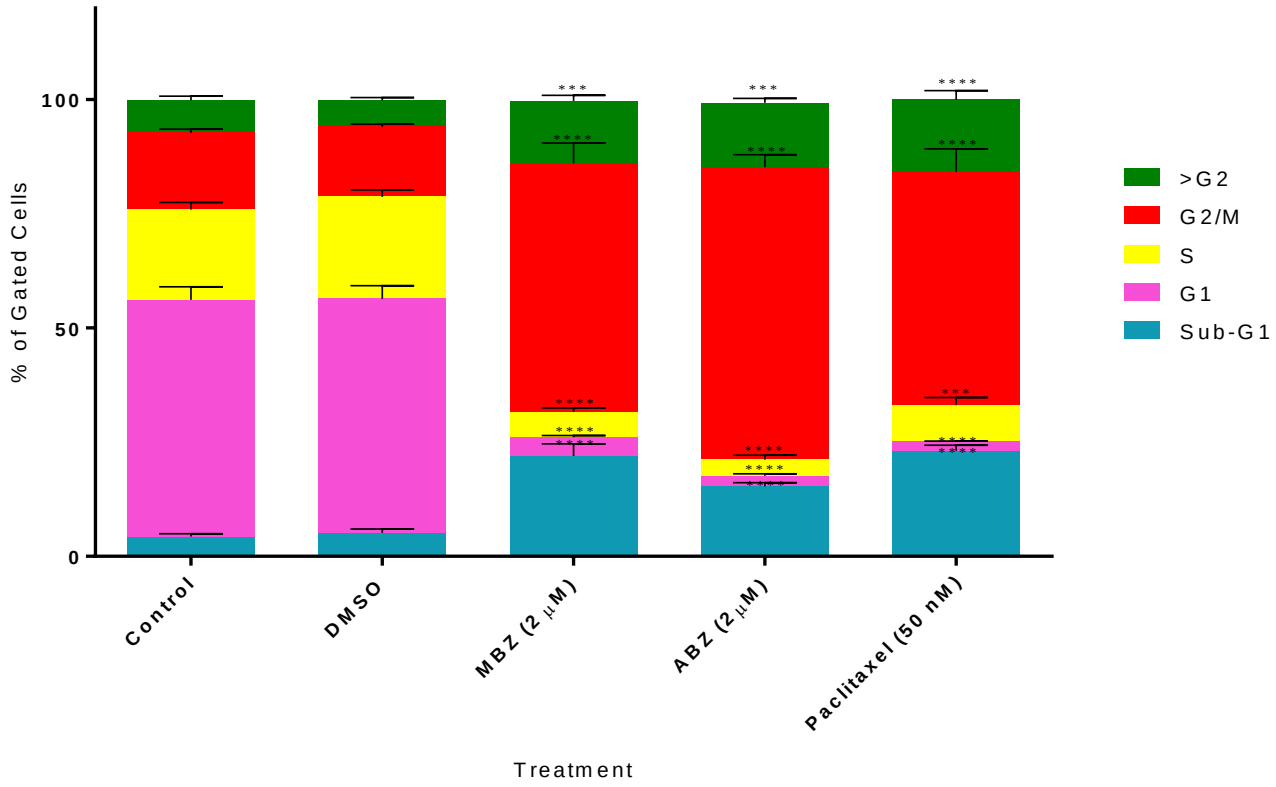

Figure 25. MBZ, ABZ and Paclitaxel cause G2/M arrest in cell cycle following 48hr treatment. Cell cycle analysis of HT-29 cells following 48 hr treatment with MBZ (2 µM), ABZ (2 µM), paclitaxel (50 nM), DMSO (0.1% v/v) or untreated control. DNA content was assessed using PI staining. Data represent mean ± SEM of the percentage of cells at each cell cycle stage (Sub-G1; G1; S; G2/M; >G2/M). Three independent experiments were conducted in triplicate with a minimum of 50,000 stopping events for each sample. Data were analysed using a Two-way ANOVA with Dunnett's post-hoc test comparing to untreated control, where $p < 0.05$ was considered statistically significant. ***$p < 0.001$, ****$p < 0.0001$

4.9 Tubulin Staining

Figure 26 shows nuclear and microtubular staining of HT-29 cells following treatment with MBZ (2 µM), ABZ (2 µM), paclitaxel (50 nM) or DMSO vehicle control (0.1% v/v) for 8 hrs. MBZ, ABZ and paclitaxel all produced smaller brighter nuclei indicating nuclear condensation, as pointed out by the red arrows. Alpha- and acetylated-alpha-tubulin staining displayed a decreased fluorescent intensity following MBZ and ABZ treatment compared to control and even more so compared to paclitaxel, which increased intensity of both alpha- and acetylated-alpha-tubulin staining compared

to control. This suggests that MBZ and ABZ promote depolymerisation of microtubules, whereas paclitaxel promotes polymerisation and stabilises microtubules.

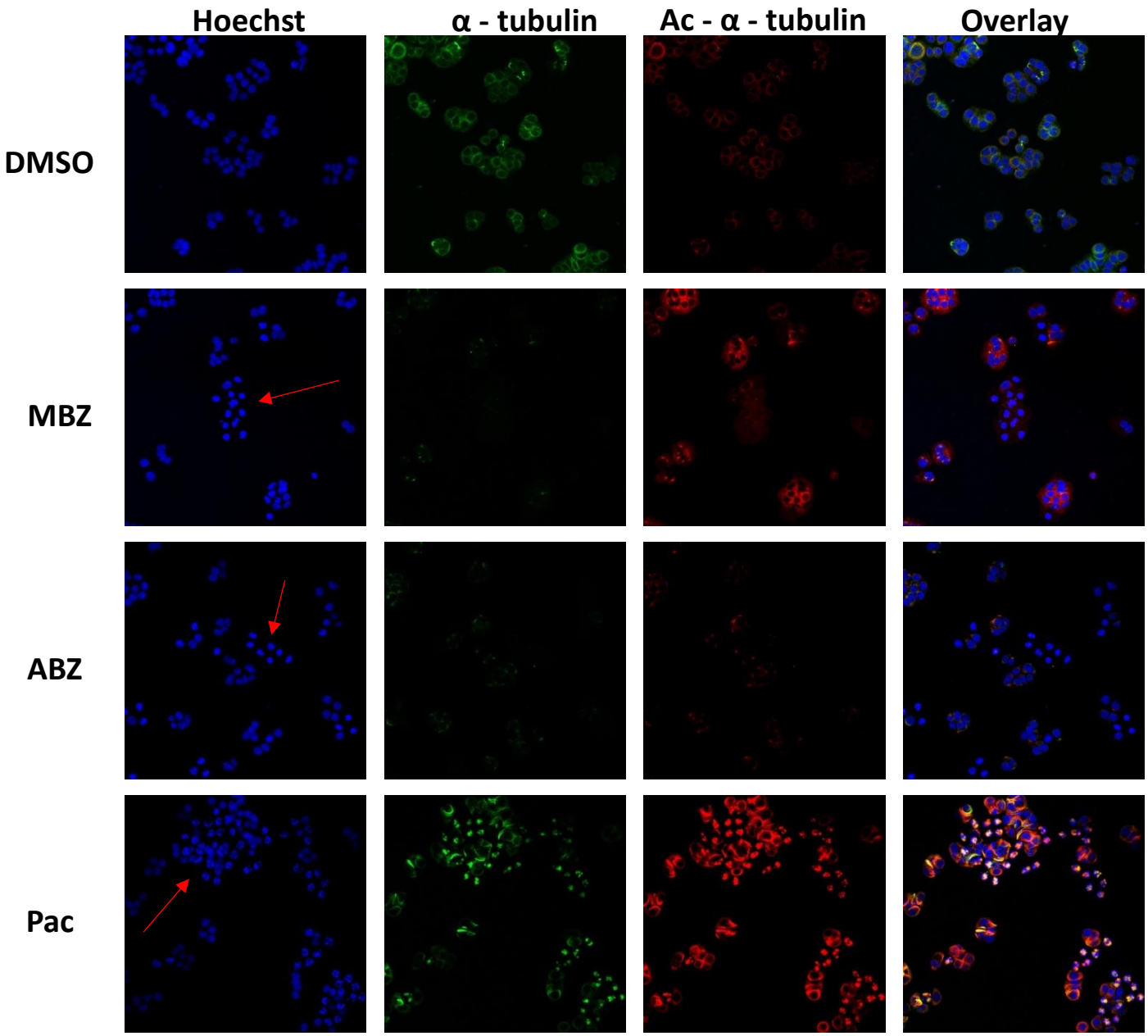

Figure 26: MBZ, ABZ and paclitaxel cause condensation of nuclei and disrupt microtubule networks. Fluorescent staining analysis of HT-29 cells treated with MBZ (2 µM), ABZ (2 µM), paclitaxel (50 nM) or DMSO vehicle control (0.1% v/v) for 8 hrs. Cells were stained with Hoechst 33342, anti-alpha-tubulin and anti-acetylated-alpha-tubulin and imaged using the Nikon AI-R inverted fluorescent microscope with Nikon Intensilight C-HGFI mercury lamp (Olympus, Japan) at 20x magnification, with consistent exposure. Red arrows point to apoptotic condensed nuclei.

Chapter 5: Discussion

The overall aim of the first part of this project was to identify the mechanism of action by which the two compounds 4-thiazolecarboxylic acid, 4, 5-dihydro-2-(4-nitrophenyl)-methyl ester (D1) and 4-thiazolecarboxylic acid, 2-(4-nitrophenyl)-methyl ester (D2) cause cytotoxicity in cancer cells. The original screening of these novel compounds and other analogues in a previous study, revealed that 4-thiazolecarboxylic acid, 2-(4-nitrophenyl)-methyl ester (D2 (12c in the Lamb *et al.* paper)) and the structurally related 4-thiazolecarboxylic acid, 2-(4-aminophenyl)-methyl ester (D3 (13c in the Lamb *et al.* paper)) were the only analogues that exhibited cytotoxicity in cancer cells below 100 µM (Lamb *et al.*, 2015). D2 (12c) caused a time-dependent decrease in cell viability of HT-29 cells at 24 hrs from 77% to 53% at 72 hrs, whereas D3 (13c) caused a decrease from 82% to 55% when cells were treated at 10 µM. These compounds were also cytotoxic towards MCF-7 breast cancer cells, again showing time-dependent decreases in cell viability over 72 hr (Lamb *et al.*, 2015). From this initial study carried out by Lamb *et al*, these two compounds and another analogue (11c), untested at the time, 4-thiazolecarboxylic acid, 4, 5-dihydro-2-(4-nitrophenyl)-methyl ester (D1), identical to D2 except lacking a double-bond in the thiazole ring, became the focus of a summer studentship project, where it was found, surprisingly, that only D1 and D2 were significantly cytotoxic in a range of cancer cell lines and D3 showed no significant biological activity. This summer project was then expanded into the current Master's project, aiming to examine the mechanism of anticancer action in depth using a variety of *in vitro* assays and techniques. Unfortunately, during the current investigation, both compounds displayed significantly decreased cytotoxicity towards cancer cells, even with a new batch, and results seen in the previous summer project were unable to be replicated. This most likely suggested that the two compounds D1 and D2 had degraded in solution over time and had lost their biological activity. Following a newly synthesised batch of both compounds, the potencies exhibited were different to the first batch and again degraded and lost activity, leading the project to investigating a completely new set of compounds.

Results from the previous summer project showed that both compounds had cytotoxic effects in breast and colon cancer cells and had IC_{50} values ranging between 50 – 100 µM following 24 hr treatment. Subsequent experiments for the Master's project were then carried out using a concentration of 50 µM of both D1 and D2 to investigate their mechanism of action. These included a range of flow cytometry assays, cell viability assays and nuclear staining. However, throughout this stage it later appeared that the two compounds had lost activity and results were not as expected, and later dose-response curves showed that the cytotoxic potency had in fact decreased.

Early results from the summer project suggested that these compounds may kill cancer cells by induction of apoptosis. This led to investigating the involvement of caspases, crucial components of the apoptotic pathway, by using a pan-caspase inhibitor z-VAD-FMK in an MTT cell viability assay. Figure 7 shows three cancer cells lines treated with D2 alone and in conjunction with the caspase inhibitor at both 0.1 and 1.0 µM. D2 alone showed significant decreases in cell viability in all cell lines, similar to the positive control paclitaxel. The caspase inhibitor exhibited no significant decreases in cell viability in any of the cell lines at either concentration, however it also failed to reduce the decrease in cell viability when treated with D2, and produce a "rescuing" effect. These results suggest that D2 could be causing cytotoxicity through a different mechanism than apoptosis, and may be independent from caspase activation. However, separate experiments using the caspase inhibitor up to 10 µM and in conjunction with the classical apoptosis inducer cisplatin showed that at any concentration of the caspase inhibitor, cell viability could not be significantly rescued, and that is was more likely that the caspase inhibitor was dysfunctional and failed to inhibit caspases (results not shown).

Cell cycle was also analysed, using propidium iodide to stain DNA content, as previous studies had suggested that structurally similar phenylthiazole compounds act through inhibition of tubulin polymerisation and lead to arrest of cell cycle at the G2/M phase and subsequent increase of hypodiploid sub-G1 phase cells, which is indicative of apoptosis (Lu *et al.*, 2009; Yu *et al.*, 2015). However, no G2/M arrest or increase in sub-G1 cells were observed in any of the cell lines (Figure

8). There were no significant changes in cell cycle following D1 or D2 treatment compared to control in MCF-7 cells. D1 exhibited a 5% decrease in G1-phase cells in MDA-MB-231 cells and a 7.5% increase in G1-phase cells and 5.6% decrease in S-phase cells in HT-29 cells. D2 had no significant effect in any cell line. These results suggest that both D1 and D2 have no significant effect on cell cycle and may not interact with tubulin polymerisation in the way that most MTAs do leading to G2/M arrest.

Figure 9 and 10 show D1 and D2's effects on mitochondrial and lysosomal membrane permeabilisation, using the fluorochromatic dyes TMRE and acridine orange, respectively. No significant changes from control were seen in either treatment in any of the cell lines, except a small decrease in the percentage of MDA-MB-231 cells with LMP following D2 treatment, which may result from error caused by manual gating during analysis. However most likely due to both compounds losing activity and thus not cytotoxic towards the cells at this stage.

Cells were also stained with Hoechst 33342 to examine nuclear morphology and identify if any treatments induced chromatin condensation, a classical marker of apoptosis. Figure 11 shows that in MCF-7 and HT-29 cells D1 and D2 produced no obvious changes in nuclear morphology compared to control and DMSO vehicle-treated cells. In MDA-MB-231 cells there are smaller brighter nuclei in D1 and D2 treated cells, however these are also seen in both control and DMSO treated cells and most likely represent the large variation of cell/nucleus size and shape of this cell line rather than an effect from a treatment.

Dose-response curves were carried out again after the previous experiments and revealed a rightward shift and decrease in potency of both D1 and D2 in all cancer cell lines (Figure 12). The 24 hr IC_{50} values of D1 were much greater than 100 µM in all cell lines with the lowest seen in MDA-MB-231 cells of 394 µM. D2 was slightly more potent with values also above 100 µM except in MCF-7 cells where the IC_{50} was approximately 66 µM. Both compounds showed relatively selective cytotoxicity

towards cancer cells as IC_{50} values were the highest in the non-transformed mesenchymal stem-cell line RCB2157, where D1 had an IC_{50} of 604 µM and D2 1223 µM.

Altogether these results show that D1 and D2 cause decreases in cell viability in cancer cells measured using the MTT assay. However, evaluating markers of apoptosis and cell cycle, both compounds exhibited no largely significant changes compared to untreated control or DMSO vehicle control, despite preliminary results suggesting that an apoptotic mechanism is involved. This suggests that a number of possibilities could be occurring. Firstly, D1 and D2 both are cytotoxic and cause decreases in cell viability, which may be due to other cell death mechanisms and not involve the apoptotic pathway however, this seems unlikely. Secondly, D1 and D2 are not actually cytotoxic, but somehow interfere with MTT producing a false positive result – this could be solved by using different cell viability assays such as sulforhodamine B or crystal violet. Again, this is unlikely as results from the summer project indicated that the compounds were cytotoxic and acting through apoptotic pathways due to observing phosphatidylserine externalisation and nuclear condensation. Thirdly and most likely, D1 and D2 are cytotoxic and do cause cell death via an apoptotic pathway, but have degraded over time and have decreased potency, therefore 50 µM was of too low a concentration to see any effects and potentially the chemical structures of the compounds had changed thus losing activity altogether.

Both D1 and D2 were obtained dissolved in 100% DMSO at stock concentrations of 10 mM and stored at room temperature for many months. In retrospect the compounds should have been given in a solid powder form, and dissolved into DMSO when required, as experiments were carried out over a period of multiple months and hence given longer exposure to the mild oxidative nature of DMSO, thus potentially resulting in the oxidation/degradation of the compounds. Previous studies have shown that the stability of compounds dissolved in DMSO greatly decrease over a period of 1 year. In one study the stability of approximately 7200 compounds stored as 20 mM DMSO solutions at room temperature was assessed. The probability of observing any one compound was 92% after 3 months of storage at room temperature, 83% after 6 months, and 52% after 1 year in DMSO

(Kozikowski *et al.*, 2003). Furthermore, the longer the compounds are stored in DMSO the greater the chance of them precipitating out, due to the hygroscopic nature of DMSO as it pulls water from the surrounding atmosphere (Waybright *et al.*, 2009). A potential solution for this is the addition of a cosolvent(s) that is not hygroscopic such as glycerol.

The second section of the project then focused on investigating two other compounds, mebendazole and albendazole. These two anthelmintic benzimidazoles are commonly prescribed to treat a range of worm infestations. Recently these drugs have shown promising results against cancer activity both *in vitro* and *in vivo* and look to be promising drug candidates to be repurposed for anticancer indication, with MBZ already in a range of clinical trials for treatment of gliomas (Pantziarka *et al.*, 2014; Castro *et al.*, 2016). These two drugs were of interest as their anthelmintic mechanism of action was well documented and due to the inhibition of tubulin polymerisation in gastrointestinal cells of helminths, however their anticancer effect was less understood but most likely involved alteration of tubulin. Similar to the investigation of D1 and D2, MBZ and ABZ were screened in three cancer cell lines and one non-transformed mesenchymal stem cell line over 24 and 48 hrs and mechanism of anticancer action investigated using a variety of flow cytometry assays, caspase-3 and ROS assays and fluorescent imaging.

MBZ and ABZ both produced dose-dependent and time-dependent decreases in the cell viability of the three cancer cell lines HT-29, MCF-7, and MDA-MB-231, as well as in the mesenchymal stem cell line RCB2157 (Figures 13-14). MBZ and ABZ were observed to have the highest IC_{50} values in the mesenchymal stem-cell line compared to any of the cancer cell lines, suggesting that these drugs may be more selectively cytotoxic towards cancer cells. Of the cancer cell lines, both MBZ and ABZ exhibited low micromolar IC_{50} values and were most potent towards the HT-29 colorectal cancer cell line, with MBZ having 24 and 48 hr IC_{50} values of 1.3 ± 0.1 μM and 0.11 ± 0.07 μM respectively, and ABZ having 1.4 ± 0.1μM and 0.69 ± 0.42 μM respectively. For practical reasons, only one cell line was used to investigate the anticancer mechanism of action of MBZ and ABZ, with the HT-29 cell line being chosen due to having the lowest IC_{50} values and potent cytotoxicity compared to the

other cancer cell lines. The concentration of 2 µM was used for both MBZ and ABZ for all further experiments based upon their respective IC_{50} values.

A possible explanation to why MBZ and ABZ are more selective towards HT-29 cells may be due to the fact that they contain the $BRAF^{V600E}$ mutation encoding for a protein involved in the RAS signalling pathway associated with cellular growth. Somatic mutations in the BRAF gene have been described in almost 50% of malignant melanomas and many other cancers including colorectal carcinoma (CRC), ovarian and papillary thyroid carcinomas (Dhomen *et al.,* 2007). The V600E is the most frequent BRAF mutation, accounting for approximately 80% of all reported mutations in CRC and is present in HT-29 cells, but not in MCF-7, MDA-MB-231 or RCB2157 cells (Davies *et al.*, 2002; Ahmed *et al.*, 2013). Previous studies, including a large screening program using the NCI 60 cell line library identified MBZ and ABZ as potential therapies for a range of CRC and identified their high affinities for these cell lines due to interaction with several protein kinases, in particular BRAF (Nygren *et al.*, 2013). Another study found that MBZ has a higher affinity for mutant $BRAF^{V600E}$ (210 nM) over wild-type BRAF (230 nM), and that MBZ selectively inhibits BRAF in refractory $NRAS^{Q61K}$ melanoma cells containing the V600E mutation, and suppresses growth in combination with trametinib – a MEK inhibitor (Simbulan-Rosenthal *et al.,* 2017). This may be an additional pathway involved in cell death/cell growth however, the scope of this project remained focused on apoptotic/necrotic pathways and involvement with microtubules.

Previous studies have suggested that MBZ and ABZ elicit their anticancer effects via induction of apoptosis in non-small cell lung cancer (NSCLC) and gastric cancer cell lines, exhibiting caspase activation, mitotic arrest, cytochrome c release and DNA fragmentation (Mukhopadhyay *et al.,* 2002; Sasaki *et al.*, 2002; Zhang *et al.*, 2017). To examine whether MBZ and ABZ cause cell death through an apoptotic pathway in HT-29 cells, cleaved caspase-3 activity, phosphatidylserine exposure and fragmented sub-G1 DNA content were analysed. Mitochondrial and lysosomal membrane permeability were also assessed to identify whether either organelle was involved in the cell death

pathway. Paclitaxel was used as a positive control in all experiments as it is a well-known inducer of apoptosis, as well as being a classical MTA.

Caspase-3 is an effector caspase involved in both the intrinsic and extrinsic pathways, where it is one of the last enzymes to be activated by cleavage, then carrying out degradation of cellular components, which result in morphological changes, and hence it is considered as a classical marker of apoptosis (Logue *et al.*, 2008). Cleaved caspase-3 activity was measured using the fluorescent substrate Ac-DEVD-AMC, which contains the selective amino acid sequence (DEVD) recognised by caspase-3 allowing cleavage of the AMC (amido-4-methylcoumarin) fluorophore, which can then be measured using a fluorometer. Figure 15 shows caspase-3 activity by intensity of fluorescence at 440 nm following 24 hr treatment with MBZ, ABZ and paclitaxel. Paclitaxel treatment exhibited a significantly large increase in fluorescent intensity compared to control and DMSO, which came of no surprise as paclitaxel's induction of cleaved caspase-3 is well documented (Oyaizu *et al.*, 1999; Lu *et al.*, 2005). MBZ appeared to significantly increase fluorescent intensity (~250 F.U (fluorescence units)) compared to control (~150 F.U), however not to the extent of paclitaxel (~450 F.U), with ABZ also increasing fluorescent intensity (~200 F.U) albeit less than MBZ. Unfortunately, this experiment was done only once, due to difficulties with standardising the assay, however the results still suggest that cleaved caspase-3 is involved and the death pathway may most likely be apoptotic. Previous studies have also confirmed increased cleavage of caspase-3 following treatment with 0.5 µM and 1.0 µM MBZ in H460 and A549 lung cancer cells as well as in M-14 and SK-Mel-19 melanoma cells where cleavage of caspase-3 was evident as early as 6 hr after treatment (Sasaki *et al.*, 2002; Doudican *et al.*, 2008). ABZ at 1 µM has also previously shown increases in caspase-3 cleavage at 8, 24 and 48 hr treatment in the same HT-29 colorectal cancer cell line (Pourgholami *et al.*, 2005).

Another classical marker of apoptosis is the externalisation of phosphatidylserine residues, which are usually restricted to the inner membrane layer, but become expressed on the surface of the cell whereby they are recognised by macrophages leading to the phagocytosis of apoptotic cells (Shiratsuchi *et al.*, 1998). Using flow cytometry and annexin V-FITC, a dye which binds specifically

to phosphatidylserine residues, along with PI, a non-permeable DNA-binding dye, cells treated with MBZ and ABZ were categorised as viable, early or late apoptotic, or necrotic following 24 and 48 hr treatments. Figure 16 shows the state of cells following 24 hr treatment with MBZ, ABZ, paclitaxel, DMSO (vehicle only) or control. Treatment with MBZ or ABZ caused significant decreases in the viability of cells and increased the percentage of cells with phosphatidylserine externalisation, indicative of early apoptosis, by approximately 25% compared to control (3%), similar to that of paclitaxel treatment. The percentage of cells positive for both annexin V and PI, indicative of late or secondary apoptosis, was also increased following treatment with MBZ, ABZ and paclitaxel. The percentage of necrotic cells, being positive for PI alone, was also slightly increased following MBZ and ABZ treatment but not paclitaxel treatment. This may be due to inaccurate compensation with spill-over of annexin-V labelled cells into the PI filter as the two labels have emission wavelengths that overlap slightly (Annexin-V 518 nm; PI 617 nm). These significant increases in apparent secondary apoptotic and necrotic cells were not observed following 48 hr treatments, whereas a large 20% increase in early apoptotic cells were still observed following treatments with MBZ, ABZ and paclitaxel (Figure 17). This suggests that along with paclitaxel, MBZ and ABZ cause significant increases in phosphatidylserine externalisation and further support their anticancer mechanism of action to involve an apoptotic pathway. This is also supported by a previous study where M-14 and SK-Mel-19 human melanoma cells were treated with 1 µM MBZ for 24 hrs and exhibited 25% and 31% of cells positive for annexin-V staining, respectively (Doudican *et al.*, 2008). ABZ has also previously been shown to increase annexin-V positive staining in SGC-7901 gastric cancer cells in a time- and concentration-dependent manner, also producing an approximate 20% increase in annexin-V positive cells following 24 hr treatment with 1 µM ABZ (Zhang *et al.*, 2017). Similar results have also been observed *in vivo* with ABZ (20 mg/kg) treatment increasing the percentage of apoptotic cells 5.4-fold compared to control ($p < 0.05$) in Ehrlich ascitic carcinoma (EAC) tumour cells grown in Balb-c mice (Castro *et al.*, 2016).

Internucleosomal DNA fragmentation is another hallmark of apoptosis. As previously mentioned, apoptosis is characterised by the activation of a range of endonucleases, particularly caspase-3 activated DNase (CAD), which once activated results in subsequent cleavage of nuclear DNA into internucleosomal fragments of roughly 180 base pairs and multiples thereof (360, 540 and so on) (Sakahira *et al.,* 1998). Following fixation with 70% ethanol which also permeabilises cell membranes, cells were stained with the DNA-binding dye propidium iodide (PI) and apoptotic cells can be identified on DNA content frequency histograms as cells with fractional ("sub-G_1") DNA content, commonly known as the Nicoletti assay (Lizard *et al.*, 1997; Riccardi *et al.*, 2006). Figure 18 shows the percentage of treated cells with sub-G1 DNA content. Similar to paclitaxel, both MBZ and ABZ exhibited time-dependent increases in the percentage of cells with sub-G1 DNA content. After 48 hr treatment, ABZ exhibited 15% of sub-G1 cells, with MBZ resulting in 22% of cells, similar to that of paclitaxel with 23% of sub-G1 cells, compared to 4% of control ($p < 0.0001$). MBZ (0.5 µM) has also previously been shown to time-dependently increase the percentage of subdiploid cells in H460 and A549 lung cancer cells. At 48 h, 35% of H460 cells and 15% of A549 cells were in the sub-G1 phase, indicating that MBZ induced cell death after mitotic arrest (Sasaki *et al.*, 2002). There is lack of sub-G1 analyses of ABZ treatment in cancer cells in the literature. However, in the same HT-29 colorectal cancer cell line using gel electrophoresis following 48 hr treatment with 1 µM ABZ, a DNA ladder effect was demonstrated indicating DNA fragmentation and activation of endonucleases (Pourgholami *et al.*, 2005).

With sufficient evidence of caspase-3 activation, phosphatidylserine externalisation and DNA fragmentation, it is clear that both MBZ and ABZ cause cell death via an apoptotic pathway in HT-29 colorectal cancer cells. Further analysis of cell cycle, mitochondrial and lysosomal membrane permeabilisation, ROS formation and tubulin alteration may lead to a better understanding as to how MBZ and ABZ induce apoptosis, and whether it is through an intrinsic or extrinsic pathway.

Mitochondrial membrane permeabilisation (MMP) is a universal feature of cell death and is often considered as the "point of no return" in the cascade of events leading to apoptosis. The

permeabilisation of the outer membrane is a sign of the intrinsic apoptotic pathway, due to the formation of MACs, composed of pro-apoptotic proteins Bax and/or Bak, causing the subsequent release of cytochrome c and other factors into the cytosol triggering the commitment step of the mitochondrial apoptotic cascade (Dejean *et al.*, 2005; Dejean *et al.*, 2006). The loss of the mitochondrial membrane potential (ΔΨm) is also associated with the permeabilisation of the outer mitochondrial membrane due to the loss of cytochrome c. Cytochrome c is essential for producing ΔΨm because it promotes the pumping the protons into the mitochondrial intermembrane space as it shuttles electrons from Complex III to Complex IV along the electron transport chain. Cytochrome c is released from the mitochondrial intermembrane space into the cytosol during apoptosis. This impairs its ability to shuttle electrons between Complex III and Complex IV and results in rapid dissipation of ΔΨm. Loss of ΔΨm is therefore closely associated with cytochrome c release during apoptosis and is often used as a surrogate marker for cytochrome c release in cells. The net negative charge across a healthy mitochondrion is maintained at approximately -180 mV, which can be detected by staining cells with positively charged dyes such as tetramethylrhodamine ethyl ester (TMRE). TMRE emits a red fluorescence that can be detected by flow cytometry or fluorescence microscopy and the level of TMRE fluorescence in stained cells can be used to determine whether mitochondria in a cell have high or low ΔΨm (Crowley *et al.*, 2016b).

Figure 19 shows the percentage of cells with depolarised ΔΨm/permeabilised mitochondrial membranes following treatment with MBZ, ABZ or paclitaxel. Approximately 20% of cells treated with either MBZ, ABZ or paclitaxel for 24 hrs exhibited depolarised ΔΨm, 6-fold higher than that of either control of DMSO treated cells. Similar results were seen following 48 hr treatment, however slightly less percentage of depolarised cells than 24 hrs, due to increased treatment exposure resulting in a greater number of dead cells. These results suggest that both MBZ and ABZ may induce apoptosis via the intrinsic pathway involving the permeabilisation of mitochondrial membranes, similar to that of paclitaxel which has also previously been shown to cause MMP and subsequent depolarisation of the ΔΨm in cancer cells (Ahn *et al.*, 2004). MMP induced by MBZ treatment in cancer cells has

currently not been directly examined in the literature however, these results are further supported by MBZ exhibiting significant dose-dependent (0.2 – 1.0 µM) increases in cytochrome c release in A549, H460 and H1299 lung cancer cells following 12 and 24 hr treatments (Mukhopadhyay *et al.*, 2002; Sasaki *et al.*, 2002). ABZ's direct effect on ΔΨm has previously been examined in MCF-7 breast cancer cells where it was shown that 100 µM ABZ significantly ($p < 0.1$) decreased ΔΨm compared to untreated control by approximately 20% following 6 hr treatment, which was restored when treated with 5 mM of the antioxidant N-acetylcysteine (NAC) (Castro *et al.*, 2016). There were no significant changes using concentrations less than 100 µM however, this may be due to the fact that MCF-7 cells are less sensitive to ABZ as seen in this present study (Figure 13-14), and that exposure for 6 hr may not have been a long enough time to witness any changes using lower concentrations of ABZ. The authors also describe that ABZ treatment increases the ratio of mitochondrial Bax/Bcl-xL, which induces Bax activation and cytochrome c release from the mitochondria, thereby confirming that ABZ induces the mitochondrial-associated pathway of apoptosis (Castro *et al.*, 2016).

To determine whether lysosomes played a role in the anticancer mechanism of action of MBZ and ABZ, LMP was measured in conjunction with cellular membrane permeabilisation using the dichromatic dye acridine orange. Figure 20 shows the percentage of cells with LMP following 24 and 48 hr treatment with MBZ, ABZ and paclitaxel, whereas Figure 21 shows the percentage of cells with permeabilised outer cell membranes. Following 24 hr treatment with either MBZ or ABZ there is a significant 33% increase in the percentage of cells with LMP compared to control ($p < 0.0001$, which proved to be even greater than paclitaxel (~20%). Forty-eight-hour treatment exhibited similar significant increases in the percentage of cells with LMP, however slightly less with MBZ and ABZ but a greater time-dependent increase was seen with paclitaxel (Figure 13). The reason for this may be similar to that of Figure 19 and MMP, with the longer treatment period resulting in more dead cells and less cells in the process of dying and with a measurable LMP. However, interestingly paclitaxel treatment caused a time-dependent increase in the percentage of cells with LMP. The results seen in Figure 21 involving the percentage of cells with permeabilised outer cell membranes

almost exactly match that of the LMP results (Figure 20) with both MBZ and ABZ treatment, as well as with paclitaxel. All three treatments caused significant cell membrane permeabilisation to the same extent as LMP at both 24 and 48 hrs. This suggests that both MBZ and ABZ treatments do not target the lysosome and promote permeabilisation directly, which would lead to lysosomal-triggered apoptosis, as the percentage of LMP would be greater than cell membrane permeabilisation at any one time. Results rather suggests that LMP is a symptom of apoptosis triggered elsewhere, independent to the lysosome, as the percentage of cell membrane permeabilisation is virtually equal to that of the percentage of cells with LMP. Also, the results seen from MBZ and ABZ treatment are similar to that of paclitaxel, which is not a lysosomotropic compound and does not target the lysosome directly to cause apoptosis, but rather exhibits LMP following apoptosis induction (Bröker *et al.*, 2004). To further confirm that MBZ and ABZ are not directly targeting the lysosome and inducing LMP, earlier time points should be examined in the future such as at 3, 6 and 12 hours. Currently, this is believed to be the only assessment of MBZ and ABZ treatment on LMP in cancer cells.

Limited studies have been performed on assessing ROS in cells treated with MBZ and ABZ. As both mitochondrial and lysosomal membranes have been determined to permeabilise following MBZ and ABZ treatment, releasing their contents into the cytosol, it was hypothesised that there would be an increase in the production of ROS, as mitochondria are the major ROS-generating organelle and lysosomes contain H_2O_2 as well as the main pool of chelatable iron, capable of catalysing Fenton-type reactions. The DTNB assay which measures free sulfhydryl content, as an indirect measurement of ROS formation was used, as ROS such as hydroxyl and peroxyl radicals, superoxide and hydrogen peroxide cause damage by reacting with macromolecules like lipids, DNA and proteins where they are able to oxidise sulfhydryl groups (Liou *et al.*, 2010). MBZ, ABZ and paclitaxel all exhibited significant decreases in free sulfhydryl content to nearly 50% of both control and DMSO vehicle-control following 48 hr treatments (Figure 22). This suggested that both MBZ and ABZ cause increases in ROS and may contribute to their mechanism of anticancer action, however as this was only carried out following 48 hrs of treatment, it is likely that this increase in ROS activity (as

measured by decreases in free sulfhydryl content) is merely a symptom of apoptosis that has already been induced by the permeabilisation and leakage of mitochondria and lysosomes. Paclitaxel has previously been shown to produce apoptosis in leukaemia cells via intracellular ROS generation and activation of the JNK pathway, independent to its microtubule action and may suggest that MBZ and ABZ may behave similarly (Meshkini *et al.,* 2012). However, there is very little examination of MBZ and ABZ on ROS production in cancer cells in the literature, but one previous study has shown that ABZ induces oxidative stress promoting DNA fragmentation and triggering apoptosis and inducing cell death (Castro *et al.*, 2016). Future studies with MBZ and ABZ should investigate earlier time-points, with additional assays that measure ROS production more directly such as with the DCFDA assay, as well as using antioxidants like NAC and examine whether they can rescue the effects seen with MBZ and ABZ treatments.

As MBZ and ABZ are known to inhibit tubulin polymerisation in helminths and likely to interact with tubulin in cancer cells, the effect of treatment on cell cycle was then assessed. Other MTAs such as paclitaxel and nocodazole are well known to affect the cell cycle and cause arrest leading to the induction of apoptosis (Blajeski *et al.*, 2002). Figures 23-25 show the effects of MBZ, ABZ and paclitaxel on cell cycle following 24 and 48 hr treatments. At both time-points all three treatments exhibited significant changes in the percentage of cells in sub-G1, G1, S, G2/M and >G2/M phases compared to untreated control and DMSO vehicle control. As already discussed, all three treatments caused significant time-dependent increases in the percentage of cells in the sub-G1 phase. However, the most important results seen here are the significantly large increases in the percentage of cells in the G2/M phase following treatment with either MBZ or ABZ, at both 24 and 48 hrs, similar to that of the paclitaxel treatment. These large increases in the percentage of cells in the G2/M phase lead to a subsequent decrease in the percentage of cells in both the G1 and S phases. Not surprisingly, paclitaxel caused significant G2/M arrest, which has been well documented before in a range of cancer cell lines including ovarian, breast, lung and glioma, and caused hyperstabilisation of microtubule dynamics leading to mitotic arrest in the G2/M phase and thus causing subsequent

induction of apoptosis (Shu *et al.*, 1997; Vikhanskaya *et al.*, 1998; Das *et al.*, 2001; Han B., 2016). However, it is worth noting that paclitaxel may also cause induction of apoptosis in a manner independent to G2/M arrest, and still kill cells via the microtubule system but uncoupled from mitotic arrest and cause apoptosis during other phases of the cell cycle, as well as the possibility of causing apoptosis through altering gene expression (Fan, 1999). From these results it is clear to see that both MBZ and ABZ cause significant increases in cells arrested in the G2/M phase, similar to paclitaxel, indicating that they interact with microtubule dynamics and cause mitotic arrest leading to induction of apoptosis. This is supported by previous studies, which have also observed significant G2/M cell cycle arrest following treatment with MBZ or ABZ. In the H460 lung cancer cell line MBZ (0.5 µM) treatment caused significant time-dependent increases in cells arrested at the G2/M phase (Mukhopadhyay *et al.*, 2002; Sasaki *et al.*, 2002). The authors found that the cells were blocked at the G2-M phase 12 h after MBZ treatment before undergoing apoptosis. Cells were rounded and partly detached after 12 h of MBZ treatment. However, after 24 h of treatment, cell shrinkage occurred, and nuclear bodies were evident; the cells subsequently underwent apoptosis. After 48 h of MBZ treatment, ~60% of the cells had undergone apoptosis with characteristic nuclear fragmentation. Similar results have also been observed in melanoma and triple-negative breast cancer cell lines, in particular refractory $NRAS^{Q61K}$ melanomas where MBZ (0.1 µM) caused significant ($p < 0.01$) increases in cells at the G2/M phase following 8 hr treatment, and also in SUM159PT cells where MBZ (0.35 µM) caused a significant ($p < 0.001$) increase in the percentage of cells in the G2/M phase following 24 hr treatment (Simbulan-Rosenthal *et al.*, 2017; Zhang *et al.*, 2019). ABZ has also previously been shown to induce G2/M arrest in a dose-dependent manner (0 – 1 µM) over 24 hrs in the human gastric cancer cell lines MKN-45, SGC-7901 and MKN-28 (Zhang *et al.*, 2017). ABZ (20 mg/kg) also significantly ($p < 0.001$) increased the percentage of EAC cells in the G2/M phase, obtained from inoculated balb-c mice, treated once daily for nine days (Castro *et al.*, 2016). ABZ (1 µM) also exhibited time-dependent increases in the percentage of HT-29 cells in the G2/M phase,

where during the first 24 hrs cells in the G2/M phase increased from 1.3 ± 0.3% to 88.1 ± 0.9% (Pourgholami *et al.*, 2005).

There is a high likelihood that the reason behind the G2/M arrest caused by ABZ and MBZ treatment is due to interactions with microtubules, such as promoting depolymerisation. However, there is still the possibility of microtubule-independent causes, such as altered gene expression and inhibition/induction of microtubule-associated proteins (MAPs) and other cell cycle regulators such as cyclins and cyclin-dependent kinases (CDKs). Unfortunately, no such assessments were carried out in this study but previous studies have given understanding as to how MBZ and ABZ affect these other potential targets. In the NSCLC cells A549 and H460 it was found that MBZ (0.5 μM) induced depolymerisation of tubulin and inhibited normal spindle formation in NSCLC cells, resulting in mitotic arrest at the G2/M phase and cell death (Sasaki *et al.*, 2002). MBZ treatment also induced changes in the expression of cell cycle-regulatory proteins and initiated a phosphorylation cascade resulting in the phosphorylation of MPM-2 and Cdc25C in NCSLC cells. These dynamic changes in protein expression and modification are consistent with mitotic arrest (Morris *et al.*, 2000). During a normal cell cycle, the progression of G2 cells to M phase is triggered by the activation of MPF, whose activity is predominantly regulated by the phosphorylation/dephosphorylation of CDK1, as well as the synthesis, degradation and subcellular localisation of cyclin B1. Previous studies have found that the M/G1 transition requires the degradation of cyclin B1 (Surana *et al.*, 1993; Yamano *et al.*, 1996). Therefore, high levels of cyclin B trigger cell cycle arrest during the M phase; however, they also prevent cell division (Gallant *et al.*, 1992; Choi *et al.*, 2011). Treatment of SGC-7901 cells with various concentrations of ABZ (0.25-1.0 μM) for 24 h dose-dependently led to increased expression of cyclin B1 up to two-fold higher than control, which may be a plausible reason for the M-phase arrest observed (Zhang *et al.*, 2017). However, in the same study ABZ was observed to cause depolymerisation of microtubules and prevent spindle formation and this is likely to be the main reason behind the G2/M arrest.

Identifying G2/M arrest following ABZ/MBZ treatment is not sufficient enough evidence to indicate the interference with microtubule dynamics. Therefore, using fluorescent microscopy and antibodies for alpha-tubulin – a main component of the tubulin dimer that polymerises to form microtubules – and acetylated-alpha-tubulin – an indicator of stabilised microtubules – it was possible to observe the effects of both ABZ and MBZ treatment on microtubules of HT-29 cells, and compare that to untreated control as well as paclitaxel. Figure 26 shows treated cells stained with Hoechst 33342, alpha-tubulin and ac-alpha-tubulin antibodies. Staining was not quantified however, but provides a visual indication as to how MBZ and ABZ affect microtubule and nuclear morphology. From the nuclear staining, both MBZ and ABZ treatments show brighter smaller nuclei compared to control, indicating the condensation of nuclei, a classical marker of apoptosis. This is also seen with paclitaxel treatment, however interestingly also observed in only paclitaxel treatment were cells with multiple nuclei, which is common in cells exiting mitosis following treatment with taxanes or vinca alkaloids as they often develop lobulated nuclei and multiple micronuclei, hinting at the possible differences between MBZ/ABZ and other MTAs (Jordan *et al.*, 1992; Theodoropoulos *et al.*, 1999). Both MBZ and ABZ produced diminished fluorescent intensities of cells stained with both alpha-tubulin and ac-alpha-tubulin compared to control. Whereas paclitaxel treatment produced much greater intensities with both alpha-tubulin and ac-alpha-tubulin stained cells compared to control. This suggests that MBZ and ABZ may destabilise microtubules and promote depolymerisation as ac-alpha-tubulin staining is a marker of stabilised cells, which is very prominent in paclitaxel treated cells as paclitaxel is a well-known hyperstabiliser of microtubule dynamics (Al-Bassam *et al.*, 2012). The decreased intensity of cells stained with the anti-alpha-tubulin following MBZ and ABZ treatment was unexpected, as it was only hypothesised that they would only decrease the intensity of the stabilised acetylated form. However, in paclitaxel treated cells there was a higher intensity of fluorescence of alpha-tubulin, therefore it may be possible that the antibody only optimally binds or fluoresces when tubulin is in the polymerised form, hence giving a low fluorescence intensity following MBZ and ABZ treatment as these drugs promote depolymerisation. Previous studies have also shown similar

results with MBZ treatment using fluorescent microscopy. In A549 lung cancer cells following 14 hr MBZ (0.5 µM) treatment, many mitotic cells had abnormally reduced numbers of spindles or had monopolar (monoaster) spindles. These spindle abnormalities were very similar to those in cells treated with nocodazole, a similar structurally-related benzimidazole, but completely different from the aggregated spindles present in paclitaxel-treated cells (Sasaki *et al.*, 2002). In the melanoma cell lines melan-a, M-14, and SK-Mel-19, cells were treated with MBZ (0.5 µM) for 14 hrs and stained with anti-alpha-tubulin. Overall microtubular network disarray in melan-a, M-14, and SK-Mel-19 cells were observed following MBZ treatment, characterized by diffuse staining. This is in contrast to the vehicle-treated melanocytes and melanoma cells which displayed discrete networks of microtubule structure. Furthermore, mitotic figures, when observed in MBZ-treated cells, had an abnormal appearance with improperly aligned chromosomes (Doudican *et al.*, 2008). ABZ treatment has also been shown to cause similar results in the human gastric cancer cell line SGC-7901 (Zhang *et al.*, 2017). The untreated control SGC-7901 cells showed an organised distribution of microtubules; treated cells that were exposed to 0.5 µM ABZ for 18 hr displayed irregular microtubule formation. In interphase cells, microtubules were less well dispersed with a fuzzy network structure, and appeared thicker and depolymerised. Mitotic cells were notably increased in size and primarily featured multipolar spindles and uncompressed chromosomes.

These microscopy results, in conjunction with results from previous literature, suggest that both MBZ and ABZ affect tubulin structure in cancer cells and promote depolymerisation, in contrast to paclitaxel which affects tubulin dynamics by promoting polymerisation and stabilisation. This has been further confirmed with both MBZ and ABZ treatment producing increases in the soluble/insoluble tubulin ratios in cancer cells, i.e. decreasing the amount of insoluble polymerised tubulin - an indicator of tubulin depolymerisation. In A549 lung cancer cells the ratio of depolymerised: polymerised tubulin was 0.75 ± 0.12 for MBZ-treated cells, 1.46 ± 0.25 for nocodazole-treated cells, 0.16 ± 0.03 for paclitaxel-treated cells, and 0.42 ± 0.06 for DMSO-treated

control cells (Sasaki *et al.*, 2002). Even 4 hrs of incubation with MBZ was enough to significantly enhance the depolymerisation of tubulin in A549 cells compared to vehicle-control cells, but the magnitude of this effect by MBZ was significantly less than that by nocodazole, which is a well-known potent microtubule depolymerising agent (Blajeski *et al.*, 2002). Paclitaxel further decreased the ratio in contrast to MBZ and nocodazole treated cells, which is expected due to paclitaxel promoting polymerisation and causing greater amounts of insoluble microtubules. ABZ has also been shown to significantly decrease the insoluble fraction (polymerised) of microtubules in SGC-7901 cells in a dose-dependent (0.25 – 1 μM) manner over 24 hrs, also confirming the depolymerising nature of ABZ (Zhang *et al.*, 2017).

Future directions for this study would also include confirming the destabilisation of microtubules by MBZ and ABZ, which has already been carried out and proven *in vitro* as previously mentioned (Blajeski *et al.*, 2002; Sasaki *et al.*, 2002; Bai *et al.*, 2011; Zhang *et al.*, 2017), as well as identifying the binding site to which MBZ and ABZ interact with microtubules. The microtubule binding site of MBZ and likely that of ABZ as well, has already been confirmed to be the same as the colchicine site in helminths and has more recently been shown to be the same with mammalian tubulin (Friedman *et al.*, 1980; Laclette *et al.*, 1980; Russell *et al.*, 1995; Jornet *et al.*, 2016). Using laser flash photolysis, Jornet *et al* showed that MBZ and related anticancer benzimidazoles act by binding the β-subunit of tubulin before dimerisation with α-tubulin with subsequent blocking of microtubule formation.

The next step with MBZ and ABZ would include animal studies and looking at the anticancer effects *in vivo*. Fortunately, a few studies have already proven the anticancer potential of both MBZ and ABZ *in vivo*, with MBZ (p.o) treatment significantly inhibiting tumour growth in human adrenocortical carcinoma and lung cancer cells implanted in mice (Mukhopadhyay *et al.*, 2002; Martarelli *et al.*, 2008). ABZ (150 mg/kg, i.p.) has also been shown to significantly ($p < 0.001$) suppress tumour growth in a xenograft model of peritoneal carcinomatosis using nude mice implanted with HT-29 cells (Pourgholami *et al.*, 2005). MBZ (50 mg/kg, p.o) and ABZ (150 mg/kg, p.o) have both exhibited significant inhibition in cancer cell growth in both *in vitro* and *in vivo* models of glioblastoma

multiforme (GBM), with MBZ proving to be more efficacious most, likely due to the difference in bioavailability in these models (Bai *et al.*, 2011). The limited solubility of ABZ and MBZ in water and organic solvents greatly affects absorption and behaviour in the body, with ABZ reported to have between 5-10% bioavailability whereas MBZ has been reported to have between 5-10% and 17-22% in healthy human volunteers, with both drugs undergoing extensive first-pass metabolism (Dayan, 2003). In GBM cell lines, MBZ displayed cytotoxicity, with half-maximal inhibitory concentrations ranging from 0.1 to 0.3 μM, much more potent than in the colorectal HT-29 cancer cells. MBZ disrupted microtubule formation in GBM cells, and *in vitro* activity was correlated with reduced tubulin polymerisation. Subsequently, the authors showed that MBZ significantly extended mean survival up to 63% in syngeneic and xenograft orthotopic mouse glioma models (Bai *et al.*, 2011).

Based on the evidence supplied, it is in contention that human clinical trials of MBZ in a range of cancer types is warranted, with MBZ preferred over ABZ due to being more efficacious and having a better safety profile. The known pharmacokinetics, relatively low toxicity (even with extended high-dosing protocols), low cost, and strong pre-clinical evidence make this an ideal candidate for re-purposing. Currently, there are two early phase clinical trials getting under way, both in glioma and a relatively recent trial in GI cancer and cancer of unknown origin NCT01729260, NCT01837862, NCT03628079. In addition to these, the evidence suggests that candidate cancer types to take to human trial include: melanoma (Doudican *et al.*, 2013), non-small cell lung cancer (Sasaki *et al.*, 2002), adrenocortical cancer (Martarelli *et al.*, 2008), and colon cancer (Mukhopadhyay *et al.*, 2002).

5.1 Conclusion

Overall, the results from this study have identified that both MBZ and ABZ produce cell death via an intrinsic apoptotic pathway, stemming from cell cycle arrest at the G2/M phase due to the depolymerisation of microtubules. Significant caspase-3 activation, phosphatidylserine externalisation and DNA fragmentation were all observed following treatment with MBZ or ABZ suggesting that cell death is via an apoptotic pathway, supported by other previous studies.

Mitochondrial membrane permeabilisation suggests that apoptosis follows the intrinsic pathway, rather than the receptor-mediated extrinsic pathway, with evidence of increased ROS production. Lysosomal membrane permeabilisation is also evident with both MBZ and ABZ treatments, however its involvement remains to be further elucidated as at the time points tested it appears to be a symptom of already induced apoptosis rather than the causative effect. Finally, both MBZ and ABZ cause mitotic arrest at the G2/M phase of the cell cycle, indicative of MTAs, and appear by fluorescent staining to be in agreement with published literature, where they cause depolymerisation of microtubules.

Chapter 6: References

Ahmed D, Eide PW, Eilertsen IA, Danielsen SA, Eknæs M, Hektoen M*, et al.* (2013). Epigenetic and genetic features of 24 colon cancer cell lines. Oncogenesis **2**(9)**:** e71.

Ahn HJ, Kim YS, Kim J-U, Han SM, Shin JW, Yang HO (2004). Mechanism of taxol-induced apoptosis in human SKOV3 ovarian carcinoma cells. J Cell Biochem **91**(5)**:** 1043-1052.

Aits S, Jäättelä M (2013a). Lysosomal cell death at a glance. J Cell Sci **126**(9)**:** 1905-1912.

Akhmanova A, Steinmetz MO (2015). Control of microtubule organization and dynamics: two ends in the limelight. Nat Rev Mol Cell Biol **16:** 711.

Al-Bassam J, Corbett KD (2012). α-Tubulin acetylation from the inside out. Proceedings of the National Academy of Sciences **109**(48)**:** 19515-19516.

Alushin Gregory M, Lander Gabriel C, Kellogg Elizabeth H, Zhang R, Baker D, Nogales E (2014). High-Resolution Microtubule Structures Reveal the Structural Transitions in αβ-Tubulin upon GTP Hydrolysis. Cell **157**(5)**:** 1117-1129.

Appelqvist H, Johansson AC, Linderoth E, Johansson U, Antonsson B, Steinfeld R*, et al.* (2012). Lysosome-mediated apoptosis is associated with cathepsin D-specific processing of bid at Phe24, Trp48, and Phe183. Ann Clin Lab Sci **42**(3)**:** 231-242.

Ashburn TT, Thor KB (2004). Drug repositioning: identifying and developing new uses for existing drugs. Nat Rev Drug Discov **3**(8)**:** 673-683.

Bai RY, Staedtke V, Aprhys CM, Gallia GL, Riggins GJ (2011). Antiparasitic mebendazole shows survival benefit in 2 preclinical models of glioblastoma multiforme. Neuro Oncol **13**(9)**:** 974-982.

Blajeski AL, Phan VA, Kottke TJ, Kaufmann SH (2002). G(1) and G(2) cell-cycle arrest following microtubule depolymerization in human breast cancer cells. J Clin Invest **110**(1)**:** 91-99.

Borisy GG, Taylor EW (1967a). THE MECHANISM OF ACTION OF COLCHICINE. Binding of Colchincine-3H to Cellular Protein. J Cell Biol **34**(2)**:** 525-533.

Borisy GG, Taylor EW (1967b). The mechanism of action of colchicine. Colchicine binding to sea urchin eggs and the mitotic apparatus. J Cell Biol **34**(2)**:** 535-548.

Boya P, Gonzalez-Polo RA, Poncet D, Andreau K, Vieira HL, Roumier T*, et al.* (2003). Mitochondrial membrane permeabilization is a critical step of lysosome-initiated apoptosis induced by hydroxychloroquine. Oncogene **22**(25)**:** 3927-3936.

Boya P, Kroemer G (2008b). Lysosomal membrane permeabilization in cell death. Oncogene **27**(50)**:** 6434-6451.

BPAC (2012). Surveillance of people at increased risk of colorectal cancer. BPJ(44)**:** 18-25.

Brinkley W (1997). Microtubules: a brief historical perspective. J Struct Biol **118**(2)**:** 84-86.

Bröker LE, Huisman C, Span SW, Rodriguez JA, Kruyt FAE, Giaccone G (2004). Cathepsin B Mediates Caspase-Independent Cell Death Induced by Microtubule Stabilizing Agents in Non-Small Cell Lung Cancer Cells. Cancer Res **64**(1)**:** 27-30.

Brunk UT, Dalen H, Roberg K, Hellquist HB (1997). Photo-oxidative disruption of lysosomal membranes causes apoptosis of cultured human fibroblasts. Free Radic Biol Med **23**(4)**:** 616-626.

Castro L, Kviecinski MR, Ourique F, Parisotto EB, Grinevicius V, Correia JFG*, et al.* (2016). Albendazole as a promising molecule for tumor control. Redox Biol **10:** 90-99.

Choi HJ, Fukui M, Zhu BT (2011). Role of cyclin B1/Cdc2 up-regulation in the development of mitotic prometaphase arrest in human breast cancer cells treated with nocodazole. PLoS One **6**(8)**:** e24312.

Cirman T, Oresic K, Mazovec GD, Turk V, Reed JC, Myers RM*, et al.* (2004). Selective disruption of lysosomes in HeLa cells triggers apoptosis mediated by cleavage of Bid by multiple papain-like lysosomal cathepsins. J Biol Chem **279**(5)**:** 3578-3587.

Conus S, Perozzo R, Reinheckel T, Peters C, Scapozza L, Yousefi S*, et al.* (2008). Caspase-8 is activated by cathepsin D initiating neutrophil apoptosis during the resolution of inflammation. J Exp Med **205**(3)**:** 685-698.

Cory S, Adams JM (2002). The Bcl2 family: regulators of the cellular life-or-death switch. Nat Rev Cancer **2**(9)**:** 647-656.

Crowley LC, Christensen ME, Waterhouse NJ (2016b). Measuring Mitochondrial Transmembrane Potential by TMRE Staining. Cold Spring Harb Protoc **2016**(12).

Das GC, Holiday D, Gallardo R, Haas C (2001). Taxol-induced cell cycle arrest and apoptosis: dose-response relationship in lung cancer cells of different wild-type p53 status and under isogenic condition. Cancer Lett **165**(2)**:** 147-153.

Davies H, Bignell GR, Cox C, Stephens P, Edkins S, Clegg S*, et al.* (2002). Mutations of the BRAF gene in human cancer. Nature **417**(6892)**:** 949-954.

Dayan AD (2003). Albendazole, mebendazole and praziquantel. Review of non-clinical toxicity and pharmacokinetics. Acta Tropica **86**(2)**:** 141-159.

Dejean LM, Martinez-Caballero S, Guo L, Hughes C, Teijido O, Ducret T*, et al.* (2005). Oligomeric Bax is a component of the putative cytochrome c release channel MAC, mitochondrial apoptosis-induced channel. Mol Biol Cell **16**(5)**:** 2424-2432.

Dejean LM, Martinez-Caballero S, Manon S, Kinnally KW (2006). Regulation of the mitochondrial apoptosis-induced channel, MAC, by BCL-2 family proteins. Biochim Biophys Acta **1762**(2)**:** 191-201.

Delgado ME, Olsson M, Lincoln FA, Zhivotovsky B, Rehm M (2013). Determining the contributions of caspase-2, caspase-8 and effector caspases to intracellular VDVADase activities during apoptosis initiation and execution. Biochim Biophys Acta **1833**(10)**:** 2279-2292.

Desai A, Mitchison TJ (1997). Microtubule polymerization dynamics. Annu Rev Cell Dev Biol **13:** 83-117.

Dewson G, Kratina T, Czabotar P, Day CL, Adams JM, Kluck RM (2009). Bak activation for apoptosis involves oligomerization of dimers via their alpha6 helices. Mol Cell **36**(4)**:** 696-703.

Dhomen N, Marais R (2007). New insight into BRAF mutations in cancer. Curr Opin Genet Dev **17**(1)**:** 31-39.

Dorléans A, Gigant B, Ravelli RBG, Mailliet P, Mikol V, Knossow M (2009). Variations in the colchicine-binding domain provide insight into the structural switch of tubulin. Proceedings of the National Academy of Sciences **106**(33)**:** 13775-13779.

Doudican N, Rodriguez A, Osman I, Orlow SJ (2008). Mebendazole Induces Apoptosis via Bcl-2 Inactivation in Chemoresistant Melanoma Cells. Mol Cancer Res **6**(8)**:** 1308-1315.

Doudican NA, Byron SA, Pollock PM, Orlow SJ (2013). XIAP downregulation accompanies mebendazole growth inhibition in melanoma xenografts. Anticancer Drugs **24**(2)**:** 181-188.

Droga-Mazovec G, Bojic L, Petelin A, Ivanova S, Romih R, Repnik U*, et al.* (2008). Cysteine cathepsins trigger caspase-dependent cell death through cleavage of bid and antiapoptotic Bcl-2 homologues. J Biol Chem **283**(27)**:** 19140-19150.

Elie-Caille C, Severin F, Helenius J, Howard J, Muller DJ, Hyman AA (2007). Straight GDP-Tubulin Protofilaments Form in the Presence of Taxol. Current Biology **17**(20)**:** 1765-1770.

Ellman GL (1959). Tissue sulfhydryl groups. Archives of Biochemistry and Biophysics **82**(1)**:** 70-77.

Elmore S (2007). Apoptosis: a review of programmed cell death. Toxicol Pathol **35**(4)**:** 495-516.

Enari M, Sakahira H, Yokoyama H, Okawa K, Iwamatsu A, Nagata S (1998). A caspase-activated DNase that degrades DNA during apoptosis, and its inhibitor ICAD. Nature **391**(6662)**:** 43-50.

Fadok VA, Voelker DR, Campbell PA, Cohen JJ, Bratton DL, Henson PM (1992). Exposure of phosphatidylserine on the surface of apoptotic lymphocytes triggers specific recognition and removal by macrophages. J Immunol **148**(7)**:** 2207-2216.

Fan W (1999). Possible Mechanisms of Paclitaxel-Induced Apoptosis. Biochem Pharmacol **57**(11)**:** 1215-1221.

Fan Z, Beresford PJ, Oh DY, Zhang D, Lieberman J (2003). Tumor suppressor NM23-H1 is a granzyme A-activated DNase during CTL-mediated apoptosis, and the nucleosome assembly protein SET is its inhibitor. Cell **112**(5)**:** 659-672.

Feldstein AE, Werneburg NW, Li Z, Bronk SF, Gores GJ (2006). Bax inhibition protects against free fatty acid-induced lysosomal permeabilization. Am J Physiol Gastrointest Liver Physiol **290**(6)**:** G1339-1346.

Fesik SW, Shi Y (2001). Structural biology. Controlling the caspases. Science **294**(5546)**:** 1477-1478.

Fojo AT, Menefee M (2005). Microtubule Targeting Agents: Basic Mechanisms of Multidrug Resistance (MDR). Seminars in Oncology **32:** 3-8.

Friedman PA, Platzer EG (1980). Interaction of anthelmintic benzimidazoles with Ascaris suum embryonic tubulin. Biochim Biophys Acta **630**(2)**:** 271-278.

Fu P, MacMillan JB (2015). Thiasporines A–C, Thiazine and Thiazole Derivatives from a Marine-Derived Actinomycetospora chlora. J Nat Prod **78**(3)**:** 548-551.

Gallant P, Nigg EA (1992). Cyclin B2 undergoes cell cycle-dependent nuclear translocation and, when expressed as a non-destructible mutant, causes mitotic arrest in HeLa cells. J Cell Biol **117**(1)**:** 213-224.

Gigant B, Wang C, Ravelli RBG, Roussi F, Steinmetz MO, Curmi PA*, et al.* (2005). Structural basis for the regulation of tubulin by vinblastine. Nature **435:** 519.

Greenhalgh DG (1998). The role of apoptosis in wound healing. Int J Biochem Cell Biol **30**(9)**:** 1019-1030.

Gududuru V, Hurh E, Dalton JT, Miller DD (2005). Discovery of 2-Arylthiazolidine-4-carboxylic Acid Amides as a New Class of Cytotoxic Agents for Prostate Cancer. J Med Chem **48**(7)**:** 2584-2588.

Han B. LM (2016). Paclitaxel-Induced G2/M Arrest via Different Mechanism of Actions in Glioma Cell Lines with Differing p53 Mutational Status. Int J Pharmacol **12**(1)**:** 19-27.

Hay M, Thomas DW, Craighead JL, Economides C, Rosenthal J (2014). Clinical development success rates for investigational drugs. Nat Biotechnol **32**(1)**:** 40-51.

Hitoshi Y, Lorens J, Kitada SI, Fisher J, LaBarge M, Ring HZ*, et al.* (1998). Toso, a cell surface, specific regulator of Fas-induced apoptosis in T cells. Immunity **8**(4)**:** 461-471.

Hsu H, Xiong J, Goeddel DV (1995). The TNF receptor 1-associated protein TRADD signals cell death and NF-kappa B activation. Cell **81**(4)**:** 495-504.

Johnson IS, Armstrong JG, Gorman M, Burnett JP, Jr. (1963). THE VINCA ALKALOIDS: A NEW CLASS OF ONCOLYTIC AGENTS. Cancer Res **23:** 1390-1427.

Jordan MA, Thrower D, Wilson L (1992). Effects of vinblastine, podophyllotoxin and nocodazole on mitotic spindles. Implications for the role of microtubule dynamics in mitosis. J Cell Sci **102**(3)**:** 401-416.

Jordan MA, Wilson L (2004). Microtubules as a target for anticancer drugs. Nat Rev Cancer **4:** 253.

Jornet D, Bosca F, Andreu JM, Domingo LR, Tormos R, Miranda MA (2016). Analysis of mebendazole binding to its target biomolecule by laser flash photolysis. J Photochem Photobiol B **155:** 1-6.

Kagedal K, Johansson AC, Johansson U, Heimlich G, Roberg K, Wang NS*, et al.* (2005). Lysosomal membrane permeabilization during apoptosis--involvement of Bax? Int J Exp Pathol **86**(5)**:** 309-321.

Kagedal K, Johansson U, Ollinger K (2001a). The lysosomal protease cathepsin D mediates apoptosis induced by oxidative stress. Faseb j **15**(9)**:** 1592-1594.

Kagedal K, Zhao M, Svensson I, Brunk UT (2001b). Sphingosine-induced apoptosis is dependent on lysosomal proteases. Biochem J **359**(Pt 2)**:** 335-343.

Kajstura M, Halicka HD, Pryjma J, Darzynkiewicz Z (2007). Discontinuous fragmentation of nuclear DNA during apoptosis revealed by discrete "sub-G1" peaks on DNA content histograms. Cytometry A **71**(3)**:** 125-131.

Kataoka T, Schroter M, Hahne M, Schneider P, Irmler M, Thome M*, et al.* (1998). FLIP prevents apoptosis induced by death receptors but not by perforin/granzyme B, chemotherapeutic drugs, and gamma irradiation. J Immunol **161**(8)**:** 3936-3942.

Kavallaris M (2010). Microtubules and resistance to tubulin-binding agents. Nat Rev Cancer **10:** 194.

Kavallaris M, Tait AS, Walsh BJ, He L, Horwitz SB, Norris MD*, et al.* (2001). Multiple microtubule alterations are associated with Vinca alkaloid resistance in human leukemia cells. Cancer Res **61**(15)**:** 5803-5809.

Kellogg EH, Hejab NMA, Howes S, Northcote P, Miller JH, Díaz JF*, et al.* (2017). Insights into the Distinct Mechanisms of Action of Taxane and Non-Taxane Microtubule Stabilizers from Cryo-EM Structures. J of Mol Biol **429**(5)**:** 633-646.

Kerr JF (2002). History of the events leading to the formulation of the apoptosis concept. Toxicol **181-182:** 471-474.

Kerr JF, Wyllie AH, Currie AR (1972). Apoptosis: a basic biological phenomenon with wide-ranging implications in tissue kinetics. Br J Cancer **26**(4)**:** 239-257.

Kim H-E, Du F, Fang M, Wang X (2005a). Formation of apoptosome is initiated by cytochrome c-induced dATP hydrolysis and subsequent nucleotide exchange on Apaf-1. Proceedings of the National Academy of Sciences of the United States of America **102**(49)**:** 17545-17550.

Kim H, Tu HC, Ren D, Takeuchi O, Jeffers JR, Zambetti GP*, et al.* (2009). Stepwise activation of BAX and BAK by tBID, BIM, and PUMA initiates mitochondrial apoptosis. Mol Cell **36**(3)**:** 487-499.

Kim H, Yang I, Patil RS, Kang S, Lee J, Choi H*, et al.* (2014). Anithiactins A–C, Modified 2-Phenylthiazoles from a Mudflat-Derived Streptomyces sp. J Nat Prod **77**(12)**:** 2716-2719.

Kim HE, Du F, Fang M, Wang X (2005b). Formation of apoptosome is initiated by cytochrome c-induced dATP hydrolysis and subsequent nucleotide exchange on Apaf-1. Proc Natl Acad Sci U S A **102**(49)**:** 17545-17550.

Kischkel FC, Hellbardt S, Behrmann I, Germer M, Pawlita M, Krammer PH*, et al.* (1995). Cytotoxicity-dependent APO-1 (Fas/CD95)-associated proteins form a death-inducing signaling complex (DISC) with the receptor. Embo j **14**(22)**:** 5579-5588.

Kozikowski BA, Burt TM, Tirey DA, Williams LE, Kuzmak BR, Stanton DT*, et al.* (2003). The Effect of Room-Temperature Storage on the Stability of Compounds in DMSO. Jf Biomol Screening **8**(2)**:** 205-209.

Kurz T, Terman A, Gustafsson B, Brunk UT (2008a). Lysosomes and oxidative stress in aging and apoptosis. Biochim Biophys Acta **1780**(11)**:** 1291-1303.

Kurz T, Terman A, Gustafsson B, Brunk UT (2008b). Lysosomes in iron metabolism, ageing and apoptosis. Histochem Cell Biol **129**(4)**:** 389-406.

Laclette JP, Guerra G, Zetina C (1980). Inhibition of tubulin polymerization by Mebendazole. Biochem Biophys Res Coms **92**(2)**:** 417-423.

Lamb RA, Badart MP, Swaney BE, Gai S, Baird SK, Hawkins BC (2015). The Synthesis and Biological Evaluation of Anithiactin A/Thiasporine C and Analogues. Aust J Chem **68**(12)**:** 1829.

Lazic SE (2010). The problem of pseudoreplication in neuroscientific studies: is it affecting your analysis? BMC Neurosci **11**(1)**:** 1-17.

Liou GY, Storz P (2010). Reactive oxygen species in cancer. Free Radic Res **44**(5)**:** 479-496.

Lizard G, Miguet C, Gueldry S, Monier S, Gambert P (1997). [Flow cytometry measurement of DNA fragmentation in the course of cell death via apoptosis. New techniques for evaluation of DNA status for the pathologist]. Ann Pathol **17**(1)**:** 61-66.

Locksley RM, Killeen N, Lenardo MJ (2001). The TNF and TNF receptor superfamilies: integrating mammalian biology. Cell **104**(4)**:** 487-501.

Logue SE, Martin SJ (2008). Caspase activation cascades in apoptosis. Biochem Soc Trans **36**(Pt 1)**:** 1-9.

Lu KH, Lue KH, Chou MC, Chung JG (2005). Paclitaxel induces apoptosis via caspase-3 activation in human osteogenic sarcoma cells (U-2 OS). J Orthop Res **23**(5)**:** 988-994.

Lu Y, Li C-M, Wang Z, Ross CR, Chen J, Dalton JT*, et al.* (2009). Discovery of 4-Substituted Methoxybenzoyl-aryl-thiazole as Novel Anticancer Agents: Synthesis, Biological Evaluation, and Structure−Activity Relationships. J Med Chem **52**(6)**:** 1701-1711.

Ly JD, Grubb DR, Lawen A (2003). The mitochondrial membrane potential (deltapsi(m)) in apoptosis; an update. Apoptosis **8**(2)**:** 115-128.

Martarelli D, Pompei P, Baldi C, Mazzoni G (2008). Mebendazole inhibits growth of human adrenocortical carcinoma cell lines implanted in nude mice. Cancer Chemother Pharmacol **61**(5)**:** 809-817.

Martello LA, Verdier-Pinard P, Shen HJ, He L, Torres K, Orr GA*, et al.* (2003). Elevated levels of microtubule destabilizing factors in a Taxol-resistant/dependent A549 cell line with an alpha-tubulin mutation. Cancer Res **63**(6)**:** 1207-1213.

Medellin DC, Zhou Q, Scott R, Hill RM, Frail SK, Dasari R*, et al.* (2016). Novel Microtubule-Targeting 7-Deazahypoxanthines Derived from Marine Alkaloid Rigidins with Potent in Vitro and in Vivo Anticancer Activities. J Med Chem **59**(1)**:** 480-485.

Meshkini A, Yazdanparast R (2012). Involvement of oxidative stress in taxol-induced apoptosis in chronic myelogenous leukemia K562 cells. Exp Toxicol Path **64**(4)**:** 357-365.

Miltenburg NC, Boogerd W (2014). Chemotherapy-induced neuropathy: A comprehensive survey. Cancer Treat Rev **40**(7)**:** 872-882.

Mindell JA (2012). Lysosomal acidification mechanisms. Annu Rev Physiol **74:** 69-86.

Ministry of Health. 2016. Cancer: New registrations and deaths 2013. Wellington: Ministry of Health. ISBN: 978-0-947515-75-1 (online)

Mitchison T, Kirschner M (1984). Dynamic instability of microtubule growth. Nature **312:** 237.

Moriyama Y, Takano T, Ohkuma S (1982). Acridine orange as a fluorescent probe for lysosomal proton pump. J Biochem **92**(4)**:** 1333-1336.

Morris MC, Heitz A, Mery J, Heitz F, Divita G (2000). An essential phosphorylation-site domain of human cdc25C interacts with both 14-3-3 and cyclins. J Biol Chem **275**(37)**:** 28849-28857.

Mosmann T (1983). Rapid colorimetric assay for cellular growth and survival: application to proliferation and cytotoxicity assays. J Immunol Methods **65**(1-2)**:** 55-63.

Mozzetti S, Ferlini C, Concolino P, Filippetti F, Raspaglio G, Prislei S*, et al.* (2005). Class III beta-tubulin overexpression is a prominent mechanism of paclitaxel resistance in ovarian cancer patients. Clin Cancer Res **11**(1)**:** 298-305.

Mukhopadhyay T, Sasaki J, Ramesh R, Roth JA (2002). Mebendazole elicits a potent antitumor effect on human cancer cell lines both in vitro and in vivo. Clin Cancer Res **8**(9)**:** 2963-2969.

Nathwani S, Butler S, Fayne D, McGovern N, Sarkadi B, Meegan M*, et al.* (2009). Novel microtubule-targeting agents, pyrrolo-1,5-benzoxazepines, induce apoptosis in multi-drug-resistant cancer cells. **66**(3):585-96

Nijhawan D, Honarpour N, Wang X (2000). Apoptosis in neural development and disease. Annu Rev Neurosci **23:** 73-87.

Nogales E (2000). Structural insights into microtubule function. Annu Rev Biochem **69:** 277-302.

Nogales E, Wang H-W, Niederstrasser H (2003). Tubulin rings: which way do they curve? Curr Opin Structural Biol **13**(2)**:** 256-261.

Norbury CJ, Hickson ID (2001). Cellular responses to DNA damage. Annu Rev Pharmacol Toxicol **41:** 367-401.

Nygren P, Fryknäs M, Ågerup B, Larsson R (2013). Repositioning of the anthelmintic drug mebendazole for the treatment for colon cancer. J Cancer Res Clin Onco **139**(12)**:** 2133-2140.

Opferman JT, Korsmeyer SJ (2003). Apoptosis in the development and maintenance of the immune system. Nat Immunol **4**(5)**:** 410-415.

Orrenius S, Nicotera P, Zhivotovsky B (2011). Cell death mechanisms and their implications in toxicology. Toxicol Sci **119**(1)**:** 3-19.

Oyaizu H, Adachi Y, Taketani S, Tokunaga R, Fukuhara S, Ikehara S (1999). A Crucial Role of Caspase 3 and Caspase 8 in Paclitaxel-Induced Apoptosis. Mol Cell Biol Res Coms **2**(1)**:** 36-41.

Pantziarka P, Bouche G, Meheus L, Sukhatme V, Sukhatme VP (2014). Repurposing Drugs in Oncology (ReDO)-mebendazole as an anti-cancer agent. Ecancermedicalscience **8:** 443.

Pantziarka P, Sukhatme V, Meheus L, Sukhatme VP, Bouche G (2017). Repurposing non-cancer Drugs in Oncology — How many drugs are out there? bioRxiv.

Paweletz N (2001). Walther Flemming: pioneer of mitosis research. Nat Rev Mol Cell Biol **2:** 72.

Pourgholami MH, Akhter J, Wang L, Lu Y, Morris DL (2005). Antitumor activity of albendazole against the human colorectal cancer cell line HT-29: in vitro and in a xenograft model of peritoneal carcinomatosis. Cancer Chemother Pharmacol **55**(5)**:** 425-432.

Povea-Cabello S, Oropesa-Ávila M, de la Cruz-Ojeda P, Villanueva-Paz M, de la Mata M, Suárez-Rivero JM*, et al.* (2017). Dynamic Reorganization of the Cytoskeleton during Apoptosis: The Two Coffins Hypothesis. Int J Mol Sci **18**(11).

Pozarowski P, Darzynkiewicz Z (2004). Analysis of cell cycle by flow cytometry. Methods Mol Biol **281:** 301-311.

Prota AE, Bargsten K, Northcote PT, Marsh M, Altmann K-H, Miller JH*, et al.* (2014). Structural Basis of Microtubule Stabilization by Laulimalide and Peloruside A. Angewandte Chemie International Edition **53**(6)**:** 1621-1625.

Raguz S, Yague E (2008). Resistance to chemotherapy: new treatments and novel insights into an old problem. Br J Cancer **99**(3)**:** 387-391.

Ranaivoson FM, Gigant B, Berritt S, Joullie M, Knossow M (2012). Structural plasticity of tubulin assembly probed by vinca-domain ligands. Acta Crystallographica Section D **68**(8)**:** 927-934.

Ravelli RBG, Gigant B, Curmi PA, Jourdain I, Lachkar S, Sobel A*, et al.* (2004). Insight into tubulin regulation from a complex with colchicine and a stathmin-like domain. Nature **428:** 198.

Rello S, Stockert JC, Moreno V, Gamez A, Pacheco M, Juarranz A*, et al.* (2005). Morphological criteria to distinguish cell death induced by apoptotic and necrotic treatments. Apoptosis **10**(1)**:** 201-208.

Repnik U, Hafner Cesen M, Turk B (2014). Lysosomal membrane permeabilization in cell death: concepts and challenges. Mitochondrion **19 Pt A:** 49-57.

Riccardi C, Nicoletti I (2006). Analysis of apoptosis by propidium iodide staining and flow cytometry. Nat Protoc **1**(3)**:** 1458-1461.

Rieger AM, Nelson KL, Konowalchuk JD, Barreda DR (2011). Modified Annexin V/Propidium Iodide Apoptosis Assay For Accurate Assessment of Cell Death. J Vis Exp(50).

Rock KL, Kono H (2008). The inflammatory response to cell death. Annu Rev Pathol **3:** 99-126.

Russell GJ, Lacey E (1995). Inhibition of [3H]mebendazole binding to tubulin by structurally diverse microtubule inhibitors which interact at the colchicine binding site. Biochem Mol Biol Int **35**(6)**:** 1153-1159.

Sakahira H, Enari M, Nagata S (1998). Cleavage of CAD inhibitor in CAD activation and DNA degradation during apoptosis. Nature **391**(6662)**:** 96-99.

Sale S, Sung R, Shen P, Yu K, Wang Y, Duran GE*, et al.* (2002). Conservation of the class I beta-tubulin gene in human populations and lack of mutations in lung cancers and paclitaxel-resistant ovarian cancers. Mol Cancer Ther **1**(3)**:** 215-225.

Sasaki J, Ramesh R, Chada S, Gomyo Y, Roth JA, Mukhopadhyay T (2002). The anthelmintic drug mebendazole induces mitotic arrest and apoptosis by depolymerizing tubulin in non-small cell lung cancer cells. Mol Cancer Ther **1**(13)**:** 1201-1209.

Scaffidi C, Schmitz I, Krammer PH, Peter ME (1999). The role of c-FLIP in modulation of CD95-induced apoptosis. J Biol Chem **274**(3)**:** 1541-1548.

Scannell JW, Blanckley A, Boldon H, Warrington B (2012). Diagnosing the decline in pharmaceutical R&D efficiency. Nat Rev Drug Discov **11**(3)**:** 191-200.

Shiratsuchi A, Osada S, Kanazawa S, Nakanishi Y (1998). Essential role of phosphatidylserine externalization in apoptosing cell phagocytosis by macrophages. Biochem Biophys Res Commun **246**(2)**:** 549-555.

Shu CH, Yang WK, Shih YL, Kuo ML, Huang TS (1997). Cell cycle G2/M arrest and activation of cyclin-dependent kinases associated with low-dose paclitaxel-induced sub-G1 apoptosis. Apoptosis **2**(5)**:** 463-470.

Simbulan-Rosenthal CM, Dakshanamurthy S, Gaur A, Chen YS, Fang HB, Abdussamad M*, et al.* (2017). The repurposed anthelmintic mebendazole in combination with trametinib suppresses refractory NRASQ61K melanoma. Oncotarget **8**(8)**:** 12576-12595.

Slautterback DB (1963). CYTOPLASMIC MICROTUBULES. I. HYDRA. J Cell Biol **18:** 367-388.

Slee EA, Adrain C, Martin SJ (2001). Executioner Caspase-3, -6, and -7 Perform Distinct, Non-redundant Roles during the Demolition Phase of Apoptosis. J Bio Chem **276**(10)**:** 7320-7326.

Steinmetz MO, Prota AE (2018). Microtubule-Targeting Agents: Strategies To Hijack the Cytoskeleton. Trends Cell Biol.

Sumoza-Toledo A, Reinhold P (2011). TRPM2: a multifunctional ion channel for calcium signalling. J Physiol **589**(7)**:** 1515-1525.

Surana U, Amon A, Dowzer C, McGrew J, Byers B, Nasmyth K (1993). Destruction of the CDC28/CLB mitotic kinase is not required for the metaphase to anaphase transition in budding yeast. Embo j **12**(5)**:** 1969-1978.

Suzuki Y, Imai Y, Nakayama H, Takahashi K, Takio K, Takahashi R (2001). A serine protease, HtrA2, is released from the mitochondria and interacts with XIAP, inducing cell death. Mol Cell **8**(3)**:** 613-621.

Sylvester PW (2011). Optimization of the tetrazolium dye (MTT) colorimetric assay for cellular growth and viability. Methods Mol Biol **716:** 157-168.

Tait SW, Green DR (2010). Mitochondria and cell death: outer membrane permeabilization and beyond. Nat Rev Mol Cell Biol **11**(9)**:** 621-632.

Terman A, Kurz T, Gustafsson B, Brunk UT (2006). Lysosomal labilization. IUBMB Life **58**(9)**:** 531-539.

Theodoropoulos PA, Polioudaki H, Kostaki O, Derdas SP, Georgoulias V, Dargemont C*, et al.* (1999). Taxol Affects Nuclear Lamina and Pore Complex Organization and Inhibits Import of Karyophilic Proteins into the Cell Nucleus. Cancer Res **59**(18)**:** 4625-4633.

Vale RD (2003). The molecular motor toolbox for intracellular transport. Cell **112**(4)**:** 467-480.

Vancompernolle K, Van Herreweghe F, Pynaert G, Van de Craen M, De Vos K, Totty N*, et al.* (1998). Atractyloside-induced release of cathepsin B, a protease with caspase-processing activity. FEBS Lett **438**(3)**:** 150-158.

Verdier-Pinard P, Wang F, Martello L, Burd B, Orr GA, Horwitz SB (2003). Analysis of tubulin isotypes and mutations from taxol-resistant cells by combined isoelectrofocusing and mass spectrometry. Biochemistry **42**(18)**:** 5349-5357.

Verhagen AM, Ekert PG, Pakusch M, Silke J, Connolly LM, Reid GE*, et al.* (2000). Identification of DIABLO, a mammalian protein that promotes apoptosis by binding to and antagonizing IAP proteins. Cell **102**(1)**:** 43-53.

Vermes I, Haanen C, Steffens-Nakken H, Reutelingsperger C (1995). A novel assay for apoptosis. Flow cytometric detection of phosphatidylserine expression on early apoptotic cells using fluorescein labelled Annexin V. J Immunol Methods **184**(1)**:** 39-51.

Vikhanskaya F, Vignati S, Beccaglia P, Ottoboni C, Russo P, D'Incalci M*, et al.* (1998). Inactivation of p53 in a Human Ovarian Cancer Cell Line Increases the Sensitivity to Paclitaxel by Inducing G2/M Arrest and Apoptosis. Exp Cell Res **241**(1)**:** 96-101.

Wajant H (2002). The Fas signaling pathway: more than a paradigm. Science **296**(5573)**:** 1635-1636.

Wani MC, Taylor HL, Wall ME, Coggon P, McPhail AT (1971). Plant antitumor agents. VI. The isolation and structure of taxol, a novel antileukemic and antitumor agent from Taxus brevifolia. J Am Chem Soc **93**(9)**:** 2325-2327.

Waybright TJ, Britt JR, McCloud TG (2009). Overcoming problems of compound storage in DMSO: solvent and process alternatives. J Biomol Screen **14**(6)**:** 708-715.

Weisenberg RC, Deery WJ, Dickinson PJ (1976). Tubulin-nucleotide interactions during the polymerization and depolymerization of microtubules. Biochemistry **15**(19)**:** 4248-4254.

Yamano H, Gannon J, Hunt T (1996). The role of proteolysis in cell cycle progression in Schizosaccharomyces pombe. Embo j **15**(19)**:** 5268-5279.

Yang C-P, Horwitz S (2017). Taxol®: The First Microtubule Stabilizing Agent. Int J Mol Sci **18**(8)**:** 1733.

Youle RJ, Strasser A (2008). The BCL-2 protein family: opposing activities that mediate cell death. Nat Rev Mol Cell Biol **9**(1)**:** 47-59.

Yu CC, Liu SP, Hsu JL, Hsu JTA, Kudryavtsev KV, Guh JH (2015). KUD773, a phenylthiazole derivative, displays anticancer activity in human hormone-refractory prostate cancers through inhibition of tubulin polymerization and anti-Aurora A activity. J Biomed Sci **22**(1).

Yu Z, Li W, Brunk UT (2003). 3-Aminopropanal is a lysosomotropic aldehyde that causes oxidative stress and apoptosis by rupturing lysosomes. Apmis **111**(6)**:** 643-652.

Yuan S, Yu X, Topf M, Ludtke SJ, Wang X, Akey CW (2010). Structure of an apoptosome-procaspase-9 CARD complex. Structure **18**(5)**:** 571-583.

Zhang L, Bochkur Dratver M, Yazal T, Dong K, Nguyen A, Yu G*, et al.* (2019). Mebendazole Potentiates Radiation Therapy in Triple-Negative Breast Cancer. Int J Radiation Oncol Biol Phys **103**(1)**:** 195-207.

Zhang X, Zhao J, Gao X, Pei D, Gao C (2017). Anthelmintic drug albendazole arrests human gastric cancer cells at the mitotic phase and induces apoptosis. Exp Ther Med **13**(2)**:** 595-603.

Zhao M, Antunes F, Eaton JW, Brunk UT (2003). Lysosomal enzymes promote mitochondrial oxidant production, cytochrome c release and apoptosis. Eur J Biochem **270**(18)**:** 3778-3786.